Chem Soc Rev

Clay nanotube-metal core/shell catalysts for hydroprocesses

Journal:	*Chemical Society Reviews*
Manuscript ID	CS-REV-05-2021-000502
Article Type:	Review Article
Date Submitted by the Author:	28-May-2021
Complete List of Authors:	Glotov, Aleksandr; Gubkin Russian State University of Oil and Gas Vutolkina, Anna; Gubkin Russian State University of Oil and Gas; Lomonosov Moscow State University Pimerzin, Aleksey; Gubkin Russian State University of Oil and Gas; Samara State Technical University Vinokurov, Vladimir; Gubkin Russian State University of Oil and Gas Lvov, Yuri; Louisiana Tech University, Institute for Micromanufacturing

Clay nanotube-metal core/shell catalysts for hydroprocesses

Aleksandr Glotov[1*], Anna Vutolkina[1,2], Aleksey Pimerzin[1,3], Vladimir Vinokurov[1], Yuri Lvov[4]**

[1]Gubkin Russian State University of Oil and Gas (NRU), 119991, Russia, Moscow, 65 Leninsky Prospekt

[2]Lomonosov Moscow State University, 119991, GSP-1, Russia, Moscow, 1-3 Leninskiye Gory

[3]Samara State Technical University, 443100, Russia, Samara, 244 Molodogvardeyskaya st.

[4]Louisiana Tech University, Institute for Micromanufacturing, 71272, USA LA, Ruston, 505 Tech Drive

Corresponding authors: Aleksandr Glotov (Gubkin University, glotov.a@gubkin.ru) and Yuri Lvov (Louisiana Tech University, ylvov@latech.edu)

Abstract

Catalytic hydroprocesses take a significant role in oil refining and petrochemistry. The tailored design of new metal nanosystems and optimization of their support, composition, and structure is a prospective strategy for enhancing efficiency of the catalysts. Mesoporous support impacts the active component by binding it to the surface, which leads to the formation of tiny highly dispersed catalytic particles stabilized from aggregation and with minimized leaching. The structural and acidic properties of the support are crucial and determine the size and dispersion of the active metal phase. Currently, the research efforts are shifted toward the design of nanoscale porous materials, where homogeneous catalysis is displaced by heterogeneous one. Ceramic materials, such as 50-nm diameter natural halloysite nanotubes are of special interest for this. Much attention to halloysite clay is due to it's tubular structure with the hollow 10-15 nm diameter internal cavity, textural characteristics, and different chemical compositions of the outer/inner surfaces allowing for the nanotube selective modification. Loading halloysite with metal particles or placing them outside the tubes provided stable and efficient mesocatalysts. The low cost of this abundant nanoclay makes it a good choice for the scaled-up architectural design of core-shell catalysts, containing active metal sites (Au, Ag, Pt, Ru, Co, Mo, Fe_2O_3, CdS, CdZnS, Cu-Ni) located inside or outside of the tubular template. These alumosilicate nanotubes are environment-friendly and are available in thousand tons.

Here we summarized the advances of halloysite-based composite materials for hydroprocesses focusing on the selective binding metal particles. We analyze the tubes' morphology adjustments and size selection, physicochemical properties of pristine and modified halloysite (e.g., acid-etched or silanized), methods of metal clusters formation, and their localization. We indicate prospective routes for architectural design of stable and efficient nanocatalysts based on this safe and natural clay material.

Authors

Dr. Aleksandr P. Glotov is a leading researcher, and he is the head of the catalysis laboratory in the Gubkin Russian State University of Oil and Gas. He earned a Ph.D. in petroleum chemistry from Lomonosov Moscow State University in 2015. He is an expert in micro/mesoporous functional materials design, including self-assembly, template synthesis and modification of zeolites, ordered mesoporous silicas, and aluminosilicate nanotubes for different refining and petrochemical processes. Dr. Glotov organized the catalysis laboratory and succeeded in the synthesis of materials with specified textural properties and porosity, applied as a support for catalysts tested in industrial petrochemical processes. A. Glotov was awarded with the Moscow Government Prize for his research excellence in natural nanomaterials.

Dr. Anna V. Vutolkina is a senior researcher at Lomonosov Moscow State University and Gubkin University of Oil and Gas. She earned her Ph.D. in Petroleum Chemistry from Lomonosov Moscow State University. Dr. Vutolkina is working on developing hydrotreatment of unconventional hydrocarbon feeds (renewable organic feeds, biomass, highly viscous and bituminous oils, bio-oil, and oil sludge) and designing hydroprocessing catalysts based on mesoporous well-ordered silicas and aluminosilicates. She is an expert in self-assembly methods applied to unsupported sulfide nanocatalysts for sulfur removal. In 2019, she was awarded with the honorable research scholarship by the President of Russia.

Dr. Aleksey A. Pimerzin is a senior researcher at Samara State Technical University. He earned a Ph.D. in chemistry in 2015 from Samara State Technical University, chemical-technological department. The field of his scientific interests focused on heterogeneous catalysts, hydroprocesses, and oil refinery with novel materials and technologies application.
The results were presented at multiple international conferences on catalysis in 2017-2021. He was awarded with a medal of the Russian Academy of Sciences as an outstanding young scientist.

Prof. Vladimir A. Vinokurov earned a Ph.D. in Chemistry from Gubkin University in 1975, has been working as a leader of Surfactants Organic Chemistry, and is the Head of the Physical and Colloid Chemistry Division. In 1989, he earned a Doctor of Science (habilitation) in Chemistry. His area of interest is nanomaterials (halloysite nanotubes, nanocellulose, renewable materials) for a wide range of industrial applications, especially catalysis, smart materials, and coatings. He pioneered multiple formulations for oil drilling technologies and advanced catalysis protected with 40 patents and published 200 peer-reviewed papers. Prof. Vinokurov is honored petrochemist, oilman, and distinguished worker of university education of the Russian Federation. He has supervised more than 25 Ph.D's.

Prof. Yuri M. Lvov earned Ph.D. from Lomonosov Moscow State University. He has worked in world-famous centers: Max Planck Institute for Colloids, Potsdam, National Institute of Materials Science, Tsukuba, and the Naval Research Laboratory, Washington DC. In 2000 Dr. Lvov moved to Louisiana Tech University. His area of expertise is micro/nano technology including assembly of ultrathin organized films, ordered shells on tiny templates, and nanotubes for controlled release of chemical agents. He was a pioneer of layer-by-layer self-assembly method and developed halloysite clay nanotubes for functional composites and core-shell metal/ceramic catalystic mesosystems. Lvov's publications have been cited 35,000 times. He chaired 8 nanomaterial symposiums at American Chem. Soc. National Meetings and in China. Y. Lvov was awarded with the A. von Humboldt Prize for lifetime achievements in nanochemistry.

Outline

1. Introduction 5

2. Petrochemical hydroprocesses 9

2.1. Hydrogenation of nitroarenes and aromatics.....9

2.2. Hydrogenation of phenols and reduction of nitrophenols.....18

2.3. Hydroformylation.....24

2.4. Fischer-Tropsch synthesis 26

2.5. Hydroisomerization over halloysite supported catalysts.....28

3. Hydroprocessing in oil refining: sulfur removal assisted with the clay nanotubes.....31

3.1. Hydrocracking and hydrotreatment 31

3.2. Fluid catalytic cracking 34

4. Gas-phase catalysis.....36

4.1. Dry reforming of methane.....36

4.2. Pollutants removal.....39

4.3. Hydrogen production and storage.....43

5. Conclusions and prospective 49

1. Introduction

Catalytic hydroprocesses (carried out under hydrogen pressure) take a significant role among the oil refining and petrochemistry. The latter involves the hydrogenation of nitroarenes to anilines which are intermediates for the production of a diverse range of chemicals; hydroconversion of aromatics to corresponding cyclic compounds, i.e. benzene to cyclohexane, phenol to cyclohexanol, used as solvent or reagent for organic synthesis, polymers, fibers, paints, and varnishes production, in pharmacology; reduction of nitrophenol to aminophenol used for black-and-white film and acetaminophen production. Petrochemical hydroprocesses also include hydroisomerization of xylenes and ethylbenzene to *p*-isomer used for the production of terephthalic acid. The gas-phase processes are alkenes hydroformylation yielded aldehydes for production of alcohols, acids, esters, surfactants, plasticizers, and Fisher-Tropsch synthesis converting syn-gas into light hydrocarbons. The importance of hydroprocesses in oil refining is defined by increasing oil processing depth. There is a growing demand for gasoline and diesel with sulfur content less than 10 ppm, fuel with lower cloud point for cold climate usage, gasoline with a high octane number, and high-quality jet fuel.

The involvement of low-quality heavy feeds, including non-traditional unconventional components (tar, black oil, shale-oil, natural bitumen, bituminous sands) and renewable bio-feeds, demands hydroprocessing catalysts to have a high surface area and mesoscale porosity providing proper transport channels for the transformation of bulk molecules, including heteroatomic compounds, and reducing diffusion limitations. The industry needs catalysts with high adsorption capacity to sulfur compounds and appropriate acidity for C-S bond scission with high selectivity to distillates and low yield of hydrocarbon gaseous products. To achieve the desirable conversion of heavy cuts to low sulfur fuel, the active metal component has to be highly dispersed over the support surface. For petrochemistry, the main problem in hydrogen-assisted processes is metal leaching, agglomeration, and aggregation of catalytic particles resulting in a decrease of the efficiency. Some processes also face difficulties in separating catalysts from products and in recycling. Therefore, the design of catalysts with highly dispersed metal nanoparticles over mesoporous supports with tunable properties is challenging.

Hydroprocessing catalysts for isomerization and hydrocracking are bifunctional systems, where metal particles accelerate the hydrogenation reaction and the support provides acidic sites for the bond cleavage. The catalytic efficiency depends on the balance between these two functionalities. The support acts as a metal binder determining the particularization and dispersity of the active component allowing for enhancing activity, selectivity and preventing agglomeration and metal leaching. The support structure, specific surface area, pore size, and regularity of the porous arrangement provide a capacity to absorb reagent molecules and sieving properties for high product selectivity. The acidic properties of the support influence reaction routes and suppress by-products formation. Therefore, the tuned support properties are crucial for catalytic behavior of the metal-based systems. The design of new metal-ceramic core-shell systems and optimization of their properties by adjusting the structure of supports is a prospective strategy for enhancing efficiency of the catalysis.

Alumina, silica, or zeolites are widely used as a support for industrial hydroprocessing. The ubiquitous usage of aluminum oxide is determined by the ease of preparation, adjustable dispersivity, and the state of oxide surface maximize cohesiveness. Zeolites are well-ordered microporous materials with a high specific surface and narrow pore size distribution providing sieving properties. The properties of these synthetic aluminosilicates depend on the choice of the

structure-directing agent and are turned during the crystallization. The alumina or zeolite-supported catalysts have high activity but suffer several drawbacks. Due to the diffusion and mass-transfer limitation in a micro-scale porous for bulk organic molecules, these materials are restricted for hydroconversion of low-quality heavy feeds. The hindered transformation leads to activity and catalyst lifetime decreases due to pore blockage by the coke. Since the product diffusion is restricted by steric hindrances, the secondary cracking over strong acid sites also may occur giving gaseous products. The latest research in tailored catalyst design focuses on the development of meso- or micro-porous materials with appropriate porosity and acidity. The well-ordered silicates, aluminosilicates, zirconium and titanium oxides were established as support materials with enhanced acidic and textural properties for bulk molecules transformation with minimized diffusion limitations. The controlled isomorphous substitution of silica to aluminum, titanium, or zirconium allows tuning the acidity and product selectivity. The high specific surface area for such supports provides their good sorption capacity that combined with appropriate acidity and metal-support binding leads to nano-particularization and high dispersity of active phase. The main industrial disadvantage of current mesoporous molecular sieves is low thermal stability and mechanical strength, which restrict their applications in high-temperature hydroprocessing. Moreover, the high cost of these synthetic materials influences their ubiquitous use. We are considering as advantageous alterative shifting efforts towards mesoporous aluminosilicates with tubular structures [1-10]. Natural halloysite clay nanotubes may be the components of catalysts with tunable properties.

The halloysite is an aluminosilicate of the kaolin group with the chemical formula of $Al_2Si_2O_5(OH)_4{*}nH_2O$, n=2, having a hollow tubular multi-layered wall structure (Fig. 1). Much attention to halloysite clay is given due to it's unique tubular structure with the hollow internal cavity and the chemical properties of the surfaces that allow for selective modification. The external and internal tube's surfaces consist of siloxane (Si–O–Si) and aluminol (Al–OH) groups (Fig. 1a). The aluminosilicate layers in the wall are linked by hydrogen bonds and are stabilized by water molecules incorporated into interlayer space, resulting in spacing of 7.2 nm [11].

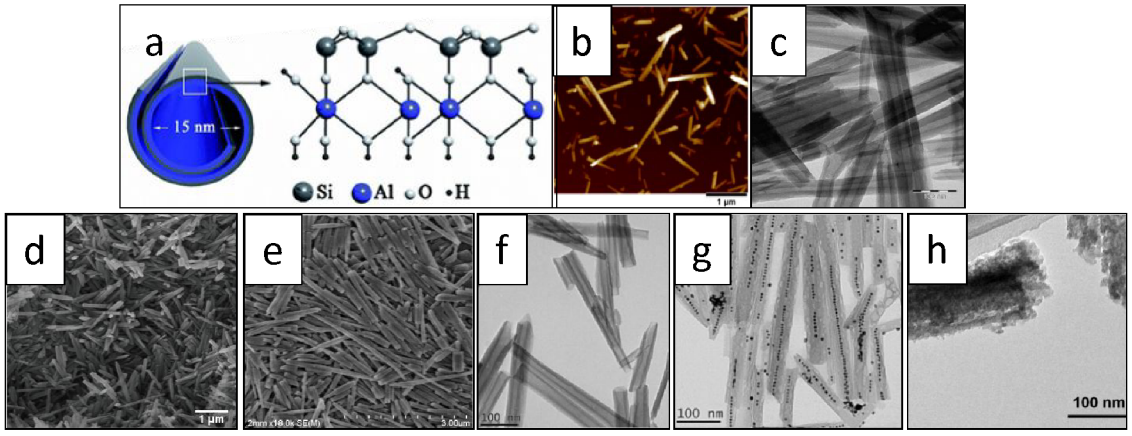

Fig. 1. (a) The schematic illustration of halloysite structure, reprinted from our works with permission [12], copyright (2012) American Chemical Society; (b-d) 50-nm diameter halloysite tubes from Applied Minerals Inc, Utah, USA: AFM, TEM, SEM reprinted from [13], copyright (2020) with permission from Elsevier; (e) SEM image of larger 130-nm diameter halloysite tubes provided by Northstar Mine Co, Utah, USA; (f, g) TEM images of empty and gold loaded halloysite nanotubes, reprinted with permission from [14] copyright (2017) American Chemical Society; (h) TEM image of halloysite etched for 20 hrs in 1 M H_2SO_4, reprinted with permission from [15], copyright (2012) American Chemical Society.

Halloysite is a natural low-cost clay available in tons; it is a safe and environment-friendly material. The weathering, hydrothermal alteration of aluminum silicates under geological volcanic conditions, leads to the accumulation of halloysite clay mineral [11]. Deposits with available commercial halloysite of purity above 90 % are located in the USA, China, New Zealand, and Australia [11, 16]. Almost any kaolin deposit has halloysite, but for industrial production, one has to find reach pockets, containing almost pure nanotubes, which minimizes the purification processes. Depending on the deposit, sizes of hydrated tubes are as follows: length 0.5 to 1.5 μm, external diameter of 40 to 100 nm with 10 to 20 nm diameter lumens. Halloysite available for a large purchase as a fine white dry powder may be found at 3-4 companies and these products have ca. 95 % tubes with a diameter of 50-60 nm, length of 0.5-1.0 μm, and the periodicity in the tubes' wall multilayer packing is 0.72 nm in a dry state (row wet halloysite has wall periodicity of ca. 1.0 nm) [11]. Halloysite is a very stable material. For example, we kept these dried nanotubular minerals on a shelf at room temperature for ten years and did not recognize any changes in their phys-chemical properties [17].

Different chemistry (outermost siloxane (Si–O–Si) and inside (Al–OH) groups) of the tube's surface and internal space, also called lumen, is the unique properties of the clay nanotubes. This causes the different charges of the inner lumen (positive) and the outer surface (negative) at pH range 4 to 9, which allows for the selective surface modification exploiting an electrostatic attraction of reagents [2, 7]. Halloysite nanotubes (HNTs) have a density of 2.53 g/cm^3, a surface area of 60-70 cm^2/g, pore volume of 0.3-0.7 cm^3/g, cation exchange capacity of 11 meq/100g, and electric zeta-potential in water at pH 5-9 of –30 mV making them moderately stable in water dispersions. It precipitates during 10-15 hours with smaller tubes staying longer at the upper column area. Contrary to other clays (kaolin, montmorillonite, bentonite), halloysite tubes are not stacked in multilayers and may be easily exfoliated by stirring. Pure commercial halloysite has less than 1 wt % of quarts admixture, ca 0.1 % of iron oxide with Fe^{3+} partially substituting Al^{3+} (it may give slightly brownish color if presents at higher amounts) and below 0.1 % of TiO_2 and CaO; other metals (Co, Cu, Cr, Ni, Pb, Zn) present in a trace amount of 1-5 ppm[1]. A single halloysite tube has a Young modulus of 130 GPa. Tubular morphology of halloysite is preserved at least up 1200 ºC with a 12 % mass decrease at 490 ºC due to the loss of interlayer water [1, 10]. Etching of halloysite for 10-15 hours in a hot strong acid allows dissolving alumina while preserving silica, enlarging lumens, and, finally, converting these solid nanotubes into highly porous (300 cm^2/g) hollow silica cylinders, Fig. 1h [15].

The unique tubule structure, surface chemistry, phys-chem properties, and wide opportunities for modification make halloysite attractive for a wide range of applications. According to the data analysis related to the term "halloysite", the number of publications increased 8 times in the last decades reaching 600 per year, mostly in materials sciences with the pioneering paper by R. Price, B. Gaber, and Y. Lvov in 2001[18]. Due to biocompatibility, halloysite nanotubes were used as containers for sustained drug delivery, for tissue engineering, bone implants and wound care, and in anticancer therapy [16]. These clay-based materials are also used to reinforce the polymeric matrix, to fabricate high-quality ceramics and porcelain, and for protective coatings[2, 19-21]. Due to the high surface area and adsorption capacity, halloysite is suggested for remediation of oil spills with Pickering emulsification and the removal of aqueous dyes [19]. These clay nanotubes are also used in cosmetics and personal care [19, 22]. The concept of tubular nanotemplates for architectural core-shell design of materials with different inside/outside compositions is a central strategy for many of halloysite research papers. [1, 13, 18, 23].

The tunable properties of halloysite allow for its application as support for enhanced catalysts. For example, by varying the number and strength of acid sites, the activity of clay-based catalysts can be adjusted. Acid activation of clay minerals leads to the formation of Brønsted acidity, which is essential for the number of organics transformation [24-28]. It affects the reaction route, efficiency, and isomers' selectivity. The design assumes selective modification of inner/outer halloysite surfaces exploiting metal ions impregnation and reduction. Since the inner cavity and outer surface have positive and negative charges at pH 4-9, the halloysite enables the selective placement of metal clusters inside or outside the clay tubes. Thus, positively charged cations adsorb on the outer tubes' surface, while the negatively charged species can be loaded inside the lumen [29-31]. Metal nanoparticles, intercalated into the inner cavity, are stable toward leaching as compared to those located on the outer surface [13, 29, 32]. Such clay-metal encapsulation prevents nanoparticle aggregation and allows for stabilized and high activity at 400-450 °C as we have shown for Cu-Ni nitric oxide catalytic removal at auto exhausting system [32]. This tubular nanoclay has been suggested as a support for precious metal catalysts for a wide range of reactions and industrial processes [4, 10, 13, 29, 33-35]. Among them are photocatalysis [3, 36, 37], coupling reactions [8, 9, 38-50], catalytic hydrogenation of benzene [23, 51, 52], phenol [23, 33], nitroarenes [44, 53-59], cyclohexene oxidation with molecular oxygen [60, 61], benzyl alcohol oxidation [62], methane oxidation reaction [63], reduction of nitrophenols [64-66], isomerization of aromatics [67], and hydroconversion of n-decane [68, 69]. Halloysite has also been used as a component of sulfur reduction additives for fluid catalytic cracking (FCC) [10, 23], and as a template for hydrocracking [70-76], FCC [77, 78], and Fischer-Tropsch synthesis [79] catalysts.

The research and development in traditional heterogeneous processes are shifting towards nanoscale porous materials. We summarize here the advances of halloysite-based core-shell catalysts focusing on the tubes' size selection, physicochemical properties of the pristine and modified nanoclay (e.g., acid-etched or silanized), methods of metal clusters formation and positioning, and catalytic optimization under the reaction conditions, Fig. 2.

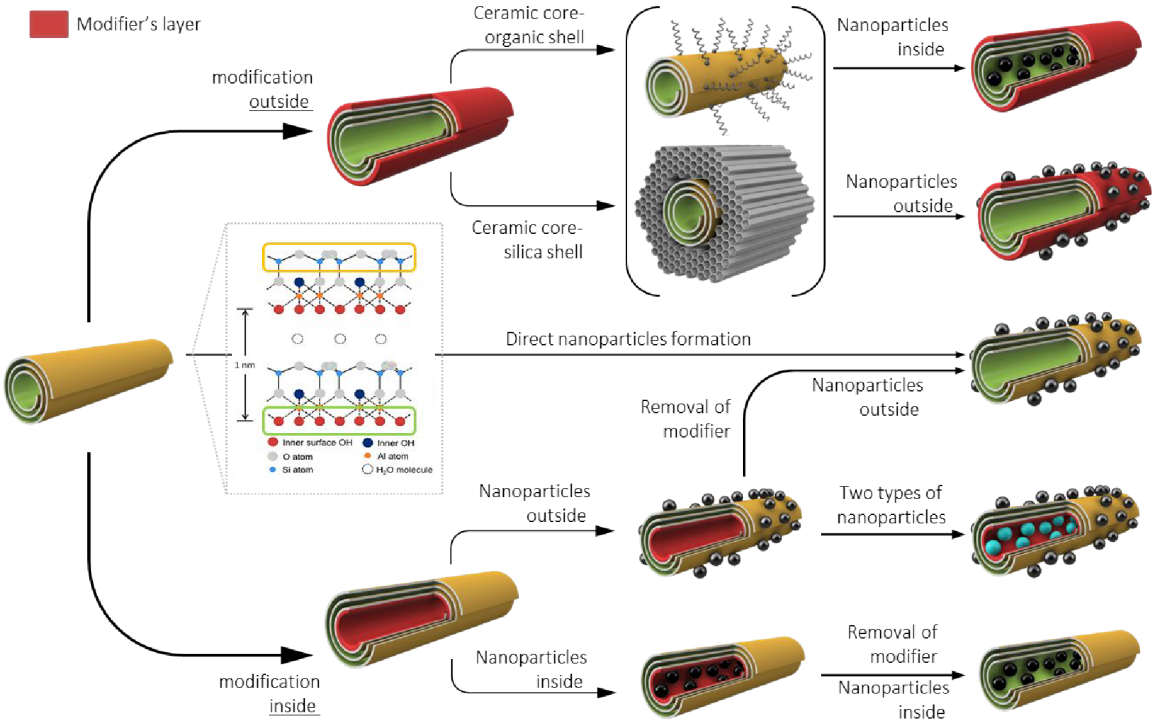

Fig. 2. Strategy and pathways of architectural design of core-shell metal-ceramic nanosystems.

We cover the catalytic performance of halloysite-based materials for hydroprocesses focusing on selective binding metal particles inside or outside the nanotubes, optimizing behavior under reaction conditions, and indicating further routes for design of more stable and efficient catalyst.

2. Petrochemical hydroprocesses

Petrochemical processes via hydrogenation are divided into homogeneous and heterogeneous catalyzes. The latter is the most prospective due to low costs and the simplicity of product recovery. Hydrogenation of nitroarenes to anilines, reduction of nitrophenols to aminophenols, are used for black-and-white film and acetaminophen production, gas-phase processes like hydroformylation of alkanes yielded aldehydes for the production of alcohols, acids, esters, surfactants, plasticizers, Fisher-Tropsch synthesis converting syn-gas into light hydrocarbons are among the most famous petrochemical hydroprocesses. The second group of heterogeneous processes includes hydrogenation of aromatics to corresponding cyclic compounds, i.e. benzene to cyclohexane, phenol to cyclohexanol, used as solvent or reagent for organic synthesis, polymers, fibers, paints, and varnishes production, in pharmacology, hydroisomerization of xylenes and ethylbenzene to *p*-isomer needed for the production of terephthalic acid as a monomer for polymeric manufacturing. In heterogeneous processes, metal leaching, agglomeration, and aggregation of nanoparticles lead to a decrease in catalytic efficiency. Therefore, the tailored design of catalysts with well-dispersed nanoparticles is of great interest. We discuss application of halloysite-supported catalysts for transformation of a wide range of chemicals into value-added products focusing on enhancing activity, selectivity, and stability.

2.1.Hydrogenation of nitroarenes and aromatics

The particularization of metals over porous support is related to the increasing activity and selectivity due to reactant molecules can reach as many active metal sites as possible. However, catalyst nanoparticles may agglomerate, particularly at high metal loading or elevated reaction temperatures, thus decreasing the conversion efficiency. To prevent the agglomeration of metal particles, they are anchored to the support surface. Many attempts have been made to develop hybrid organic-inorganic materials for the immobilization of metal particles[80-82]. Among them, nanotubular inorganic support, in particular halloysite, has attracted attention due to it's high specific surface area, thermal and mechanical resistance, and a hollow inner cavity with nanoconfined space for particle formation. Halloysite provides an opportunity for strong anchoring of metal particles inhibiting their aggregation[7] and preventing leaching. The halloysite nanotubes are prospective for environmentally benign carbonaceous heterogeneous catalysts which do not require a complicated chemical synthesis allowing for essentially "green" and scaled-up production.

One of the main catalyst characteristics is selectivity to the nitro group reduction, adjusted by the modification of the halloysite surface with organosilanes or polymers. These polymer-clay nanocomposites exhibit enhanced mechanical strength, flame retardancy, and reduced thermal expansion. The adjustable catalytic properties are achieved by selective metal loading and by improved clay dispersion in a solvent. Selective outer or inner halloysite tubes modification for loading of Ru, Cd, Ag, Au, Co-Ni were proposed in [1, 6, 29, 30, 33, 83, 84]. These studies were extended by the application of amphiphiles, polymers, and cyclodextrins for selective decoration of the

nanotubes' surface to enhance the metal loading [9, 44, 45, 47, 49, 53, 55-57, 59, 85]. This approach prevented aggregation of metal nanoparticles and improved the dispersion of catalysts' active phase. All of these methods imply varying the content of modifier's groups covered the halloysite surface to control the metal deposition and particle size.

The modification of the external surface of halloysite nanotubes (further we used also shortening: HNTs) by the poly(methyl methacrylate-co-maleic anhydride) was applied to enhance the efficiency of Pd catalysts in hydrogenation of nitroarenes [9]. Functionalization of the external halloysite' surface by polymers enhances the support capacity to metal particles anchored over the outer surface and encapsulated into the internal cavity. It leads to metal particles stabilization and an increase in the selectivity of the Pd-containing catalyst (Pd@HNT-Gua-Poly) toward the nitro group, converted to amine (Table 1).

Table 1. Comparison of the catalytic activity of halloysite-based palladium catalysts for hydrogenation of nitroarenes

Entry	Substrate	Time, min	Catalyst	Reaction condition (1 mmol of substrate in water, 50 °C, 1 atm H_2 pressure)	Yield[e] (%)	Ref
1	Nitrobenzene	80	Pd@HNT-Gua-Poly l	A	95	9
		80	Pd@HNT	A	65	9
		80	Pd@Poly	A	70	9
		60	Pd@HTMCa	B	100	44
		45	Pd@C	C	100	86
		60	Pd@HNT@Glu-Fe-C	D	98	58
2	1-Nitronaphthalene	120	Pd@HTMCa	B	100	44
		155	Pd@C	C	85	86
		155	Pd@HNT@Glu-Fe-C	D	80	58
3	4-Nitroacetophenone	90	Pd@HTMCa	B	100	44
		100	Pd@C	C	90	86
		90	Pd@HNT@Glu-Fe-C	D	90	58
4	4-Nitroaniline	180	Pd@C	C	55	86
		110	Pd@HNT@Glu-Fe-C	D	87	58
5	1-Bromo-2-nitrobenzene	165	Pd@C	C	60	86
		200	Pd@HNT@Glu-Fe-C	D	68	58

[a] catalyst (1 mol%) in water (5 mL)
[b] catalyst (1 wt%) in water (2 mL)
[c] catalyst (0.85 mol%) in water (5 mL)
[d] catalyst (0.5 mol%) in water (5 mL) at 40 °C
[e] Isolated yield

This strategy was also applied in the work [54], where the outer surface of the tubes was decorated with 3-(trimethoxysilyl) propylisocyanate followed by Pd loading. The resulting catalyst exhibited high activity in the hydrogenation of nitroarenes. The highest selectivity to the nitro group was achieved when the ligand consisted of two methylenic moieties between both amine groups. The shorter or longer carbon chain, as well as more rigid ones, the lower selectivity was achieved. Considering the synergism between halloysite, cyclodextrins (CD), and carbon porous materials, the authors suggested the Pd-containing catalyst supported on the halloysite, decorated with cyclodextrin and melamine-based polymer, for conversion of nitroarenes to the corresponding anilines [44] (Fig. 3 a, d). According to TEM images, the fine sheets of CD-modified melamine-based polymer cover the outer surface of HNTs (Fig. 3 b, c). This functionalization leads to the formation of Pd particles with 7.0±0.1 nm in diameter strongly bonded with the support surface. It provides protecting from metal leaching and

prolonging catalysts' lifetime [87]. The authors proposed that cyclodextrin not only promotes the formation of an inclusion complex with a hydrophobic substrate and transfers it into the aqueous media, but cyclodextrin also acts as a capping agent, stabilizing Pd nanoparticles. The mesoscale inner cavity of the halloysite also provides the higher selectivity toward the nitro group, when a substrate containing keto-functionality is a competing group (Table 1).

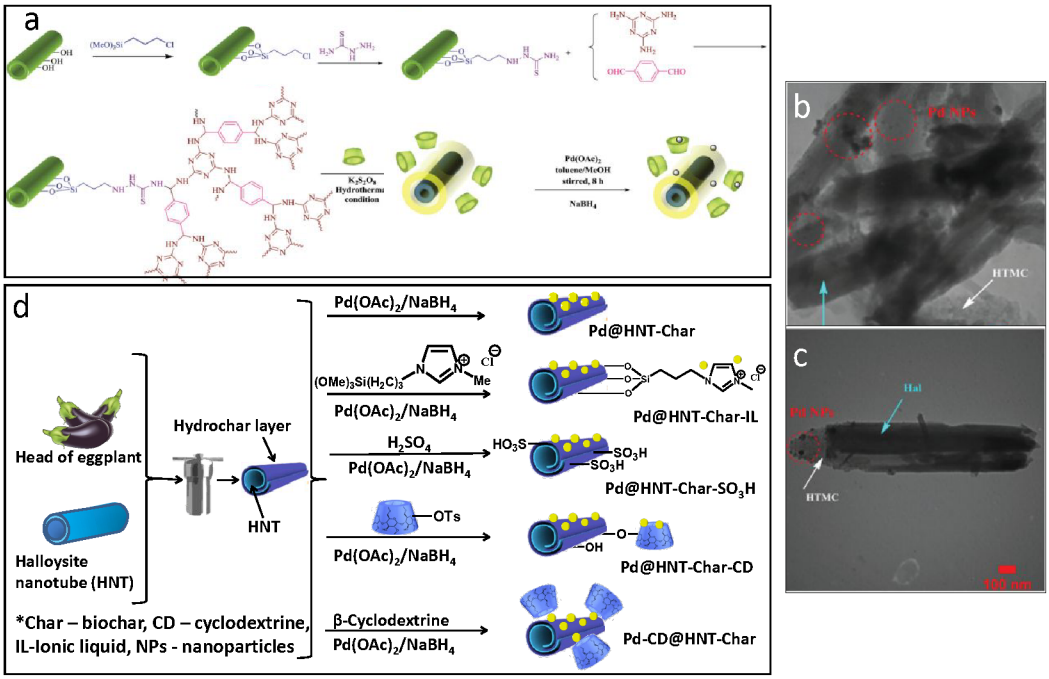

Fig. 3. (a) The schematic of the synthesis of Pd-containing catalyst on halloysite, decorated with cyclodextrin and melamine-based polymer (reproduced from [44] with permission from the Royal Society of Chemistry), and (b, c) TEM images of the resulted catalysts (reproduced from [44] with permission from the Royal Society of Chemistry); (d) The proposal pathways for the modification of eggplant-derived biochar-halloysite used as a support for Pd catalysts (adopted from [56]).

Following the improvement of catalysts' activity and stability by constructing halloysite-based support, researchers were focused on the functionalization of nanotubes through the β-cyclodextrin (β-CD) and glycidyl methacrylate polymerization to form a polymeric network (HNT-P-CD)[85]. Halloysite nanotubes (HNTs) were carbonized to prepare the HNT-C composite, afterward used as a template for the immobilization of Pd nanoparticles, producing Pd@HNT-C catalyst. Since the cyclodextrin acts both as a phase transfer and a capping agent, the Pd nanoparticles were immobilized over the outer surface of the halloysite. The authors assumed that an application of halloysite as the backbone component of the catalyst allows for increasing Pd content and improving catalytic activity. This carbonized halloysite-based exhibited superior activity in hydrogenation of nitrobenzene as compared to polymer-containing counterpart.

The importance of bio-char arming by halloysite for Pd nanoparticles immobilization was shown in[56]. The synthetic procedure is exhibited in Fig. 3d. The covering of the outer surface of the halloysite by bio-char resulted in uniform Pd distribution. The metal particles were well-dispersed, and no aggregation of Pd was observed. The synergistic effect of halloysite nanotubes with chair leads to the high activity of the nanocomposite-based Pd catalyst in the hydrogenation of nitroarenes when adding cyclodextrin (Table 2). Based on zeta-potential measurements, the halloysite decorated with char biopolymer enhances the stability of colloidal dispersion, which

prevents the aggregation of the metal particles. Better interaction between the substrate and the catalytic species resulted in increasing conversion and turnover frequency (TOF) values.

Table 2. The catalytic activity, the average Pd particle size, and the loading of the catalytic samples [a], [56]

Entry	Catalyst	Aniline Yield (%)[b]	Naphthylamine Yield (%)[b]	Pd loading (mmol.g^{-1})	Pd Particle Size (nm)	TOF for Aniline (h^{-1})	TOF for Naphthylamine (h^{-1})
1	Pd@HNT	30	10	0.027	4.8±1.3	1297	307
2	Pd@HNT+β-CD[c]	65	60	0.027	4.8±1.3	2810	1844
3	Pd@Char	40	30	0.026	3.6±1.1	1307	693
4	Pd@Char+β-CD	75	50	0.026	3.6±1.1	1951	1156
5	Pd@HNT-Char	75	65	0.028	3.7±1.0	2435	1490
6	Pd@HNT-Char+β-CD	100	95	0.028	3.7±1.0	3226	2179
7	Pd@HNT-Char-IL[d]	60	30	0.041	4.5±1.1	1612	570
8	Pd@HNT-Char-IL+β-CD	90	45	0.041	4.5±1.1	2406	834
9	Pd@HNT-Char-SO_3H[e]	45	50	0.028	3.9±1.0	1524	1204
10	Pd@HNT-Char-SO_3H+β-CD	55	55	0.028	3.9±1.0	1863	1324
11	Pd@HNT-Char-CD	60	50	0.025	4.9±1.7	2662	1696
12	Pd-CD@HNT-Char	50	40	0.032	3.8±1.0	1451	825

[a] Reaction condition: Substrate (1 mmol), catalyst (0.03 mol%), β-CD (0.004 mmol), H_2O (2 mL), H_2 (1 bar) at 25 °C in 1 h.
[b] Isolated yields
[c] Use of β-CD in its free form
[d] Trimethoxysilyl propyl imidazolium ionic liquid (IL) grafted on HNT-Char
[e] Functionalized HNT-Char using H_2SO_4

An interesting approach was proposed in [86], where halloysite nanotubes (HNTs) were used as porogen for the synthesis of nitrogen-doped porous carbon materials for Pd nanoparticles immobilization to produce catalysts for aqueous hydrogenation of nitroarenes under atmospheric hydrogen pressure (Fig. 4). The opportunities of halloysite for modification with nitrogen groups, resulting in hydrophobization of its outer surface, provide Pd anchoring and prevent metal leaching. A high mechanical and chemical stability of halloysite nanotubes allows for preservation of the composite structure under acid treatment. This provides high porosity and enhances the catalytic activity by facilitating the mass transfer. The tests showed highly active Pd@C catalyst for the conversion of nitrobenzenes as well as 1-nitro naphthalene and 4-nitro acetophenone with high selectivity towards hydrogenation of NO_2 functionality (Table 1).

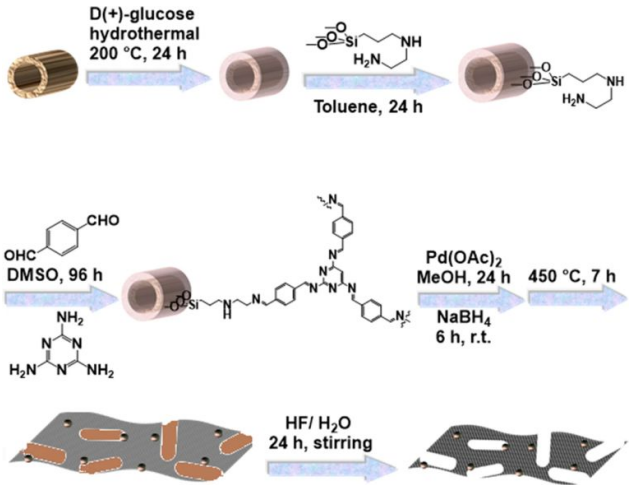

Fig. 4. The synthesis route of the Pd@C catalyst. CC BY license, 2020, Springer Nature, Scientific Reports [86].

The effective nanoparticle separation based on magnetic halloysite (with magnetite) support is described in [58]. The halloysite nanotubes (HNTs) were decorated with carbon from glucose (Glu) followed by coating with resorcinol-formaldehyde (RF) polymeric shell, its carbonization, and immobilization of magnetic nanoparticles to produce a magnetic carbon-coated composite. Then, Pd nanoparticles were impregnated (Fig. 5). The catalyst promoted hydrogenation of nitroarenes with high selectivity toward the nitro group in the aqueous media at low temperature. Comparing catalytic behavior of Pd@HNT, Pd@HNT@Glu, Pd@HNT@Glu-Fe, Pd@HNT@Fe-C, Pd@HNT@Glu-Fe-RF, and Fe@HNT@Glu-Pd-C catalysts (Table 3) in nitrobenzene hydrogenation, the impact of Glu-modified halloysite was evaluated as stabilization of Pd nanoparticles. Similar to cyclodextrin-modified halloysite, the Glu shell acts as a capping agent, decreasing the specific surface area of the catalyst. The functionalization of the halloysite by Glu leads to Pd nanoparticles deposition on the external surface providing higher metal loading for better activity. The Glu was exhibited to improve the recovery and recyclability of the catalyst due to the anchoring of magnetic nanoparticles. Glu was the best carbon precursors, optimizing the content of carbon on the halloysite surface. Meanwhile, magnetic nanoparticles, allowing for recyclability manipulations, do not influence the Pd loading.

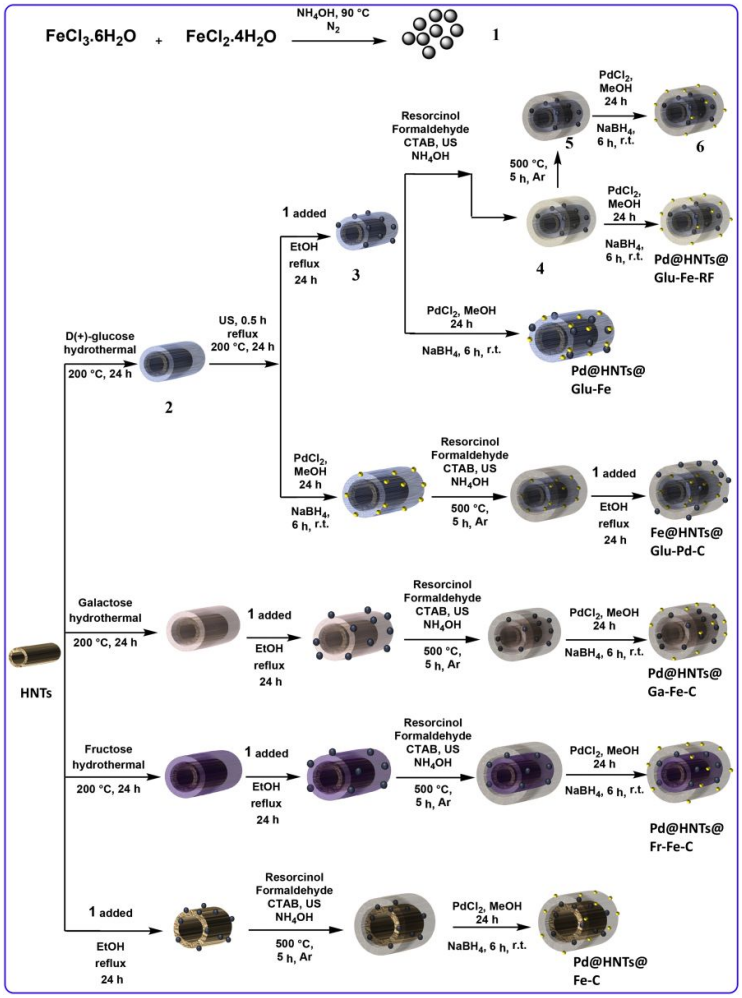

Fig. 5. The scheme of Pd@HNT@Glu-Fe-C synthesis (adapted from [58], copyright (2019) with permission from Elsevier). * HNTs – halloysite nanotubes, EtOH – ethanol, MeOH – methanol, $NaBH_4$ - sodium tetraborate, Glu – glucose, Ga – galactose, Fr – fructose, RF – resorcinol formaldehyde, CTAB – cetyl trimethylammonium bromide, US – ultra-sonication, r.t. – room temperature.

Table 3. Comparison of the activity, Pd loading, and specific surface area of the HNT catalyst in the hydrogenation reaction[a] [58]

Catalyst	Loading Pd (mmol*g^{-1})	S_{BET} (m^2 g^{-1})	Yield[b] (%)
Pd@HNT@Glu-Fe-C	0.058	195	98
Pd@HNT@Glu-Fe-C (Pd 2wt%)	0.040	218	60
Pd@HNT@Glu-Fe-C (Pd 3 wt%)	0.047	208	85
Fe@HNT@Glu-Pd-C	0.049	171	80
Pd@HNT@Fe-C	0.041	188	65
Pd@HNT@Glu-Fe-RF	0.051	99	76
Pd@HNT@Glu-C	0.058	206	98
Pd@HNT@Glu	0.030	27	55
Pd@HNT	0.025	45	50
Pd@HNT@Fr-Fe-C	0.051	171	78
Pd@HNT@Ga-Fe-C	0.052	189	90

[a] Reaction condition: nitrobenzene (1 mmol), catalyst (0.5 mol%) in water (5 mL) at 40 °C under 1 atm H_2 gas. Time, 60 min
[b] Isolated yield.

The modification of halloysite by ionic liquids (IL) was found to provide high metal loading as well as active phase dispersion over the support surface [59]. The interesting point is that the IL-polymer covered the surface of the halloysite and formed a shell. It should be noted as a disadvantage, that upon IL polymerization, the specific surface area of bare halloysite decreased to 10 m^2g^{-1}, but the structure of nanotubes didn't destroy. Nevertheless, the Pd particles with an average diameter of 7 nm were well-dispersed on the support, and no aggregation was observed. The content of poly-(IL) polymer significantly affects the catalytic activity: the higher this value, the higher is the Pd content. These catalysts demonstrate excellent recyclability without destruction of the halloysite structure or Pd aggregation.

Unlike the hydrogenation of nitroarenes, there are only several examples of halloysite-supported catalysts for hydroconversion of aromatics. Most of them aimed at the selective metal loading inside the tubes or their dispersion over the external surface. The selective metal incorporation into the lumens allows for strong interaction of particles with aluminol groups, protecting the active phase from leaching and providing the substrate selectivity when molecules are diffusing through the tubular porous system to the active sites. To load the metal nanoparticles into the internal halloysite cavities (both in the lumen and in the inner-wall packing defects) the ligand-assisted metal impregnation procedure was developed [23]. This approach was applied to design Ru-HNT catalysts for hydrogenation of benzene and phenol in aqueous media. To provide the effective penetration of Ru^{3+} ions inside the halloysite clay without modification by donor organic ligands the wetness impregnation from aqueous solution under microwave irradiation was applied. The Ru impregnation was carried out via azine-assisted procedure, resulting in the formation of Ru nanoparticles with ~3.0 nm in diameter, selectively intercalated into the lumen (Fig. 6 a, b). The metal loading reached 8-9 wt %. As-constructed catalyst appeared non-sensitive both to substrate shape and concentration increase (Fig. 6e-g). Apart from standard wetness impregnation, the microwave-assisted synthesis followed by reduction with $NaBH_4$ leads to the Ru nanoparticles with ~1.4 nm in diameter located both over the external surface and inner one (Fig. 6 c, d). This catalyst demonstrated significantly higher activity in the hydrogenation of phenol and other aromatic compounds. The catalytic activity was supposed to depend on the mean particle size, and decreased in the following order benzene>toluene>ethylbenzene>xylenes.

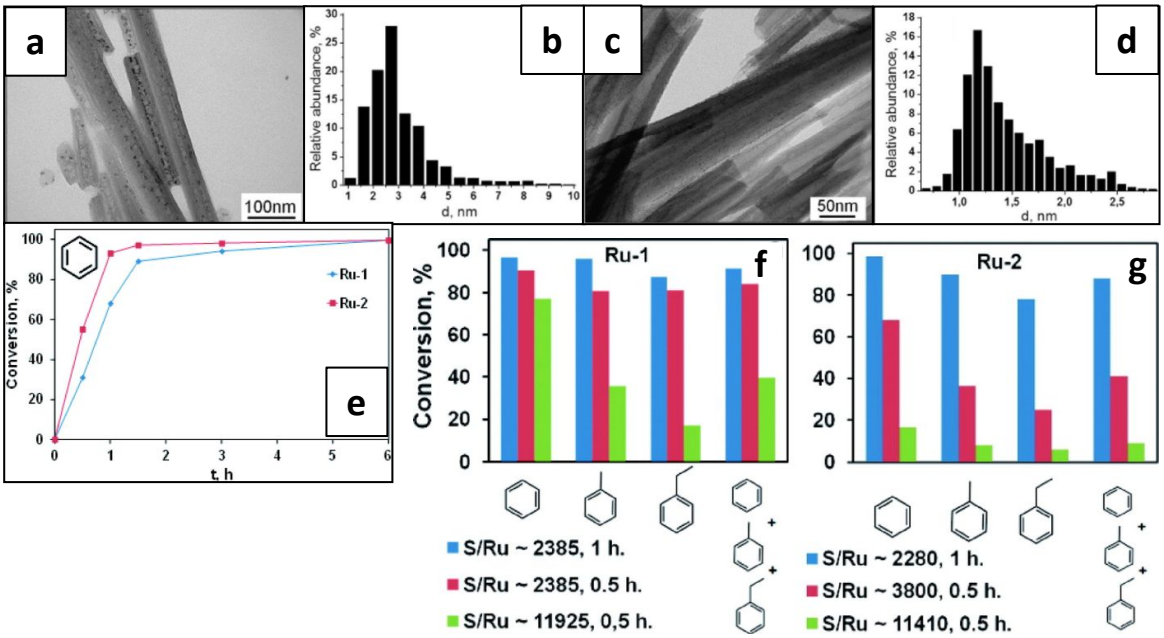

Fig. 6. TEM images of halloysite-based catalysts obtained by (a) ligand linkage standard (Ru-1) and (c) microwave-assisted (Ru-2) wetness impregnation technique; (b, d) metal particle size distribution for (b) the Ru-1 and (d) Ru-2 catalysts; (e) Hydrogenation of benzene and (f, g) one-pot hydrogenation of aromatics over Ru catalysts based on modified halloysite. For (f, g) reaction conditions: 80 °C, 3 MPa of H_2, V(substr.)=V(H_2O) [23]. Reproduced with permission from The Chemical Society of Japan (CSJ).

Using a simple procedure for modification and low-cost halloysite could speed up the application of these catalysts.

Another approach for controlling the metal localization is based on the electrostatic interaction of cationic or anionic metal species with charged halloysite surface. The charge of the halloysite surface can be changed, for example, by modification of silanol groups. Thus, the nanotubes modified with aminopropyltriethoxysilane (APTES) were used as a support (HNT-m) for Ru-containing catalysts [51]. According to zeta-potential measurements, the functionalization of the halloysite by silanes leads to the outer surface becoming less charged (Fig. 7a). For APTES-modified catalyst (Ru/HNT-m), ruthenium nanoparticles are intercalated predominantly into the lumen (Fig. 7b). The microwave-assisted Ru impregnation on the pristine halloysite (Ru/HNT catalyst) leads to smaller ruthenium nanoparticles deposited on the outer nanotubes' surface (Fig. 7c). The former catalyst has the highest content of the active metal phase.

The catalytic tests in benzene hydrogenation were carried out at the temperature of 80° C and 3 MPa hydrogen pressure both in the hydrocarbon medium and under two-phase conditions (Fig. 7d, e). Ru catalyst based on APTES-grafted halloysite (Ru/HNT-m) was the more active in benzene hydrogenation in the presence of water, providing 92 % substrate conversion for 100 min with 100 % selectivity to cyclohexane. For catalyst based on pristine halloysite (Ru/HNT) benzene conversion doesn't exceed 40 %. This difference in catalytic activity may be caused by the mass-transfer limitations, which occurred under two-phase conditions when the benzene molecules diffusing to active sites, located on the outer surface of the nanotubes. The hydrophobization with APTES protects the active phase from water while providing contacts with benzene molecules.

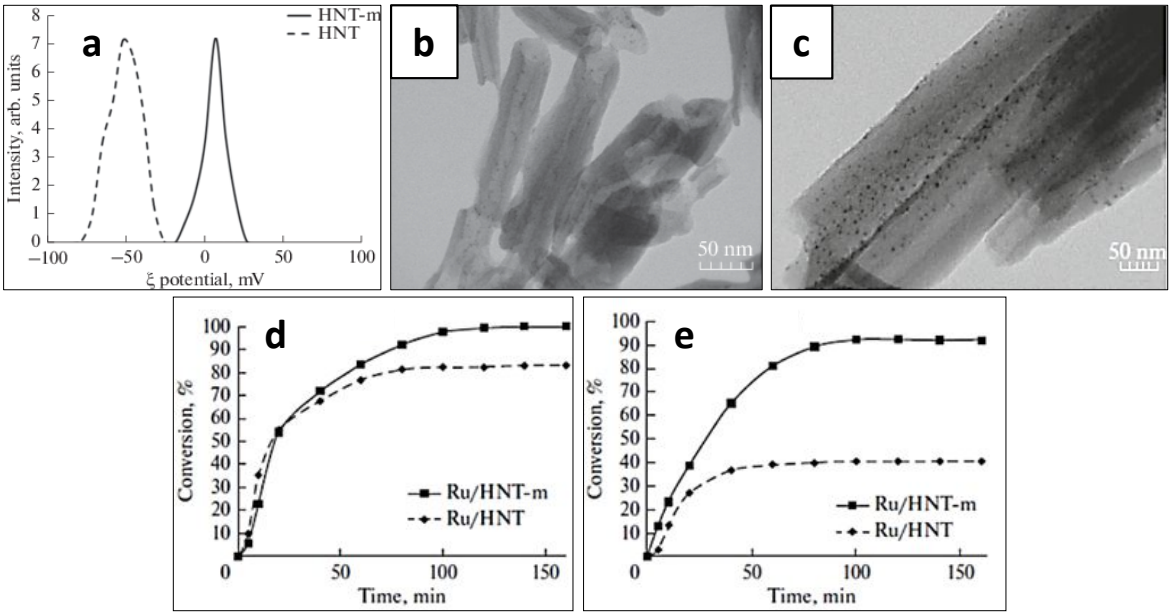

Fig. 7. (a) Zeta-potential at pH 7 for the pristine (HNT) and modified with APTES (HNT-m) nanotubes; TEM images for Ru catalysts based on (b) modified and (c) pristine halloysite nanotubes; Time dependence benzene conversion over Ru/HNT and Ru/HNT-m catalysts: (d) in the single-phase system, and (e) in the presence of water. Reprinted by permission from Springer Nature: Petroleum Chemistry [51], copyright (2018).

Recently, a new strategy to control metal localization for pristine halloysite by varying the impregnation procedure was proposed. The halloysite supported Ru catalysts were prepared by incipient wetness impregnation, the same under vacuum, and impregnation with the microwave irradiation. A high Ru content was achieved, and the metal particles were uniformly distributed mainly on the external surface of the nanotubes. It provides superior catalytic activity in the hydrogenation of benzene to cyclohexane at 80 °C, at a hydrogen pressure of 3.0 MPa [52]. While the wetness impregnation procedure provides Ru deposition on the external surface of the halloysite, the vacuum-assisted synthesis leads to the incorporation of metal nanoparticles into the internal lumen.

The metal content also affects the particles' size and localization over the nanotubes and the higher the metal loading, the larger the particles formed. This tendency was also observed for halloysite-based hierarchical nanocomposite, which is mesoporous ordered MCM-41 silica arrays placed onto halloysite nanotubes (MCM-41/HNT). This is a novel self-assembly strategy, based on the electrostatic interaction between negative outer halloysite surface and cationic amphiphile molecules of structure-directing agents. The amphiphile molecules assembled over the external tubes surface provide the direction for the mesosilica to grow around the aluminosilicate nanotubes. Practically all the tubes in the sample were covered with structured mesoporous silica. When Ru impregnation, the increasing the metal content leads to the nanoparticles intercalation into the composite porous system and agglomeration outside the mesopores (Fig. 8) [88].

The benzene hydrogenation was chosen as the test reaction to evaluate the catalytic behavior and stability depending on metal content and its placement. As expected, the higher the metal content, the lower the dispersion of the active phase was achieved, resulting in hydrogenation activity decrease. Notably, that selectivity toward cyclohexane reached 100 % independently from metal content and support composition. MCM-41/HNT composite supported Ru catalysts

demonstrated good stability under recycling, provided by the hierarchical structure and high specific surface area, resulting in ruthenium nanoparticle stabilization within the porous system. We concluded that new and strong mesocatalysts consisting of synthetic mesoporous MCM-41 silica arrays attached to the clay nanotubes are safe and could be easily scaled up for industrial application.

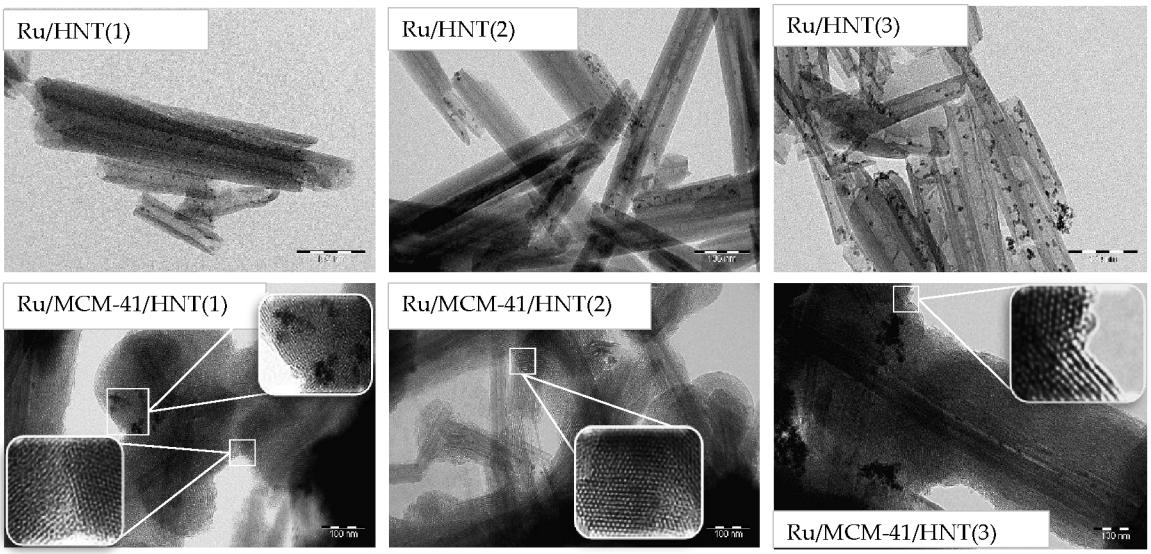

Fig. 8. TEM of Ru-particles location for Ru/HNT and Ru/MCM-41/HNT hybrid catalysts. CC BY license, 2020, MDPI, Catalysts [88].

Recently, we proposed the modification of halloysite nanotubes by different chain-length alkyltriethoxysilanes constructing an outer shell with an optimal hydrophobicity for selective Ru impregnation [13]. The hydrophobic shell formed by the alkyl attached prevents the adsorption of Ru-cations onto the nanotubes' outermost surface and forces them into the hydrophilic lumens (Fig. 9).

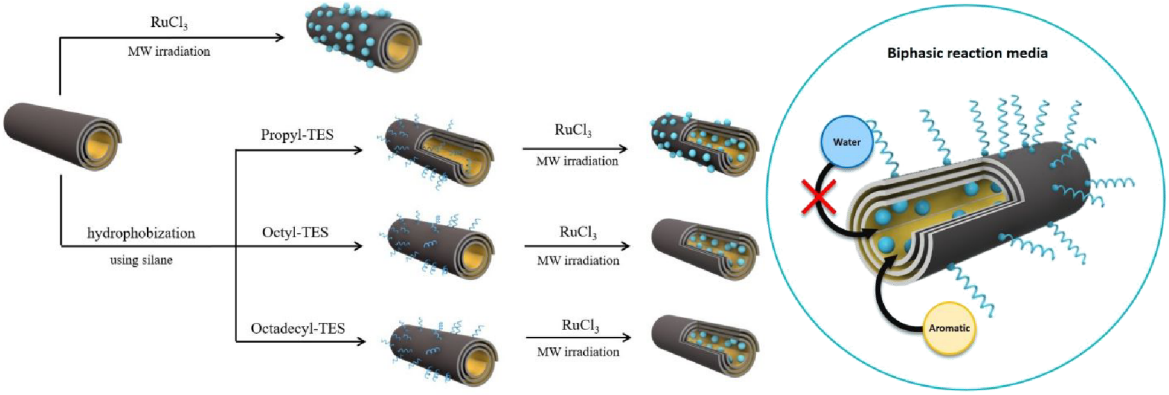

Fig. 9. Scheme of the hydrophobization and Ru loading into the inner cavity of halloysite nanotubes to produce nanoreactors for hydrogenation of aromatics under biphasic (water-oil) conditions.

The Ru content and metal nanoparticle localization could be controlled by varying the length of the alkyl chain. The longer the alkyl tail, the higher the water contact angle and therefore hydrophobicity (Fig. 10, 1a-1b). It enhances the incorporation of metal nanoparticles into the halloysite lumen. We introduce these tubular Ru-loaded systems as nanoreactors for hydrogenation of aromatics at 80 °C and a hydrogen pressure of 3 MPa in the organic (Fig. 10,

2a, 2c, 2e) and biphasic systems (Fig. 10, 2b, 2d, 2f). The highest benzene conversion (turnover frequency of 4371 h^{-1}) with 100 % selectivity to cyclohexane in the biphasic water-oil system was achieved over halloysite modified by C_{18}-triethoxysilane supported ruthenium catalyst. The silanization prevents adsorption of the water molecules by a modified halloysite sample and therefore such core-shell tubular reactors provide shielding of the active sites from deactivation by water and prevent metal leaching. These catalytic systems remained stable after ten cycles, providing 98 % conversion (Fig. 10, 3a-3b) [13].

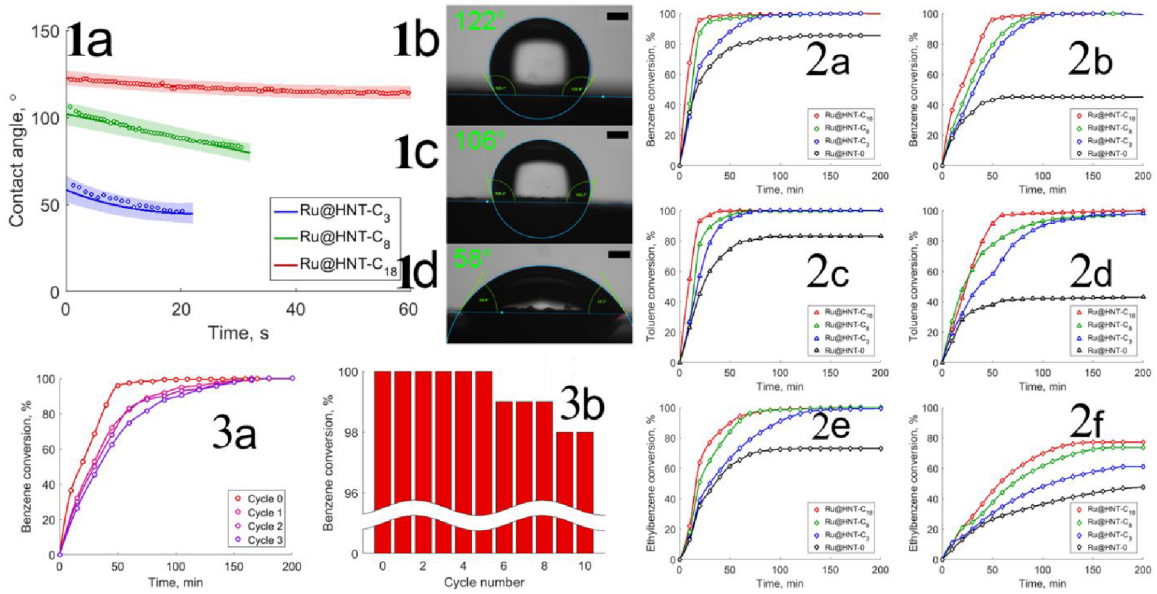

Fig. 10. (1a) Time-dependent contact angles and Sessile drop micrographs for (1b) Ru@HNT-C_{18} , (1c) Ru@HNT-C_8 , and (1d) Ru@HNT-C_3 catalysts. Aromatics hydrogenation in (2a, 2c, 2e) organic and (2b, 2d, 2f) biphasic water-containing systems over Ru@HNT-0 and Ru@HNT-$C_{3\text{-}18}$ catalysts; (3a) Kinetics curves and (3b) the final conversions for recycling tests of Ru@HNT-C_{18} catalyst in a biphasic system benzene-water (50 vol. %). Reprinted from [13], copyright (2020) with permission from Elsevier.

In conclusion, the application of halloysite nanotubes for templating of different organic molecules opens up an opportunity to fabricate hybrid organic-inorganic materials with enhanced properties for catalytic transformations. The nanoclay tubular structure provides transport channels for diffusing reactants and reinforces hybrid materials despite the presence of organic functionalities. This provides an opportunity to enhance catalysts' lifetime. Second, the dual tubes' surface chemistry allows for a wide range of modifications for tailored design. The functional group may be adopted depending on the environment of nanoparticles and concentration of the reagents near catalyst surface allowing for controlled selectivity. The functionalization provides strong anchoring of metals leading to the formation of well-dispersed nanoparticles uniformly distributed over the support surface. The demonstrated synthetic strategy is promising for industrial catalysts developing for hydroprocessing of water-containing organic feedstock and may be upscaled with abundant clay nanotubes.

2.2.Hydrogenation of phenols and reduction of nitrophenols

The catalysts for reduction of nitrophenols are heterogeneous systems containing noble metal particles and support. The immobilization of Rh, Pt, Pd, Au, and Ag nanoparticles onto silica, alumina, silica-alumina including zeolites, activated carbon, carbon nanotubes, cerium or

titanium oxides, and polymeric materials allowed for stabilizing metal clusters, enhancing performance, improving catalysts separation, and reusability[89-92]. The catalytic efficiency depends on the dispersity of active components over the support surface and one of the main goals is to achieve metal nanoparticle formation preventing their agglomeration and aggregation[93]. Acidic properties of the support are crucial for fabrication of a highly dispersed nanosized metal component. Due to the hydrogenation of phenol as well as reduction of nitrophenol are carried out in aqueous media or under two-phase conditions, the stabilization of metals to prevent leaching and rapid catalysts deactivation is the second task when developing the support.

The most applicable approach for improved stability is based on the encapsulation of metal protecting it from water. Preparation of stable catalysts with uniform small-size particles requests complex and time-consuming processing, especially for encapsulated systems. Fabrication of supports with surface groups acting as active sites for metal complexation is more practical and halloysite nanotubes are well suited for this. To achieve the bond formation for guest molecule, organosilane grafting was applied at the outer halloysite surface [13, 50, 51]. Organosilanes have alkoxy groups released through the hydrolytic reactions in aqueous media. The condensation of these functionalities resulted in silanol groups formation. They interact with halloysite hydroxyl groups providing attachment at the tubes' surface (Fig. 11).

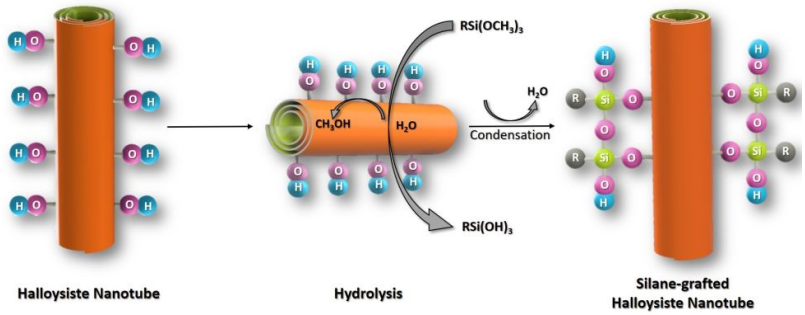

Fig. 11. Representation of organosilane coupling on halloysite nanotubes' surface.

The grafting by silanes provides the desirable density of functionalities (often amino groups) to ensure accumulation of metal clusters at the surface. This allows for selective metal loading controlling the environment of nanoparticles and concentration of the reagents under reaction conditions. The organosilane-grafted halloysite nanotubes are hybrid organic-inorganic composites, consisted of nanoscale inorganic materials and organic derivatives. For organosilane-grafted halloysite, the amino groups can link metal ions for cluster formations. Organosilane grafting allows for strong metal particles linkage to the nanoclay support. For pristine halloysite without silanization, it is difficult to control the localization of metals and their distribution over the surface. In this case, catalytic behavior depends mostly on the content of the active component. It was comprehensively studied for the reduction of 4-nitrophenol with $NaBH_4$ in alkaline aqueous solutions over halloysite-supported Ag catalyst[64].

Halloysite nanotubes functionalized by aminopropyl trimethoxysilane were used as support for Rh, Pt, and Pd deposition from an aqueous solution of metal precursors [65]. The *in situ* formation of nanoparticles was achieved by a reduction process that occurred due to protonation of amino groups in acid conditions leading to adsorption of negative metallic ions. This synthesis resulted in the formation of noble metal particles with extremely small sizes (~1.5 nm), densely and uniformly distributed both outside and inside of the nanotubes. The chelating effect provides nanoparticle stabilization through strong metal/amine coordination. The functionalization with

amino groups led to space steric hindrances preventing nanoparticle aggregation. The Rh–N-HNTs, Pt–N-HNTs, and Pd–N-HNTs nanocomposites exhibited high catalytic activity in reduction of 4-nitrophenol with excellent recyclability, and no changes in the catalysts' surface morphology, structure, and density of metal nanoparticles were observed after recycling.

Another synthetic strategy was proposed for the direct intercalation of Au or Ag nanoparticles into the internal cavity of halloysite (HNTs) [94], Fig. 12a. The (3-aminopropyl) triethoxysilane modified halloysite-based nanocomposites were fabricated. Then, Au and Ag nanoparticles were immobilized by two different approaches. The first one is based on *in situ* deposition of metals from the precursors followed by reduction leading to nanoparticle formation. The second is the impregnation of the preformed metal nanoparticles over the halloysite surface linked to amino groups. Interestingly, the characteristics of active species are independent of the impregnation procedure. The *in situ* synthesis results in Au and Ag nanoparticles of 9.0 ± 1.5 for Au and 9.0 ± 1.5 nm for Ag (Fig. 12b, c). When metal particles were preformed, 9.0 ± 0.5 gold and 8.5 ± 0.5 nm silver were well-dispersed over the external halloysite surface (Fig. 12d, e).

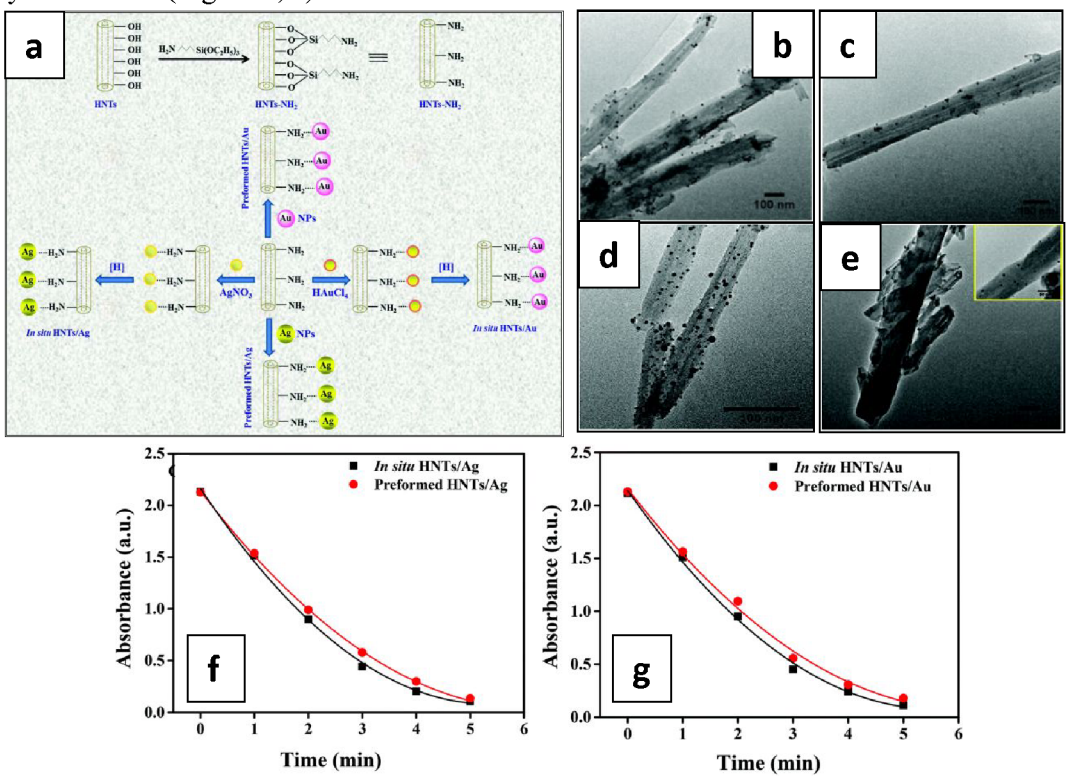

Fig. 12. (a) Presentation of the Au and Ag supported on halloysite (HNT); TEM images of (b) HNTs/Au and (c) HNTs/Ag composites synthesized with preformed metal nanoparticles as well as *in situ* synthesized (d) HNTs/Au and (e) HNTs/Ag; The plot of absorbance as a function of reduction of 4-nitrophenol using $NaBH_4$ over (a) HNTs/Ag and (b) HNTs/Au composites. Reproduced from [94] with permission from the Royal Society of Chemistry.

Due to the formation of monodispersed spherical nanoparticles, the catalytic activity of Au and Ag halloysite-based composites was close independently from the synthetic route (Fig. 12f, g). A kinetic study demonstrated the higher productivity of *in situ* prepared HNTs/Ag composites. The efficiency of 4-nitrophenol reduction decreases in the following order: *in situ* HNTs/Ag> *in situ* HNTs/Au> preformed HNTs/Ag> preformed HNTs/Au. It was explained by

the absence of any capping agent over the surface of the nanoparticles. Taking into account the almost similar particle sizes of these nanocomposites, the authors concluded that this slightly variable catalytic activity may be caused by the difference in the number of available active metal sites for reactants. For *in situ* synthesized HNTs/metal the considerable enhancement in the catalytic activity is presumably ascribed to the absence of any capping agent over the surface. The higher activity of the Ag-containing catalyst is caused by the higher affinity of Ag–N than that of Au–N [94].

Another promising approach for controlling metal nanoparticle deposition and dispersity is the grafting of the nanotubes with ionic liquids (IL). It was applied for Pd catalysts, fabricated through modification of internal halloysite cavity with (1-(2-hydroxyethyl)-3-methylimidazolium) followed by metal particles impregnation (Fig. 13a-c) [95,96]. Halloysite treatment with dimethyl sulfoxide (DMSO) was performed before IL grafting (Fig. 13b). Selective modification of the inner halloysite surface leads to formation of adsorption sites for metal particles and their anchoring via an anion-exchange mechanism, while the outer non-functionalized surface with silanol groups has a poor affinity to precursors. In contrast to grafted halloysite-based catalysts, the unmodified clay displayed randomly distributed larger size nanoparticles both inside and outside the tubes. The localization of Pd particles inside the lumen improved the catalytic activity in the reduction of 4-nitrophenol, because of increasing contact between the reactants and active metal phase (Fig. 13d).

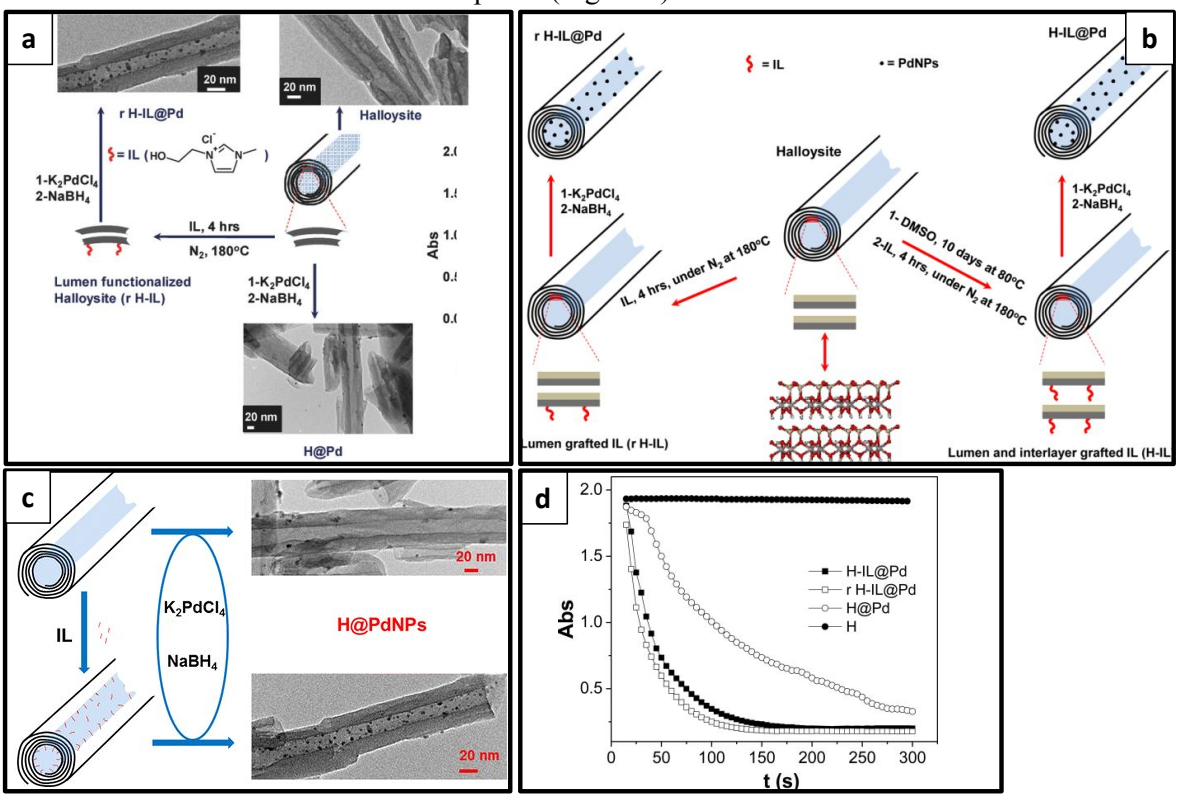

Fig. 13. (a–c) Modification of halloysite nanotubes by ionic liquids followed by Pd impregnation (for (a): reprinted with permission from [95], copyright (2018) Wiley); for (b, c): reprinted with permission from [96], copyright (2016) American Chemical Society) and (d) halloysite-Ionic Liquid-Supported Pd nanoparticles and variation of 4-nitrophenol maximum absorbance at 400 nm for various catalysts during the catalytic reduction in the presence of $NaBH_4$ (reprinted with permission from [96], copyright (2016) American Chemical Society).

Thiol-terminated organosilane was also used for anchoring Au nanoparticles to prevent their agglomeration[66]. The enhanced gold–thiol bond provides gold nanoparticle impregnation on the functionalized outer hallosyite surface (Fig. 14). The catalyst demonstrated high activity in 4-nitrophenol reduction by $NaBH_4$. Halloysite nanotubes serve as a medium for the transfer of electrons from borohydride ions to 4-nitrophenol and also modulate interfacial electron dynamics. Interestingly, that apparent kinetic constant decreases with an increasing amount of catalyst. Interestingly, that apparent kinetic constant decreases with an increasing amount of catalyst. The authors explain this by reduction of colloidal stability for the thiol-functionalized HNT-Au catalysts. When the lack of reducing agent, the higher the metal content, the larger particles were formed with aggregation which decreased the catalytic efficiency. This type of catalyst was very stable and retains activity for at least ten cycles.

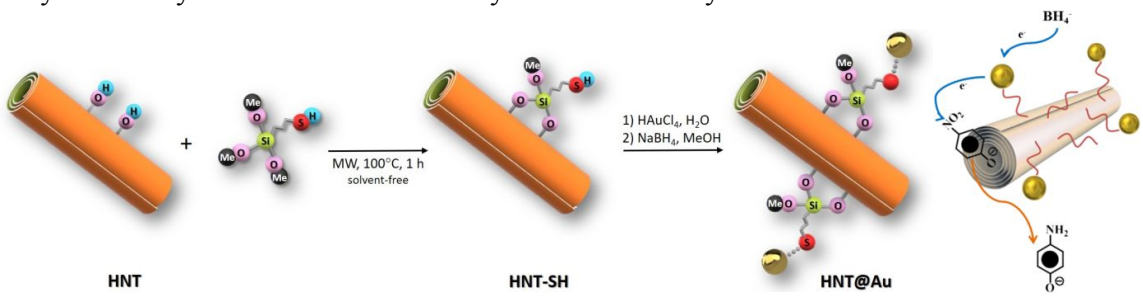

Fig. 14. Scheme of the HNT@Au synthesis and proposed reaction mechanism for 4-nitrophenol reduction [66] (adopted with permission from [66], copyright (2018) Wiley).

The different charges of halloysite inner lumen (positive) and the outer surface (negative) at pH 4-9 allows for selective surface modification with the electrostatically attracted reagents. Loading of Pt−Cu bimetallic nanoparticles inside the nanotube lumens was achieved by varying ionic precursor solutions pH. Its increase enhances dissociation of H_2PtCl_6 to $[PtCl_6]^{2-}$ which was adsorbed by cationic aluminol (Al−OH) [97]. This leads to shrinkage of bond length from Pt−Cl in $[PtCl_6]^{2-}$ to Pt−O in $[PtCl_4(OH)_2]^{2-}$ followed by Pt(IV) trapping inside the nanotubes. Cu(II) cations may complex with Pt(IV) anions forming Pt−Cu particles. This is one-step process resulted in size-controlled Pt−Cu bimetallic nanoparticles uniformly distributed over the tubes' inner surface (Fig. 15).

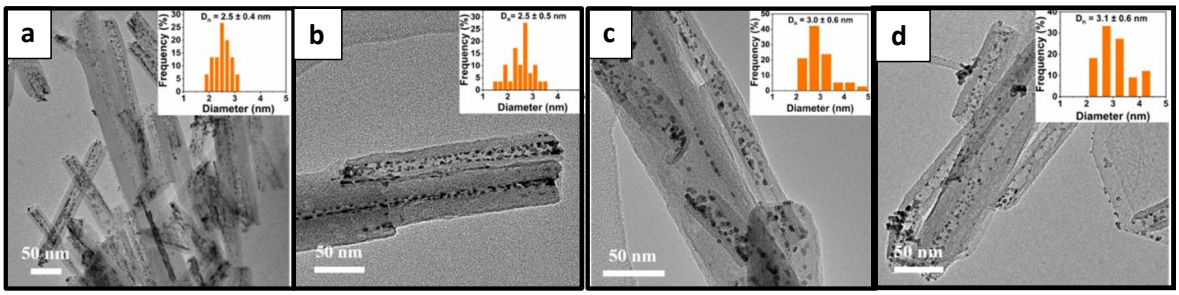

Fig. 15. TEM images of (a) Pt@HNT, (b) Pt_3Cu@HNT, (c) PtCu@HNT, and (d) $PtCu_3$@HNT catalysts. Reprinted with permission from [97], copyright (2019) American Chemical Society.

An encapsulation of metal particles in halloysite nanotubes support allows for enhancing the thermal stability, which is crucial for Pt−Cu bimetallic catalyst. Due to the protection of the active phase from aggregation and leaching, the high activity of Pt and Pt−Cu bimetallic catalyst in 4-nitrophenol reduction with sodium borohydride was retained and catalysts' lifetime was prolonged.

The metal deposition mode and halloysite pretreatment have a significant influence on the catalyst's structure and performance in the hydrogenation of phenol [23, 33]. Due to the environment of functional groups affects the nanoparticles and concentration of the reagents under reaction conditions, the modification of halloysite surface to fabricate the supports for phenol hydrogenation are differs from that for nitrophenol reduction. In this case, the strategy for metal intercalation into the lumen or deposition over the external surface is based on the tube modification with aldehyde and amine compounds (furfural and hydrazine hydrate) forming Schiff bases. It allows for the effective capturing of metal ions from an aqueous solution and their loading within the lumens. The metal content could be regulated by Schiff bases concentration on the inner halloysite surfaces and their higher density provides better Ru complexation, resulting in higher metal content. The efficiency of this method was demonstrated for the Ru nanoparticles encapsulation. Azine-linkage at the halloysite allows for metal intercalation inside the tubes (named as Ru-2 catalyst in Fig. 16) with nanoparticles of 2−3 nm in diameter. The microwave-assisted metal impregnation without pre-modification of halloysite surface by organic ligands leads to metal deposition both inside and outside surfaces (named as Ru-1 catalyst in Fig. 16) [23]. The microwave-produced Ru-1 system was more sensitive to water admixture as compared with the azine-linked Ru-2 catalyst. Ru-2 catalyst exhibited high activity in hydrogenation of phenol to cyclohexanol under biphasic conditions (Fig. 16b).

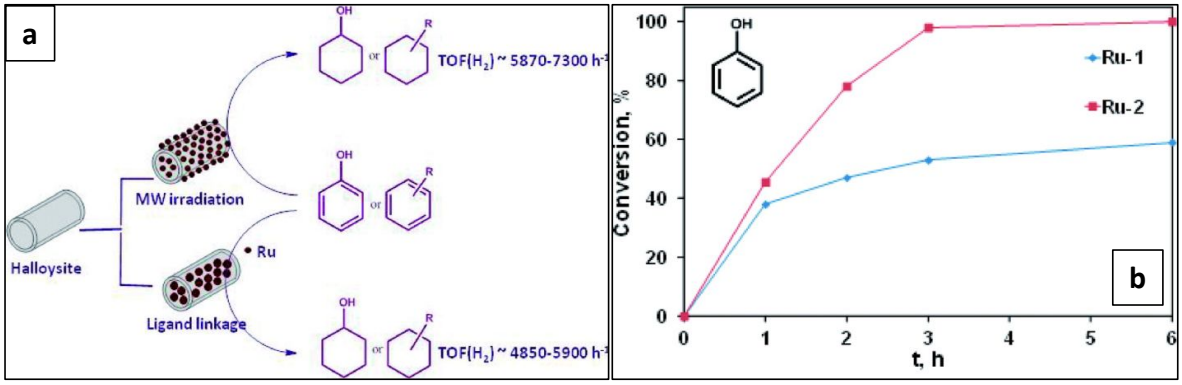

Fig. 16. (a) Two routes for the synthesis of halloysite supported Ru catalysts; (b) Hydrogenation of phenol over Ru-1 and Ru-2 halloysite catalysts. Reaction conditions are 80 °C, 3 MPa of H_2, m(PhOH)=m(H_2O), PhOH/Ru~4400[23]. Reproduced with permission from the Chemical Society of Japan (CSJ)

The selectivity of the catalysts toward phenol groups could be regulated by the varying modifier agents and metal impregnation procedure. Mainly, it is determined by the metal content, which correlates with the concentration of Schiff bases on the inner halloysite surfaces favored Ru complexation. The nature of the modifier also affects the particle size and its distribution over the support surface. Thus, Ru impregnation with salicylic aldehyde and urea occurred not regularly (Fig. 17). The higher the Schiff base loading, the more uniform the particle distribution resulted in higher catalytic activity. For hydrazine hydrate and furfural modified halloysite catalyst the highest turnover frequency calculated in terms of hydrogen uptake per metal surface was 17 282 h^{-1} with 85 % selectivity to cyclohexanol [33]. When the catalyst was recycled, some metal leaching was observed, which may be attributed to poorly retained nanoparticles located outside the nanotubes, but further Ru inner-core nanoclay catalysts can be reused 10 times without loss of activity.

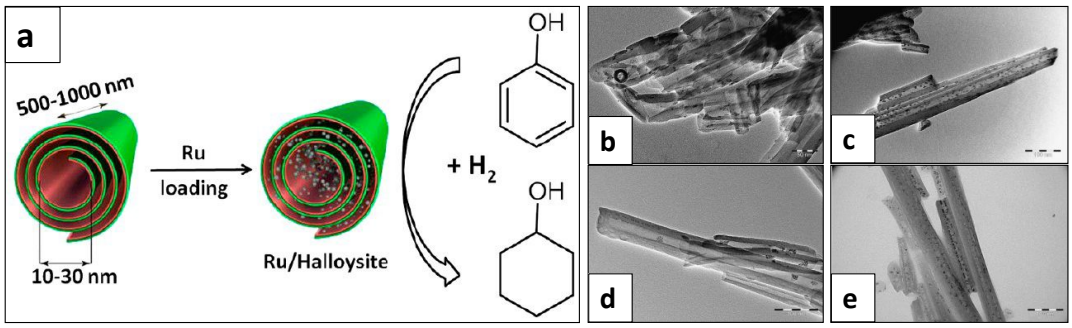

Fig. 17. TEM images and synthesis of halloysite supported Ru catalysts (a) obtained with modification of the inner halloysite surface: by hydrazine hydrate and furfural with (b, c) one-step and double (d) metal impregnation; for (e) by salicylic aldehyde and urea with one-cycle impregnation. Reprinted with permission from [33], copyright (2017) American Chemical Society.

Therefore, halloysite nanotubes were exploited as a template for inorganic-organic hybrid materials used as support for hydrogenation and reduction catalysts. These nanotubes have differently charged internal and external surfaces allowing for selective ligands immobilization. This allows for the directed complexation of metal particles with control of their localization. Selective metal loading into the lumens prevents their leaching. This is a facile *in situ* procedure to fabricate the catalysts with well-dispersed non-agglomerated nanoparticles for enhanced catalytic performance.

Content of water is crucial for the selectivity toward cyclohexanol when phenol hydrogenating, and halloysite hydrophobization protects its interior from water. The opportunities for modification of halloysite with different ligands open up the ways for regulation the selectivity by introducing functionality for effective binding and transformation of reagents, which is important for the reduction of nitrophenol with selectivity toward a nitro group because as-produced aminophenols are widely used in industry. Halloysite tubular structure provides transport channels and increases thermal stability despite the presence of organic functionalities. It allows for fabricating the catalysts with tunable selectivity and improved stability.

The advances of halloysite-based inorganic-organic hybrid materials impact the design of catalysts with enhanced properties. Future trends for these systems will also enable reactants and molecules diffusion control by the modification of nanotubes with ionic liquids and suspended nanoparticles. Homogenous transformations in heterogenous nanoreactors for selective hydrogenation may be of special interest.

2.3.Hydroformylation

Hydroformylation is ат industrial homogeneously catalytic process involving the transformation of olefins (alkenes) with syn-gas (mixture of CO and hydrogen) into corresponding linear aldehydes over noble (Rh, Ru) or transition (i.g. Co) metal catalysts[98-100]. The aldehydes are used for the production of organic acids and long-chain alkenes converted to alcohols for surfactant manufacturing. The homogeneous nature of the catalysts provides high activity and selectivity, but has complicated recycling due to the leaching of metals, making the process very expensive[101]. To enhance the recyclability of the catalysts, the ligand-assisted two-phase conditioning process was invented for the hydroformylation of olefins over water-soluble Rh catalysts[102]. With ligands, the Rh catalyst becomes water-soluble, whereas the

hydroformylation products are in the organic phase, which allows for the recycling of the precious catalyst. The main drawback is the process restriction to short-chain olefins because the longer the chain, the lower the water solubility of alkenes resulting in the poor contact of the catalysts and reactants[103]. Therefore, the hydroformylation of long-chain olefins is still a homogeneously catalyzed reaction. For catalyst separation, surfactants or solid species were added to stabilize emulsions. They provide contact between reagents and water-soluble metal complexes. The systems, stabilized by solids are the Pickering emulsions when nano/micro particles are concentrated on the phase boundary and act as the binder for metals. These emulsions are advantageous to surfactant-stabilized systems having high stability to coalescence against reaction conditions (pH, temperature)[104, 105]. These solid surfactants prevent aggregation and leaching of metal particles[106]. This is important for retaining activity and catalyst separation due to the synergetic combination of homogeneous (high selectivity and activity) and heterogeneous (efficient separation) catalysis[107, 108]. Halloysite is a good candidate as an interfacial agent for the design of the surface-active core-shell tubular catalysts for hydroformylation. These clay nanotubes form stable oil-in-water Pickering emulsions. Under two-phase conditions, the halloysite particles act as a surfactant and concentrate at the interface of 5-50 mkm oil bubles. The halloysite may act as an interfacial transferer for homogeneous reactions and two-phase processes, including hydroformylation.

Only one example of halloysite application for Pickering stabilizing during hydroformylation of a long-chain olefin was reported. It describes halloysite emulsions in catalysis of Rh linked with water-soluble sulfonated 4,5-bis(diphenylphosphino)-9,9-dimethyl xanthine for the hydroformylation of 1-dodecane. This system was advantageous as compared with fumed silica-based emulsion systems [109]. Both halloysite and silica were attached at the interfacial surface and stabilized dodecene-water Pickering emulsions. The halloysite nanotubes are larger than 100 nm length silica rods (mean length of 800 nm, the outer and diameters of 50 nm with 15 nm lumen), it forms thicker the water/oil interface, resulting in higher detachment energy and emulsion stability. The larger capillary forces provided by the halloysite lead to the higher energy of the nanotubes detachment, making the aluminosilicate particles closer packed and less mobile comparing to silica [110]. Therefore, the contact between Rh nanoparticles and reactants is interrupted and the olefine conversion decreases, whereas high selectivity to aldehydes retains. Contrary to the silica-stabilized system, the halloysite emulsion was stable after the reaction.

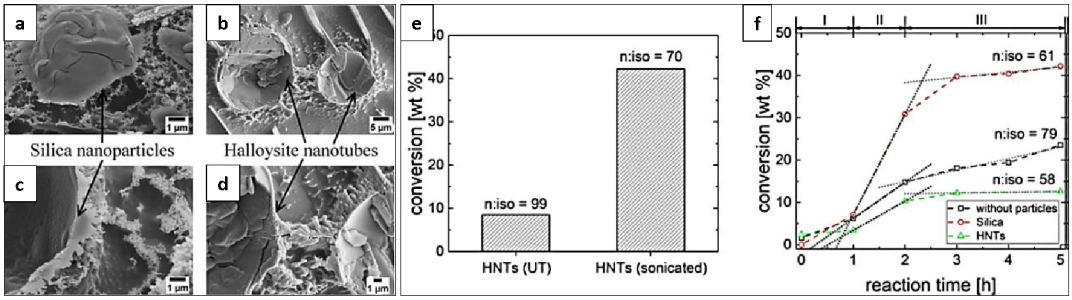

Fig. 18. (a-d) Freeze-fraction cryo-SEM of silica-stabilized and HNTs-stabilized Pickering emulsions; (e) Hydroformylation of 1-dodecene after 24 h of reaction time for HNTs-stabilized (0.50 wt. %) prepared by UT (low energy input) and for emulsions prepared by sonication (high energy input); (f) Comparison of the conversion of 1-dodecene during 5 h of reaction time (reaction time was 24 h) by stabilizing the emulsion with silica (circles, 0.50 wt. %) and HNTs (triangles, 0.50 wt. %) and without particles (square, reference system). Reprinted with permission from [109], copyright (2019) American Chemical Society.

The droplet size for both particle-stabilized emulsions is on the order of micrometers and depends on the particle concentration. When the Rh complex was added, the droplet size decreased (Fig. 18, a-d). The selectivity to aldehydes was 80 % and only a small amount of side-products (isododecene, isoaldehyde, and dodecane) was observed with 3 times less isododecane content than that for silica-based counterpart (Fig. 18, e-f).

Halloysite provides optimal stability of the emulsions, which is favorable for high conversion and allows for intensification of the hydroformylation process. Halloysite-stabilized Pickering emulsion does not block transfer between the catalyst and reactant, even at the high coverage of the droplets. It enhances the emulsion stability preventing the droplets from fast-breaking. The interfacial contact between the catalyst and 1-dodecene is enough for effective transformation, and it is favorable for catalyst separation by membrane filtration. The halloysite-stabilized emulsion is robust against mechanical and chemical stress. All these demonstrate advantages for using halloysite as emulsions stabilizer for continuous industrial processes.

A detailed investigation to evaluate the impact of a pristine halloysite on the properties of a surface-active catalyst, interfacial phenomenon, and emulsion properties like a mean droplet size, stability, energy of detachment should be in focus to improve the industrial hydroformylation of long-chain olefins.

Halloysite functional groups may be adopted depending on the environment of nanoparticles and the concentration of the reagents near the catalyst surface allowing for controlling the catalyst selectivity. For example, the functionalization with silanol groups provides appropriate wettability of the halloysite surface; modification of the halloysite surface with dendrimers or amines is also interesting. The silane-amine functionalities allow for anchoring of metal nanoparticles with selective localization: inside the tubes or over their outer surface. It gives an opportunity for the fabrication of hydroformylation catalysts, especially for two-phase catalysis. This provides a basis for an effective heterogeneous transformation of syn-gas to value-added chemicals. Halloysite-based catalysts would benefit developing nanoreactor strategies for multi-shell tubule structure formation, especially with ionic liquids for selective surface modification for biphase catalysis and diffusion control of reactants and products.

2.4.Fischer-Tropsch synthesis

Fisher-Tropsch synthesis (FTs) is one of the key industrial processes converting syn-gas to value-added hydrocarbons and oxygenates. The Ru, Pt, Pd, Fe, Co, Ni have been widely studied as catalysts for FTs[111-114]. Due to the low cost, stability, relatively high activity, and selectivity to linear hydrocarbons the Co-supported catalysts are most industrially attractive. For these catalysts, the pore diameter of the support affects the products, whereas the dispersity of Co particles and their morphology depends on the preparation. Eggshell catalysts increase the reaction efficiency. Formation of eggshell was achieved by optimization of metal content in the impregnating solution, pre-treatment of the support, processing time, and drying modes[115, 116].

Usually, the catalysts' preparation includes pre-wetness of support for optimization of the porosity followed by double-solvent methods or wetness impregnation procedure[117]. The support acidic properties influence the metal particles' formation: the higher the acidity, the stronger the interaction of metal particles with the support surface resulted in high dispersity. The acid sites anchor metal particles preventing their aggregation and leaching. On the other hand, high acidity leads to a decrease in cobalt reducibility and inhibits catalytic performance. In the case of widely applicable silica support, the acidity is not sufficient to achieve the desirable Co dispersity. On

contrary, for alumina-supported catalysts, the interaction with surface groups is strong resulting in the formation of cobalt aluminate spinels. The low acidity results in higher long-chain hydrocarbon selectivity, whereas higher acidity leads to the side-reactions (like olefin isomerization, reinsertion, and hydrogenolysis) and by-product formation. Therefore, focusing on the design of FT catalysts with optimized support acidity and the formation of metal nanoparticles with adjustable localization is a priority task[118].

Concerning all of the features, the alumosilicate halloysite is prospective mesoporous support for FT catalysts as reported in [79]. Co impregnation was carried out either with the double-solvent method or with wet impregnation. When the double-solvent method was used, most of the cobalt oxide was uniformly deposited on the nanotube walls without aggregation (Fig. 19).

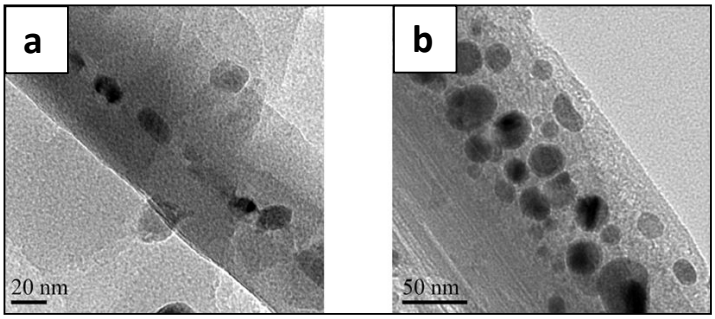

Fig. 19. TEM images of halloysite supported Co-catalysts obtained by (a) double-solvent and (b) wet impregnation. Reproduced from [79] with permission from the Royal Society of Chemistry.

The double-`solvent impregnation technique gave catalyst with higher activity in CO conversion. The nanoconfined reaction minimizes the growth of metal oxide particles and prevents their migration over the nanotubes' surface, resulting in better CO conversion and C_{5+} selectivity for FTs (Table 4).

Table 4. CO conversion and product distribution for Fischer-Tropsch reaction over HNT-based catalyst. [79]

Catalysts	CO conversion (%)	Hydrocarbon selectivity (mol %)				
		CH_4	C_2	C_3	C_4	C_{5+}
10 Co/halloysite (impregnation)	8.4	14.2	1.4	3.8	10.4	70.2
10 Co/halloysite (double-solvent)	12.2	7.7	2.0	4.4	7.3	78.6

Reaction conditions: 1.0 MPa, 503 K, molar ratio of $H_2/CO = 2$, GHSV = 4 $SL \cdot h^{-1} \cdot g^{-1}$; Fischer-Tropsch data were collected at steady state (80 h)

These results demonstrate the balanced acidity of halloysite nanotubes, provided by silica outer surface and alumina inner lumen.

In another approach, Ru-loaded halloysite tubes were used as FT nanoreactors [119]. Selective Ru deposition inside the internal tubular cavity was achieved by modification of the outer surface with ethylenediaminetetraacetic acid (HNT@Ru-1), urea (HNT@Ru-2), or acetone azine (HNT@Ru-3) catalysts. The activity and selectivity toward CH_4, C_{2-4}, and C_{5+} hydrocarbons in the FT process were affected by the total acidity and specific morphology of halloysite-based catalysts. Since the internal diameter of these clay nanotubes is 10–20-nm, the mass transfer limitations are excluded, allowing C_{5+} hydrocarbons formation. The Ru-HNT catalyst formed through urea-assisted loading demonstrated the highest C_{5+} hydrocarbons selectivity, while the

highest olefin content was achieved when the acetone azine was used for modification of the pristine aluminosilicate nanotubes (Fig. 20).

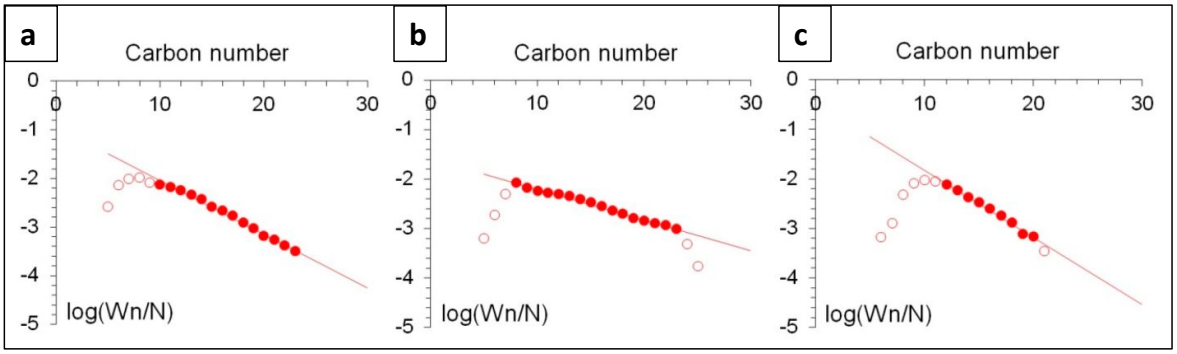

Fig. 20. Anderson–Schulz–Flory (ASF) plots of hydrocarbon formation over HNT@Ru-1 (a), HNT@Ru-2 (b), and HNT@Ru-3 catalysts (c). CC By license, 2020, MDPI, Molecules [119].

An influence of electron-donor properties of halloysite on the catalytic behavior of metal species depends on their inner/outer localization, and define adsorption of carbon monoxide and cleavage of the C−O bond during the process. Another direction is a tailored modification of the tubes' surface to adjust an appropriate acidity and selective metal deposition.

The development of halloysite-based FTs catalysts is important for converting non-petroleum feedstocks including renewable biomass and urban wastes into clean hydrocarbons or transportation fuels. Halloysite nanotubes provide transport channels for diffusion of balkier reagents and excluding mass-transfer restrictions. This effect may intensify involvement in FT processing of unconventional feeds with value-added products and clean non-sulfur fuels.

2.5.Hydroisomerization over halloysite supported catalysts

Acid-catalyzed reactions such as isomerization represent one of the most important technologies of the chemical industry. For example, the hydroisomerization of xylenes and ethylbenzene (from C_8 aromatic fraction) to *p*-xylene is an important stage for polymers manufacturing. The oxidation of as-produced *p*-xylene yielded the terephthalic acid used as monomers for polymerization [120, 121]. The hydroisomerization catalysts consist of Pt or Pd impregnated on acidic support such as alumina, zeolites, mesoporous silica sieves, aluminum, titanium, and zirconium silicates. Earlier, the multistage acid-catalyzed isomerization of xylenes was performed at atmospheric pressure[122]. Due to high coke formation and side reactions the process conditions were then shifted to higher hydrogen pressure. Recently, catalysts for effective conversion of C_8 aromatic feed into *p*-xylene with minimal xylene losses were attempted to develop. The reaction route and *p/o*-xylenes ratio when xylenes transformation depends on pore size and volume, surface area, acidity of the support, and distribution of acid sites which act as centers for isomerization. As for ethylbenzene transformation, the reaction starts from its hydrogenation over metal sites to yield cycloalkanes, while the acid sites provide the step-by-step isomerization of naphthene to dimethyl-substituted six-membered ring intermediate followed by its dehydrogenation to xylenes[123]. This pathway is possible using mesoporous support allowing for non-hindrances diffusion of bulk intermediate [123]. As for the microporous zeolite-based systems, the ethylbenzene undergoes dealkylation, and selectivity to the desired xylene decreases. The microporous zeolite facilitates direct isomerization of xylenes via 1,2-alkyl shift in a benzenium ion. Therefore, the design of hierarchical materials combining the structural features of mesoporous molecular sieves and zeolites is of interest[124]. The

halloysite tubular cavity is prospective as a support component to introduce mesoporosity and transport channels for reagents. The internal surface of the halloysite is composed of octahedral aluminum oxide which generates Brønsted acid sites necessary for isomerization. Halloysite allows for selective metal loading inside the tubes which provides effective transformation of ethylbenzene. A relatively low acidity and mesoscale transport channels prevent side reactions like dealkylation and disproportionation increasing the selectivity to xylenes and *p/o*-xylenes ratio.

Pt-containing catalysts based on hierarchical composite (consisted of halloysite nanotubes (HNTs) and ZSM-5 zeolite) were successfully applied for the isomerization of the xylenes (C_8 aromatic fraction) in a flow-type fixed-bed laboratory unit at the temperature range of 360–440°C and a hydrogen pressure of 1 MPa [125]. These Pt catalysts supported on hierarchical ZSM-5+HNT composite were prepared by standard wetness impregnation and metal particles of ca. 2.8 nm in diameter were located both on the internal and external surfaces of nanotubes (Fig. 21, a-c). The isomerization of xylenes realizes through the monomolecular (direct isomerization of *m*-xylene) and bimolecular (when *m*-xylene undergoes disproportionation followed by alkyl migration and p-xylene formation) reaction routes, leading to conversion with high *p*-xylene yield. The ZSM-5 microporous zeolite provides the appropriate acidity and halloysite introduces the mesoporosity for ethylbenzene isomerization to *p*-xylene [126]. This was proved isomerizing the C_8 aromatic fraction from the industrial unit containing xylenes and ethylbenzene. The highest ethylbenzene and *m*-xylene conversions (82 and 37 %) over the Pt/ZSM-5+HNT/γ-Al_2O_3 catalyst were achieved at 440 °C, and ethylbenzene conversion was 65 % (Fig. 21, d-e).

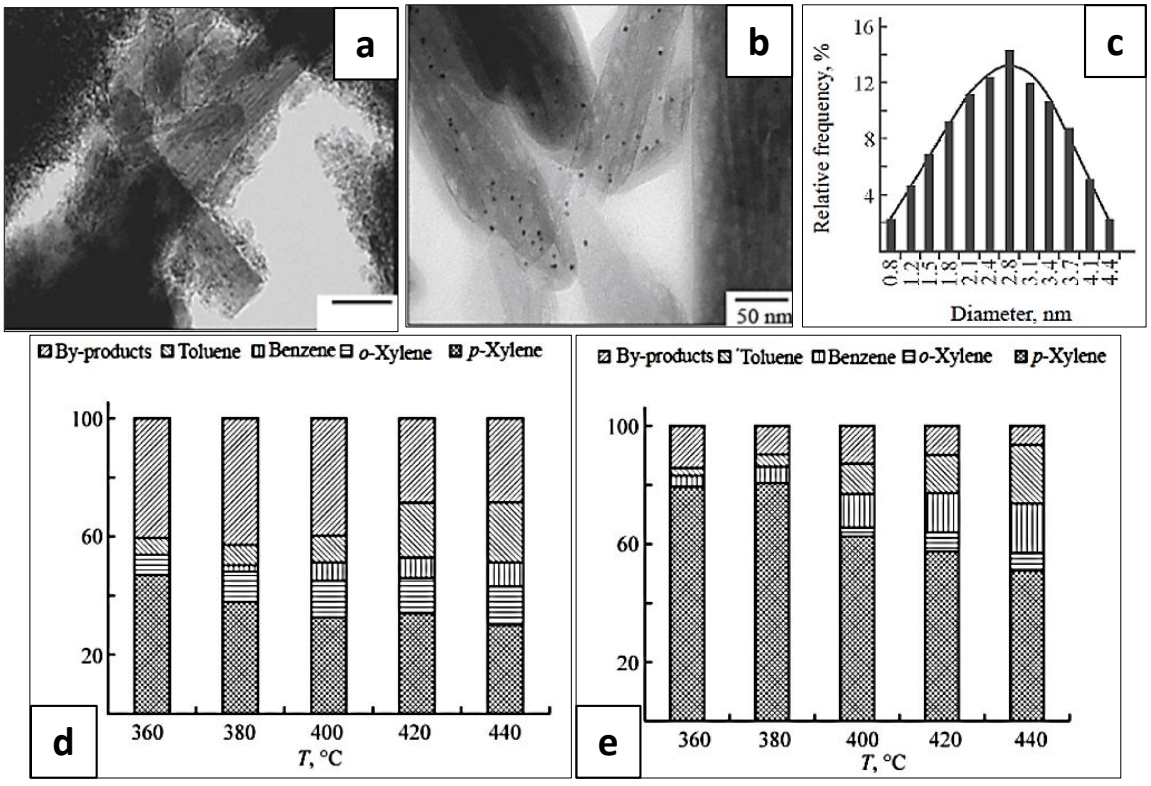

Fig. 21. TEM images of (a) ZSM-5+HNT/γ-Al_2O_3 and (b) Pt/HNT/γ-Al_2O_3 catalysts; (c) metal particle-size distribution for Pt/HNT/γ-Al_2O_3 catalyst; The product distribution for isomerization of the C_8 aromatic fraction over (d) Pt/HNT/γ-Al_2O_3 and (e) Pt/ZSM-5+HNT/γ-Al_2O_3 catalysts vs. temperature. Reprinted by permission from Springer Nature: Russian Journal of Applied Chemistry [125], copyright (2018).

An interesting approach to increase the acidity of support was suggested in [67], where hierarchical composite, consisting of ordered MCM-41 alumosilicates and halloysite nanotubes were used as a support for platinum catalysts. The TEM images prove Al–MCM-41 arrangement on the outer surface of nanotubes, and the mesoporous silica phase forms the microglobules with an ordered hexagonal packing (Fig. 22).

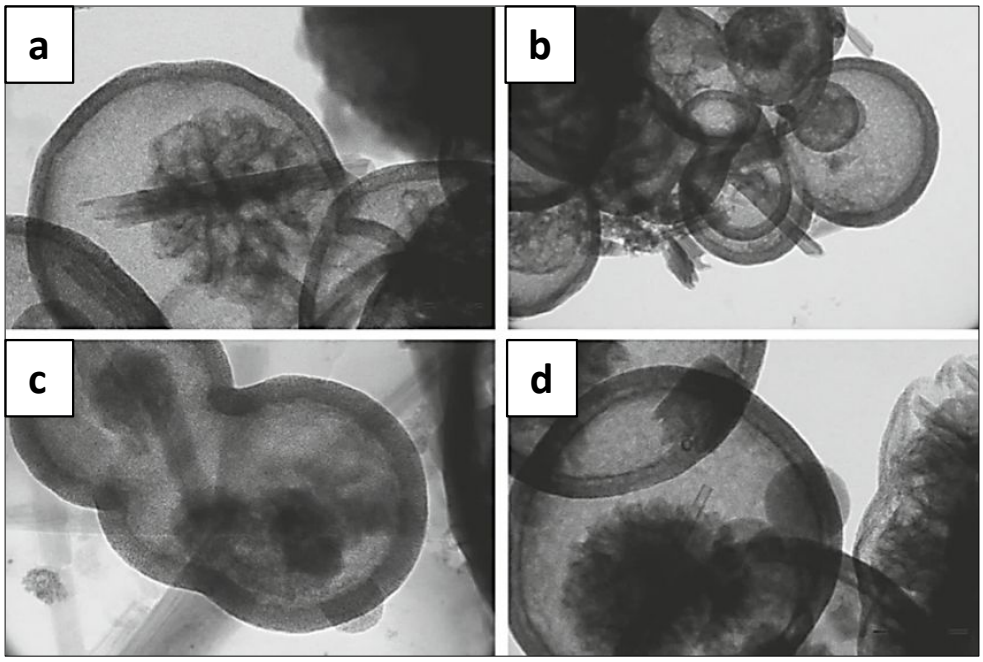

Fig. 22. TEM images of (a, b) Al–MCM-41/HNT(60:40) and (c, d) Al–MCM-41/HNT(90:10) samples. Reprinted by permission from Springer Nature: Petroleum Chemistry [67], copyright (2018).

MCM-41 type aluminosilicate incorporation allowed for an increased surface area up to 400 m^2/g, much larger than that for a pristine halloysite (ca. 60 m^2/g). One of the advantages of these materials is that optimal acidity can be adjusted by varying the Al content in MCM-41. This tunable acidity allows for controlling selectivity and stability. The Pt catalyst supported on Al–MCM-41/HNT composite with a component ratio of 90:10 provided good ethylbenzene and *m*-xylene conversion. This composite-based catalyst exhibited higher selectivity for *p*-xylene as compared to the commercial zeolite-based counterpart at the temperature range of 360–440 °C. Halloysite nanotubes, surrounded with amorphous and small pore shells of Al–MCM-41, provide thermal stability of the composite.

Concluding, the aluminosilicate composite based on halloysite are promising materials for the design of high-temperature catalysts with enhanced properties[6, 10, 23, 120]. Halloysite nanotubes act as an armoring component for enhanced thermal and mechanical stability. They may be used as a template for well-ordered silica or aluminosilicates (including zeolites) growth inside or outside the tubes introducing high porosity and surface area in the catalyst. Based on these hierarchical materials, we proposed the strategy for well-ordered silica growth inside the inner tubular clay cavity[127, 128]. This multistage procedure includes acid etching of the halloysite to remove alumina from the lumen to access the inner silica for organic modification. It allows for selective growth of MCM-41 silica embedded into the lumen (Fig. 23). The resulted halloysite-based composite exhibits enhanced textural and acidic properties, making them an attractive hybrid material for catalysts' design.

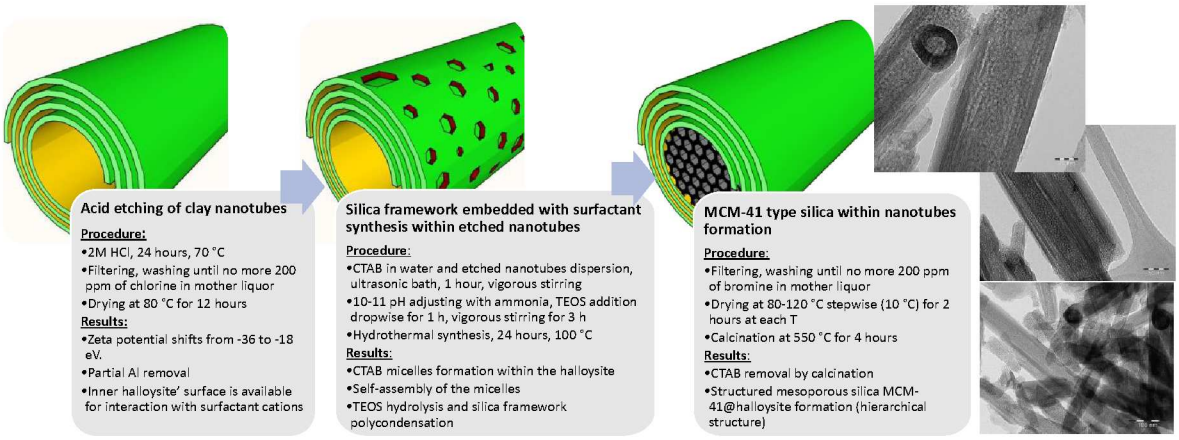

Fig. 23. Self-assembly of mesoporous MCM-4 silica embedded into halloysite lumen (TEOS – tetraethyl orthosilicate, CTAB – cetyltrimethylammonium bromide).

This research may be extended by tuning acidity of halloysite by acid/alkali etching. Finally, this natural aluminosilicate clay may be used as a silica and alumina source for the crystallization of zeolites with the desirable porous arrangement, texture, and acidity.

3. Hydroprocessing in oil refining: sulfur removal assisted with the clay nanotubes

Oil refinery involves high-temperature catalytic processing of heavy petroleum fractions into light hydrocarbons used for the production of motor and jet fuels. The hydroprocesses including hydrocracking, hydrotreatment, isomerization of gasoline and diesel fractions, and catalytic reforming take a significant role in the production of high-quality fuels. All of these processes can be divided into two groups: first is destructive processing aimed at the production of light hydrocarbon fractions (hydrocracking, catalytic cracking), and the second one allows for increasing the quality of gasoline, diesel, jet fuels without significant changing the product boiling point range as compared to that for the feedstocks (hydrotreatment, isomerization, reforming). Hydroprocessing (including hydrocracking and hydrotreatment) of non-traditional heavy and viscous oil feedstock with high content of heteroatomic (including sulfur) compounds and catalytic poisons, asphaltenes, needs efficient hybrid mesocatalysts. Mesoscale porosity provides transport channels for the transformation of bulk heteroatomic compounds without mass transfer and diffusion limitations; high adsorption capacity to sulfur compounds and appropriate acidity for C-S bond scission with high selectivity to distillates and low yield of hydrocarbon gaseous products. We described the design of halloysite-based composites for effective heavy feed transformation and sulfur removal. Halloysite-based core-shell systems demonstrate a good performance in hydroprocesses indicating possible routes for architectural design of stable and efficient catalyst based on this abundantly available natural material.

3.1. Hydrocracking and hydrotreatment

Alumina oxide or zeolites are widely applicable as support for industrial hydroprocessing. Aluminum oxide is easy in preparation and a variety of their modifications allow for developing structural features determining the dispersion and state of the oxide surface with high cohesiveness. Zeolites are well-ordered microporous materials with a high specific surface area and narrow pore size distribution depending on the choice of the structure-directing agents

turned during the crystallization[129]. The alumina- or zeolite-supported catalysts have high activity but suffer from mass-transfer limitation for bulk molecules of low-quality heavy [130-133] feeds. Since the product diffusion is restricted by the pore coke blockage, the secondary cracking over strong acid sites also may occur yielding gaseous products[134]. Therefore, research in tailored catalyst design focuses on the development of mesoporous materials such as MCM-41, SBA-15, or hierarchical zeolites of ZSM-5, Y, MOR types with appropriate secondary porosity and tuned acidity [135-138].

The halloysite nanotubes are promising support for hydrocracking and hydrotreatment catalysts. First, due to tubular mesosized morphology, halloysite provides the transport channels, excluding mass transfer and diffusion limitations for bulk organic molecules. The second reason is the aluminosilicate nature, determining acidity and activity in acid-catalyzed C-S bond scission. The acidity of halloysite also enhances the bonding of active metals to the support surface, which improves the dispersion of catalysts' nanoparticles. The mechanical and thermal stability allows halloysite usage for reinforcement of different silicates and aluminosilicates, applied as support. However, there are no detailed studies on the formation, localization, and functionality of the active phase depending on the structural features of halloysite-based composites.

Halloysite was used as a support for Ni and Mo catalysts applied in hydrocracking to obtain light oil products (gasoline and diesel fractions) from heavy residues (fuel oil) at 430 °C and 4 MPa hydrogen pressure [71]. The metal impregnation was carried out by two different methods — absorption followed by ion exchange, and dispersion of metal precursors in fuel oil reaching a homogeneous suspension. The halloysite modified by the absorption method exhibited a high conversion of fuel oil, giving 53 wt.% gasoline yield, while for catalyst obtained by the ion-exchange method, the yield achieved 83 wt.%. This higher activity may be caused by the removal of aluminum oxide from the surface of the tubes during HCl treatment. Aluminum oxide was replaced by Mo and Ni oxides on halloysite surface, which provides a uniform distribution of metal particles. When halloysite was modified by the absorption method, Al oxide remained, and metals were absorbed on the nanotube surface. The hydrocracking products are characterized by low content of aromatic and unsaturated hydrocarbons. Moreover, the octane number of this gasoline fraction was 75, and a high cetane number of 53–55 was achieved for the diesel fraction.

Similarly, the ion exchange modification of halloysite nanotubes was applied to create Mo and Ni catalysts for hydrocracking of fuel oil [74]. The substitution of Si and Al atoms by Mo and Ni provided intensification of hydrogenation and isomerization reactions, which increased the yield of liquid products up to 30 % (87wt.%) at 430 °C and a hydrogen pressure of 4.0 MPa.

Suspended highly-dispersed halloysite nanotubes modified with transition metals were tested in hydrocracking of atmospheric residue to investigate the physical-chemical properties of coked particles. When the temperature was rising to 450 °C (1.0 MPa hydrogen pressure), the yield of the coke increased[73]. This approach was also reported for hydrotreating of the diesel fraction and its mixture with cottonseed oil, as well as for the transformation of vegetable oils to paraffins through the direct decarboxylation reaction [139]. The desulfurization degree over halloysite-supported Ni-Mo oxides reached 90-95 % at 320-350 °C under 6 MPa hydrogen pressure, while the content of aromatic hydrocarbons achieved 12 wt.%.

Halloysite nanotubes were also applied as a support for transition metal-based hydrotreating catalysts [140]. The hydrotreating of diesel fraction was carried out at a temperature of 330-350 °C,

hydrogen pressure of 5.0 MPa, and the liquid hourly space velocity of 0.5-1.0 h^{-1}. The trimetallic transition metal oxides supported on halloysite exhibit catalytic activity in hydrotreatment, providing sulfur reduction, and the content of diesel fraction maintained constant with low gaseous and gasoline fraction. Of primary interest is an optimization of physical-chemical properties of the metal phase formed on the halloysite tubes and demonstrating their advantages over commonly used alumina-supported systems[141-145]. The nanoclay support plays an important role in the active phase formation process [130, 133, 146-150].

The acid or alkali treatment of halloysite nanotubes allows for controlled mesoporosity without the destruction of the template tubular structure. Such alteration of halloysite is effective for increasing transport channels and controls acidity, particle size, dispersion, and binding of metal species. Ni-Mo bifunctional catalysts based on natural clay nanotubes treated with mineral acids were evaluated in the n-decane hydroconversion [69]. This treatment increased the surface area, porosity, and acidity of the halloysite-based supports, which in turn favored dispersion of the hydrogenating phases (Ni-Mo) and enhances reactivity and molecular transport for ethyl-octanes and methyl-nonanes.

The catalytic performance in the n-decane hydroconversion over acid halloysite-based catalysts was performed[68]. Ni, Mo, and Ni-Mo clusters were impregnated on halloysite nanotubes (HNTs). The bimetallic catalyst was more efficient due to $NiMoO_4$ phase formation. The promoted Ni-effect facilitates reduction and allows formation of smaller metal particles. The catalytic activity was decreasing as follows: 5Ni15Mo/HNT-A>5Ni/HNT-A>>15Mo/HNT-A. When isomerization and cracking products were identified, the correlation of Ni, Mo, and Ni-Mo sites with the Brönsted acidity of the acid-halloysite catalysts was underlined.

Halloysite mesoporous properties and tunable acidic characteristics are the key for design and development of hydrodesulfurization catalysts for effective hydrocarbon feedstocks upgrading. Selective formation of transition metal sulfide and noble metal active sites on the outer and inner surfaces of halloysite tubes is very promising. For transition metal sulfide-based catalysts, selective lading into internal cavity allows for the protection of active phase from coking and leaching. This approach is also applicable for the layer-by-layer materials design in nanoconfined conditions limited by inner diameter of halloysite nanotubes. The intercalation of metal nanoparticles into the more acidic nanotubular lumen provides the stronger bonding of active species, enhancing the dispersion. With application of Co and Mo precursors (transition metal anionic heteropolyacids) the electrostatic interaction promotes loading of these negative species into the positively charged inner cavity. Thus, we used phosphorus molybdenum heteropolyacid for preparation of CoMo catalysts via wetness impregnation. Outstanding results on active phase particles intercalation to halloysite lumen was achieved (Fig. 24).

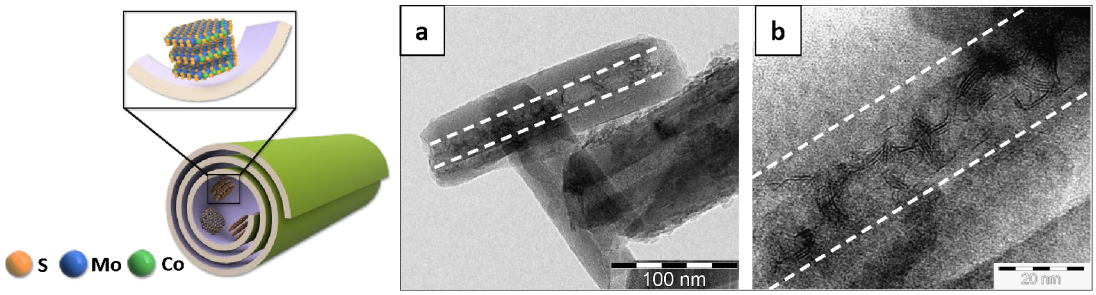

Fig. 24. Scheme and HR TEM images of halloysite supported sulfide CoMo catalyst

We are developing nano-architectural core-shell tubule formation as a promising strategy for design of CoMoS hydrodesulfurization catalysts. The constructed systems act as nanoconfined reactors for hydrotreatment. This strategy could be applied not only for hydrodesulfurization catalysts effective for stubborn sulfur compounds removal but also promises at impact for architectural design of other hybrid materials exploiting this natural nanoclay encapsulation.

3.2.Fluid catalytic cracking

Fluid catalytic cracking (FCC) is a process for alteration of heavy feedstock's boiling point range with sulfur removal yielded gasoline and diesel fractions. It was included in this review due to the hydrogen-involved mechanisms of sulfur removal. Hydrogen is transferred from the donor molecules to thiophene ring forming cyclic sulfides, which decompose to hydrogen sulfide and hydrocarbons. The catalyst ability for hydrogen transfer depends on the acidic properties, i.e. number and strength of acid sites[151, 152]. Organosulfur compounds are the Lewis bases, whereas the catalyst active centers act as Lewis acid sites. It leads to the strong adsorption of sulfur near the hydrogen donor hydrocarbons and provides an effective transformation decreasing sulfur content in liquid products[153, 154].

Halloysite as a component of support allows for mass and heat transport, and improves the mechanical and thermal stability of the catalyst. The products formed easily diffuse through the mesoporous channels without cracking to undesirable by-products [10, 151, 152].

Halloysite with large inner lumen diameter was blended with commercial FCC catalyst to introduce mesoporosity[77]. Halloysite additives were chosen as a component of FCC catalysts due to hydroxyl groups of the inner octahedral alumina surfaces, which act as active sites for acid cracking [155]. Halloysite blended with high silica Y-zeolite was very efficient in catalytic cracking of the vacuum gas oil and cottonseed oil as well as for mixture of cottonseed or sunflower oils with vacuum gas oil. When the halloysite-based additives were applied, the high gasoline yield with lower coke formation was achieved [77, 78]. The yield of gasoline achieved 46.5% (Fig. 25b) at 63% conversion (Fig. 25a), with only 2.5% coke formed (Fig. 25c). When the content of cottonseed and sunflower oils within feedstock was raised by 4%, the yield of the gasoline increased to 50% (Fig. 25) [77].

The mesoporous halloysite structure was shown to provide hydrocarbon skeletal isomerization and chain branching, causing an increase in the gasoline octane number. Halloysite pores provide efficient adsorption of heavy hydrocarbon molecules and more efficient cracking of larger molecules. When the FCC catalyst is blended with halloysite, the coke yield reduces by 7–10%. Interestingly, that coke predominantly forms at the end of the tubes. Halloysite tubes provide a linear diffusion path from the pores of larger diameter and allow for rapid removal of light hydrocarbons from the surface acid sites. It prevents the deep dehydroxylation of organic molecules and coke formation. The thermostable halloysite preserves tubular structure after catalytic cracking.

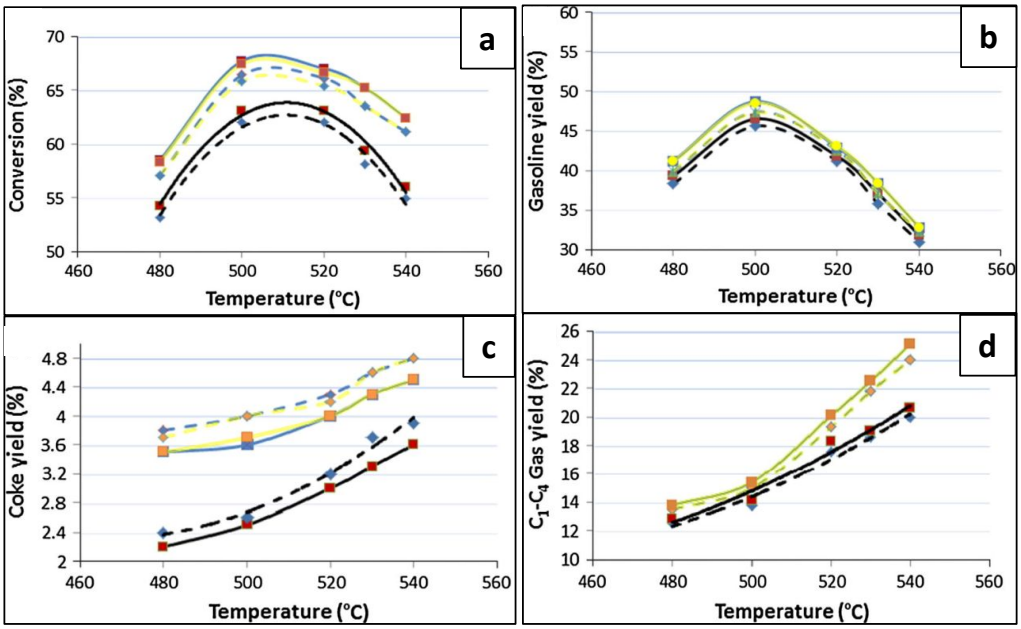

Fig. 25. (a) Conversion and (b-d) yields of cracking products of vaquum gas oil (black lines), 10% clarified slurry oil – vaquum gas oil mixture (blue lines), and 10% sun flower oil– vaquum gas oil mixture (yellow lines). Dashed lines correspond to the values for Omnikat and solid lines correspond to 10% halloysite–90% Omnikat catalyst blend. Reprinted from [77], copyright (2016) with permission from Elsevier.

Recently, the strategy for self-assembly of ordered silica arrays on aluminosilicate halloysite nanotubes was proposed to create a hierarchical support with enhancing thermal and water vapor stabilities (Fig. 26a). This approach is based on the electrostatic interaction between negative outer halloysite surface and cationic amphiphile molecules of structure-directing agents [6, 10, 23, 156]. The template concentrated over the tubes' external surface direct the mesosilica growth around halloysite. Such mesosilica organization is controlled by self-assembly of amphiphily multilayers, initiated by electrostatic attraction of the first template layer. MCM-41/HNTs composite was obtained using cetyltrimethylammonium amphiphilic molecules as a template for mesosilica, produced as a one-direction channel structure, bonded to the halloysite outer surface (Fig. 26, b-e). This novel MCM-41/HNTs composite was used as a component of sulfur reduction additives to FCC catalysts and demonstrated a good efficacy in sulfur removal from liquid products at vacuum gas oil cracking [10]. MCM-41/HNT additive to FCC catalyst reduced harmful sulfur content by 25 wt.%, while gasoline yield was preserved. Light cycle oil yield increased by 1 wt.%, and it was accomplished by decreasing coke formation. Moreover, unlike pristine mesoporous MCM-41 silica, the armoring by halloysite backbones enhanced thermal and mechanical stability of the composite up to 1100 °C and 500 MPa.

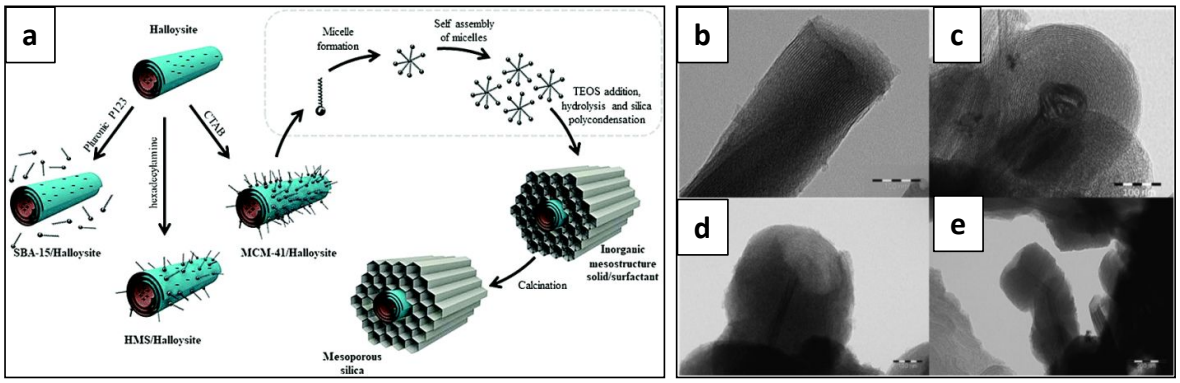

Fig. 26. (a) Scheme of the halloysite-silica hybrid synthesis using different templates (for HMS – hexadecyl amine, for SBA-15 – Pluronic P123, for MCM-41 – cetyltrimethylammonium bromide (CTAB)) and (b-e) TEM images of MCM-41/HNT composite with the nanoclay tube cross-section visible in the center. Reproduced from [10] with permission from the Royal Society of Chemistry.

The acidity of pristine halloysite is not sufficient for effective transformation of hydrocarbons during FCC, and its application as one-component support for catalysts is ot feasible. Halloysite can be exploited as reinforcing materials (kind of ceramic skeleton) with synergetically enhanced catalytic properties for oil refining.

4. Gas-phase catalysis

In addition to tunable textural and physical-chemical properties, halloysite nanotubes have high thermo-mechanical stability, helping for high-temperature gas-phase processes. Halloysite also provides strong anchoring of metal nanoparticles, preventing sintering and deactivation at high temperatures. We discuss here halloysite-based systems for dry reforming of methane aimed at utilization of greenhouse gases (this produces syn-gas for Fisher-Tropsch synthesis and hydroformylation), pollutants removal via chemical transformation of topping atmosphere residue, toxic oxides conversion into value-added chemicals, and hydrogen production and storage.

4.1.Dry reforming of methane

Due to the increase in CO_2 emissions and global temperature, there is a strong request for a decrease of the greenhouse gases (CO_2 and CH_4) by their utilization[157]. One of the methods for CO_2 transformation is dry reforming of methane, where greenhouse gases are converted into hydrogen and carbon monoxide[158, 159]. The conversion of CO_2 and CH_4 depends on the temperature, partial pressure of reagents, and volume hourly space velocity[160]. The molar ratio of CO and H_2 in the gaseous products is close to one, and as-produced syn-gas may be used as a feedstock for the Fischer–Tropsch process, hydroformylation, or carbonylation. The noble metal-based catalysts (Rh, Ru, Pt, and Pd) are the most active and resistant to coking[161]. However, they are very expensive, which limits their large-scale applications. Transition metal-based catalysts are more promising, but they suffer several disadvantages like high coke formation, metal sintering at high temperatures, and rapid deactivation[162]. The strategy to enhance their properties is introducing noble metal promoters, controlling the particle size, and intercalation them into the well-ordered support matrix.

For enhancing the coke- and sintering-resistance performance of transition metal catalysts, supports with appropriate acid-base properties and thermal conductivity have to be developed allowing for endothermic dry reforming of methane at 700-900°C[163]. The optimal acidity of the support enhances the anchoring of metal particles, resulting in high dispersity and stability to sintering. On the other hand, the high acidity inhibits the reduction of oxide species and leads to high coke formation. The basicity is crucial for CO_2 adsorption over the support surface. The activation of CH_4 through the dissociative adsorption yielded carbon species and hydrogen occurs over metal centers, whereas the basic sites are necessary for CO_2 coordination[159]. The hydrogen may react with CO_2 via reverse water gas shift reaction, while the carbon species oxidized to CO reducing the coking. Silica, alumina oxides, zirconium- and titanium-silicates were investigated as supports for dry reforming catalysts. Their basicity can be regulated by support alloying with cerium, lanthanum, calcium, and magnesium oxides[158]. Thus, Ni-Al, Mg-Al, Ni-La spinels were employed as catalysts. The halloysite is chemically inert and suffers several advantages for introducing them as a support for dry reforming catalysts. It allows for fabrication of materials with adjustable properties[156]. These clay tubes provide a heat transfer and have optimal thermal conductivity. It may also be exploited to reinforcing materials with synergetically enhanced properties.

Ni-based nanosheet-like catalysts, derived from halloysite nanotubes, were tested in CO_2 reforming of methane [164]. To expose more active sites the nanotubes were unzipped into few-layer nanosheets via ball milling during silica etching from the outermost halloysite layer (Fig. 27). As-obtained materials have defects, which confines metal nanoparticles, providing thereby high dispersion of active species, and boosts charge transfer during wet impregnation. This formulation supports Ni particles size of ~14 nm, uniformly distributed over the surface, whereas for tubular halloysite Ni particles larger sizes (~26 nm) were observed (Fig. 28, a-f). Unzipping the tubes forms more active sites, which is beneficial for the activation of CH_4 during the dry reforming. These halloysite-based Ni catalysts exhibit good performance in methane conversion with retaining of activity after a 20 h stability test (Fig. 28, g-h).

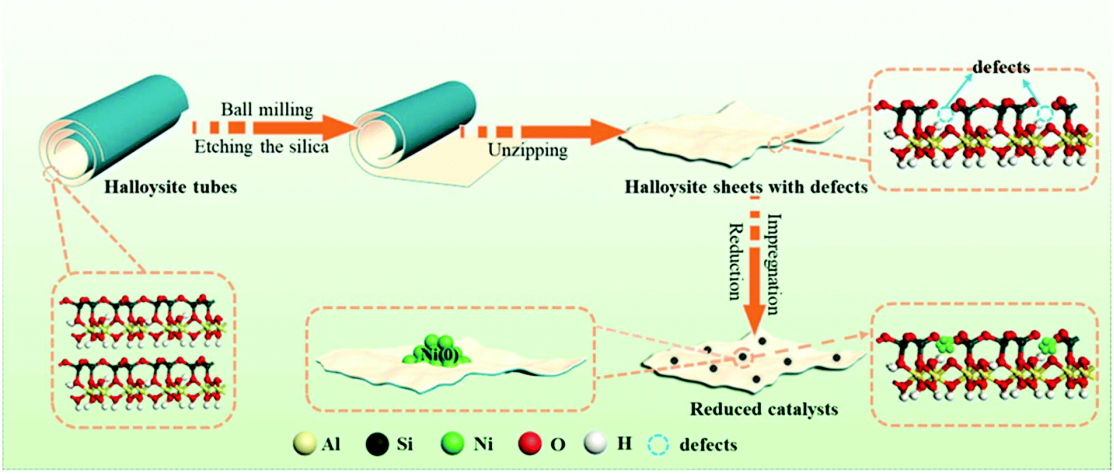

Fig. 27. Illustration of the fabrication strategy of unzipped halloysite-based catalysts. Reproduced from [164] with permission from the Royal Society of Chemistry.

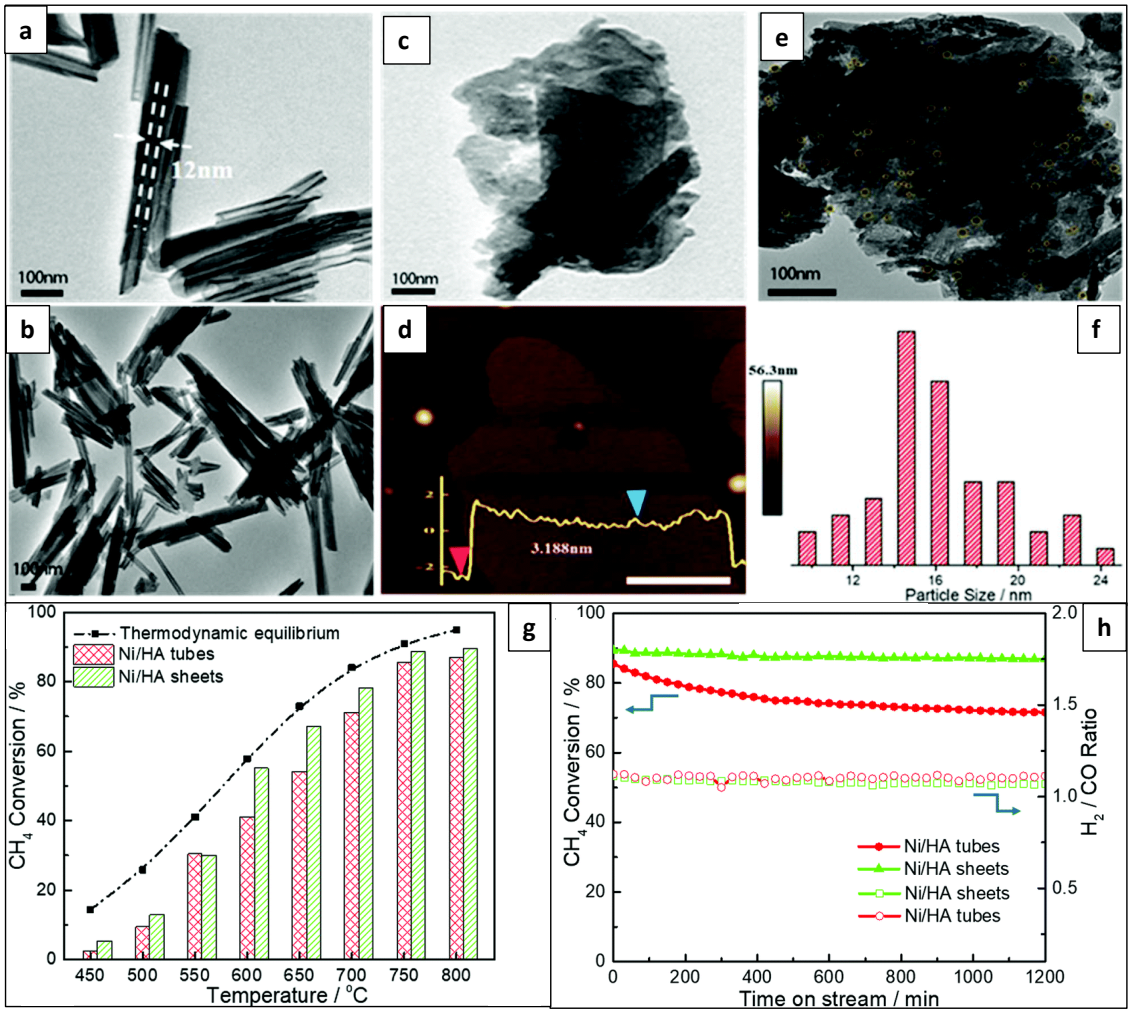

Fig. 28. TEM images of (a, b) raw HNTs; (c) HNTs sheets; (d) the corresponding height profile of the sheets (Scale bars: 1μm); (e) Ni/HNTs sheets reduced at 750 °C for 1h; (f) the corresponding particle size distribution histogram of Ni over Ni/HNTs sheets; (g) Effects of reaction temperature on the catalytic performance of catalysts; (h) Stability tests at 750 °C: CH_4 conversions and relevant H_2/CO ratio as a function of time on stream (GHSV = 15,000 mL h^{-1}gcat $^{-1}$, 750 °C, 1 atm). (a-f) Reproduced from [164] with permission from the Royal Society of Chemistry; (g, h) modified from [164] with permission from the Royal Society of Chemistry.

The halloysite-derived silica-alumina composite with nanorod structure was used as a support for Ni catalysts, having a high activity and coke-resistance towards steam-CO_2 dual reforming of methane to produce syn-gas [165]. Calcination temperature affects the dispersion of Ni nanoparticles over the halloysite surface. Despite specific surface area decreases, halloysite supported Ni catalyst calcined at 1000 °C exhibits the highest activity as well as resistance to coke and metal sintering. There is no obvious decrease in the CH_4 and CO_2 conversions as the time on stream was extended to 30 h (Fig. 29). Interestingly, that over halloysite supported Ni catalysts H_2 selectivity is slightly higher than that for CO, which may be caused by abundant surface hydroxyl group of aluminosilicate surface.

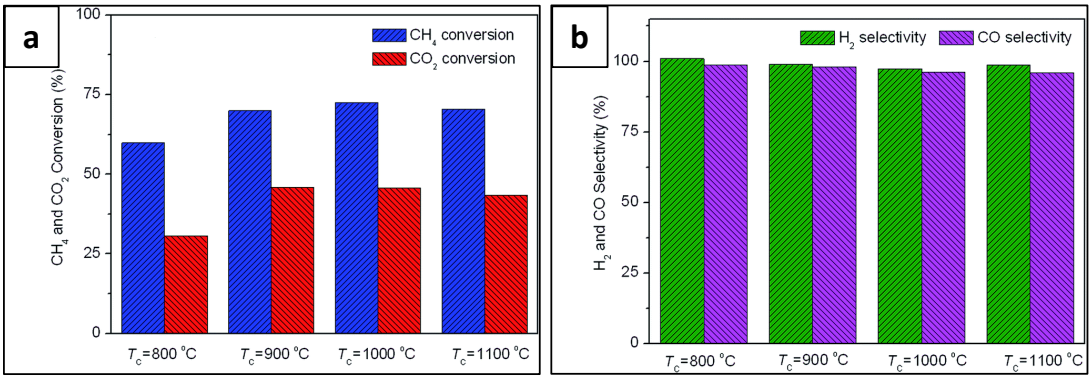

Fig. 29. Catalytic performance of the supported Ni catalysts on the silica-alumina composite oxides derived from halloysite through calcination with diverse temperatures. (a) CH_4 and CO_2 conversion, (b) H_2 and CO selectivity. Reaction condition: m_{cat}=50 mg, CH_4:CO_2:H_2O:N_2=1:0.4:0.8:1.2, GHSV=48000 mL h^{-1} g^{-1}, 700 °C, and atmospheric pressure. Reproduced from [165] with permission from the Royal Society of Chemistry.

The catalytic efficiency in methane dry reforming depends on the anchor moieties between the support and metal nanoparticles. More detailed research on the behavior of halloysite-based catalysts in dry reforming is needed. This includes i.e. investigation of reaction kinetic, mechanisms of sorption and activation of CO_2 and CH_4 depending on acid-base properties, the transformation of the active component and support structure. Halloysite nanotubes are cheap and naturally abundant clay with a wide opportunity of tuning the structural and chemical properties, and these catalysts' development may intensify industrialization of dry reforming processing. Enhanced performance of halloysite-based hybrid system both in dry reforming of methane and Fisher-Tropsch synthesis or hydroformylation allows for development of tandem process over a one-type catalyst producing the value-added chemicals or hydrocarbon fuels from methane and carbon dioxide.

4.2.Pollutants removal

Utilization of toxic wastes has attracted much attention. Chemical plants discharge toxic compounds in atmosphere and the complete and qualified technology for these gases treatment is needed[166, 167]. Mostly, the trapped toxic gas is converted via combustion or oxidation, but these low efficient technologies are restricted [168, 169]. Halloysite nanotubes have been used as low-cost adsorbents for trapping toxic gas, and it would be interesting to evaluate their peculiar properties also as transformative nanoreactors[170]. Usually, alumina, cerium, and zirconium oxide were used as a component of catalysts for conversion of toxic gases[171].

The CeO_2 system with Pd nanoparticles intercalated into halloysite nanotubes, modified with Schiff base ligand, were successfully applied for NO reduction as well as CO and C_3H_8 oxidation [172]. The hydrophilic nature of this nanoclay negatively influences the interaction with hydrophobic molecules, resulting in a weak bonding of metals with the support surface. Therefore, the catalytic system has also to include the amine source. The modification of the halloysite external surface with ethylenediamine resulted in the substitution of O-H groups into -C≡N ones. It leads to the overall negative charge increase, making the surface more attractive for metal cations accumulation. The anchoring of Schiff base ligands on the aluminosilicate allows for the strong interaction between support and metal species. Pd nanoparticles were well-dispersed over the support surface. For unmodified halloysite, Pd nanoparticles aggregate on the outer surface of nanotubes. On the contrary, the ligand-assisted catalyst exhibits a good

dispersion of Pd nanoparticles, intercalated into the multilayer wall and internal lumen of the aluminosilicate nanotubes. CeO_2 particles are deposited not only on the outer surface but also in the inner lumen of the support (Fig. 30, 1a-c).

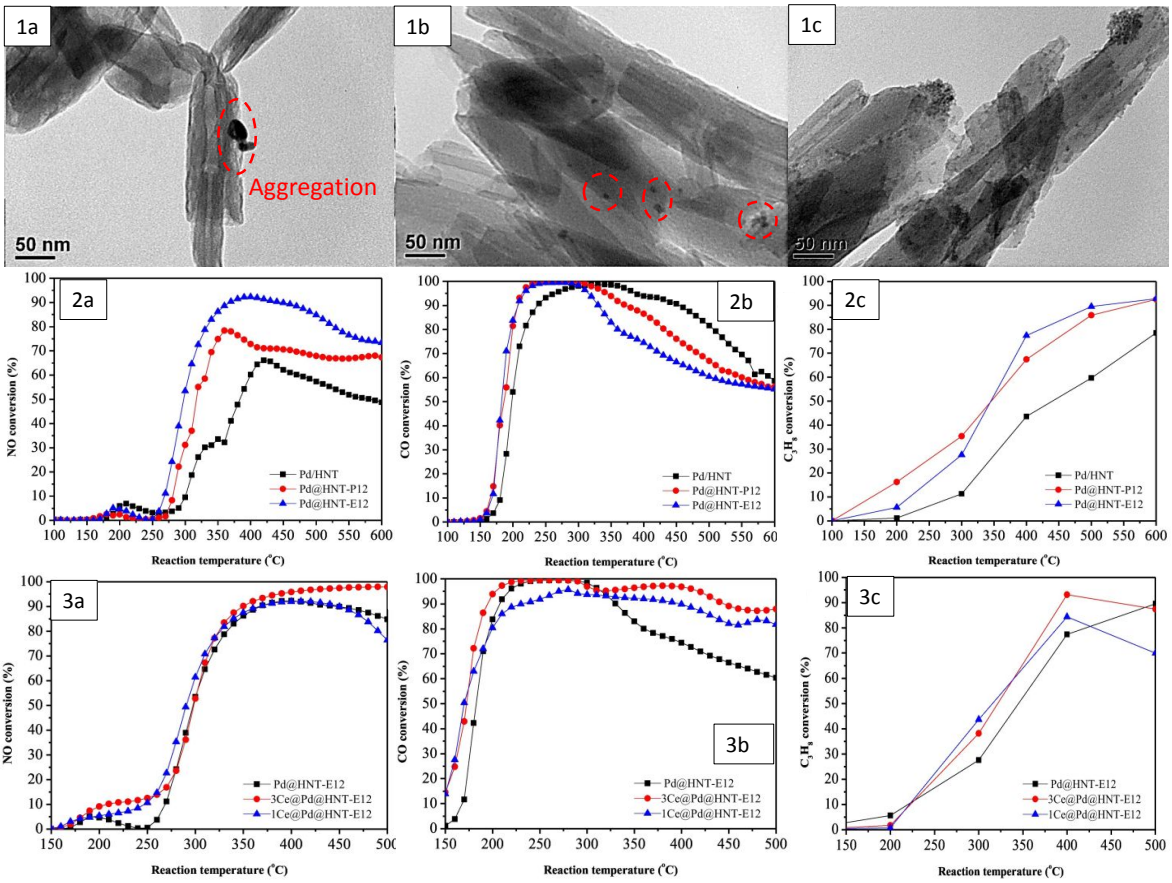

Fig. 30. TEM images of (1a) Pd/HNT, (1b) Pd@HNT-E12, and (1c) 3Ce@Pd@HNT-E12 catalysts; The conversion curves of (2a) NO, (2b) CO, and (2c) C_3H_8 for the Pd/HNT and Pd@HNT catalysts with different amine sources; The conversion curves of (3a) NO, (3b) CO, and (3c) C_3H_8 for the zCe@Pd@HNT-E12 catalyst with different Ce:Pd ratios. Reprinted from [172], copyright (2019) with permission from Elsevier.

Due to the low thermal resistance of Pd nanoparticles, suffered from agglomeration, the unmodified Pd/HNTs catalyst demonstrates lower gas conversion. The modification of halloysite nanotubes with amine groups provides formation of Pd clusters of smaller size. In this case, nanotubes act as a sintering barrier and increase the overall gas conversion, especially the NO reduction (Fig. 30, 2a). The CeO_2 shell acts as a promoter, enhancing low-temperature CO and C_3H_8 oxidation and the conversion efficiency at high temperatures. Meanwhile, the high content of Ce^{3+} implied that the enhancement of the Ce interaction with support could provide more oxygen vacancies, improving NO reduction (Fig. 30, 3a).

The NO_x reduction in the presence of SO_2 was carried out using a halloysite-supported Fe_2O_3 catalyst, promoted by CeO_2–WO_3 [173]. The metal oxides are well dispersed over the support surface (Fig. 31, a-b). Moreover, cerium and tungsten oxides are loaded on the treated halloysite lumen, and the iron oxides are located on the outer surface, forming the shell-like structure (Fig. 31, c-f). These catalysts exhibited superior activity, high N_2 selectivity over a wide temperature range (270-420 °C), and excellent sulfur-poisoning resistance (Fig. 31, g-h). When the catalyst was promoted by Fe_2O_3, the ratio of Ce^{3+} and the number of surface oxygen

vacancies increased. The interaction between active components is also enhanced due to the number of Brønsted acid sites increase. The halloysite-based Fe_2O_3 catalyst, promoted by CeO_2−WO_3, effectively prevents the irreversible binding of SO_2, providing desirable sulfur resistance.

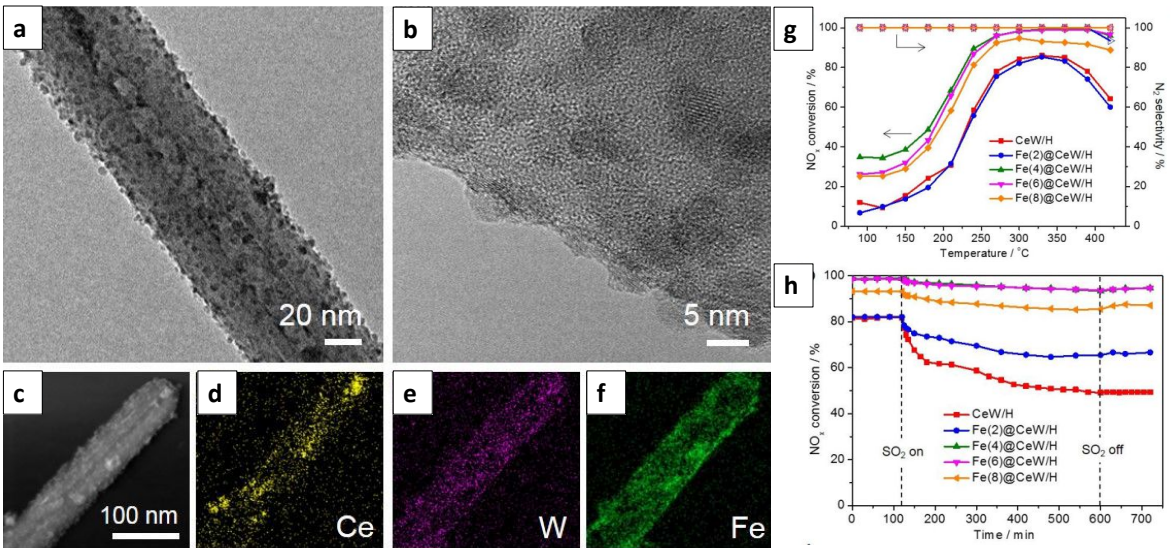

Fig. 31. (a) TEM image, (b) HRTEM image, and (c−f) EDX mapping of the Fe(4)@CeW/H catalyst; (g) NO_x conversion during the selective catalytic reduction reaction over Fe@CeW/H catalysts with different Fe_2O_3 contents and (h) NO_x conversion over Fe@CeW/H catalysts in the presence of 100 ppm SO_2. Reaction conditions: 500 ppm NO, 500 ppm NH_3, 5 vol % O_2, N_2 as the balance gas, and GHSV of 40000 h^{-1}. Reprinted with permission from [173], copyright (2019) American Chemical Society.

Halloysite clay was also applied as support for the Fe_2O_3/Y_2O_3 catalyst, which was used for topping atmosphere residue (TAR) removal [34]. This process aimed to convert the TAR compounds into H_2 and CH_4 gases over metal oxides catalysts that are highly resistive to the H_2S. The oxides were impregnated in the nanotubes via the sol-gel method using citric acid as an agent. With rising the $Fe(NO_3)_3/Y(NO_3)_3$ molar ratio, a single garnet structure of active metal phase over nanotubes' surface was formed, whereas for alumina supported catalyst multiphase structures were obtained.

Halloysite supported CeO_2-ZrO_2 hybrid (CZ-halloysite) was used for Pd and/or Rh nanoparticles impregnation[174, 175]. The resulted catalysts were tested in NO reduction as well as CO and C_nH_m oxidation. The halloysite-based catalysts have a rod-like morphology, consisting of agglomerated nanoparticles with average sizes of ca. 100 nm. SEM and TEM images also confirm that halloysite nanotubes were wrapped by the CeO_2-ZrO_2 (CZ) solid solution, which gives rise to opening lumen structure, resulting in their increased volume (Fig. 32, 1a-c).

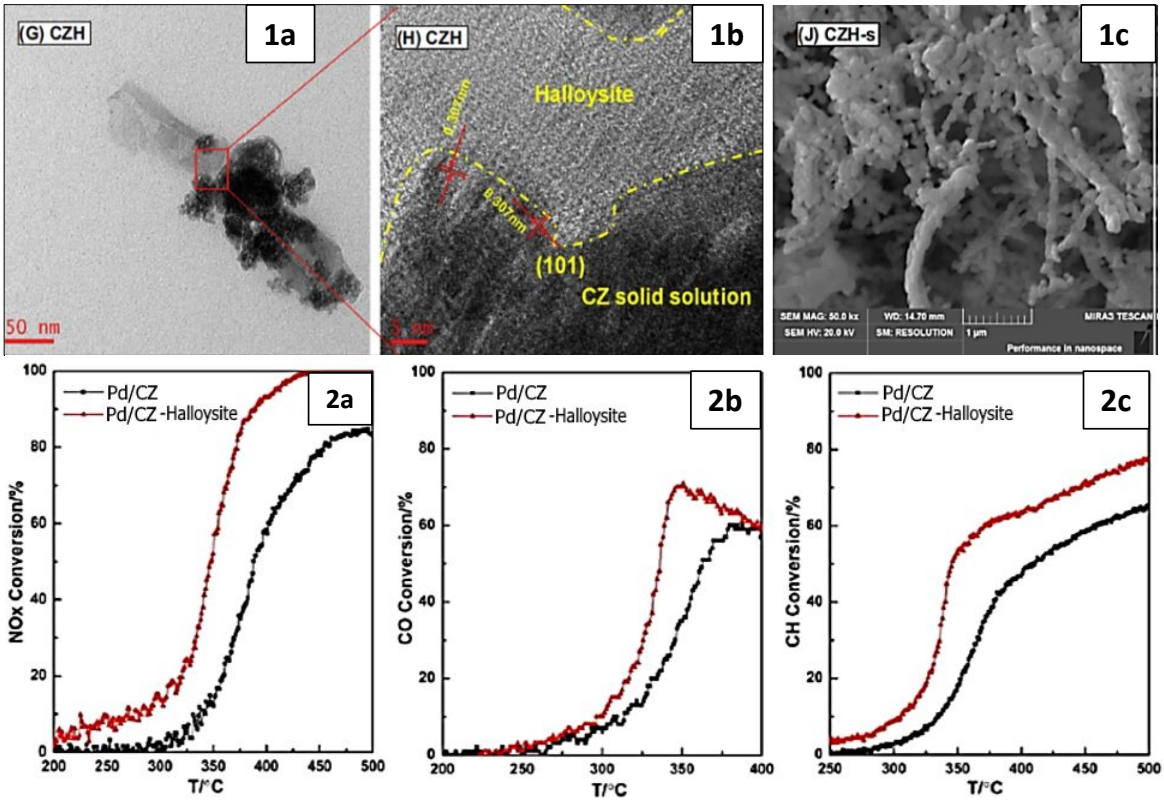

Fig. 32. (1a, b) TEM and (1c) SEM pictures of CZH hybrid sample (reprinted from [175], copyright (2017) with permission from Elsevier); Conversion curves of (2a) NO_x, (2b) CO, and (2c) C_3H_8 as a function of temperature at stoichiometry A/F ratio over the supported Pd/CZ-halloysite, compared with Pd/CZ catalysts (reprinted from [176], copyright (2016) with permission from Elsevier).

The tubular halloysite structure shortens the diffusion route of O atoms, preventing the sintering of the oxide solid solutions. Thus, the supported Pd-Rh/CZ-Halloysite catalyst showed the best performances for CO, NO_x (conversion up to 98%), and C_nH_m (70%) under low-temperature conditions (Fig. 32, 2a-c).

Similar researches are described in [176], where the halloysite-$Ce_{0.5}Zr_{0.5}O_2$ hybrid materials loaded with Pd were tested in catalytic conversion of CO, C_3H_8, and NO_x. The nanotubes were adapted through surface modification and hybridization with mixed oxides solid solutions. The halloysite-based catalyst is more active as compared to $Ce_{0.5}Zr_{0.5}O_2$ supported one (Fig. 32). The hybridization with aluminosilicate nanotubes is supposed to prevent sintering of active phase under reaction conditions, increasing the adsorption capacity in gas phase catalysts and providing gas exchange tunnel to the inner part of the metal oxides solid solution.

MnO_x/HNTs catalysts were successfully applied in low-temperature NO reduction with NH_3[177]. Halloysite provides high dispersion of the amorphous MnO_x particles over the internal and external surfaces. The catalysts provided nearly 100% NO conversion at temperatures from 60 to 250 °C. The nanosized hollow tubular structure of the halloysite is crucial for super-high catalytic efficiency at lower temperatures.

Cu–Ni catalysts supported on halloysite with exterior and interior surfaces act as an agglomeration-tolerant exhaust catalyst when copper-nickel alloy nanoparticles were immobilized at the AlO_x interior (Fig. 33) [32].

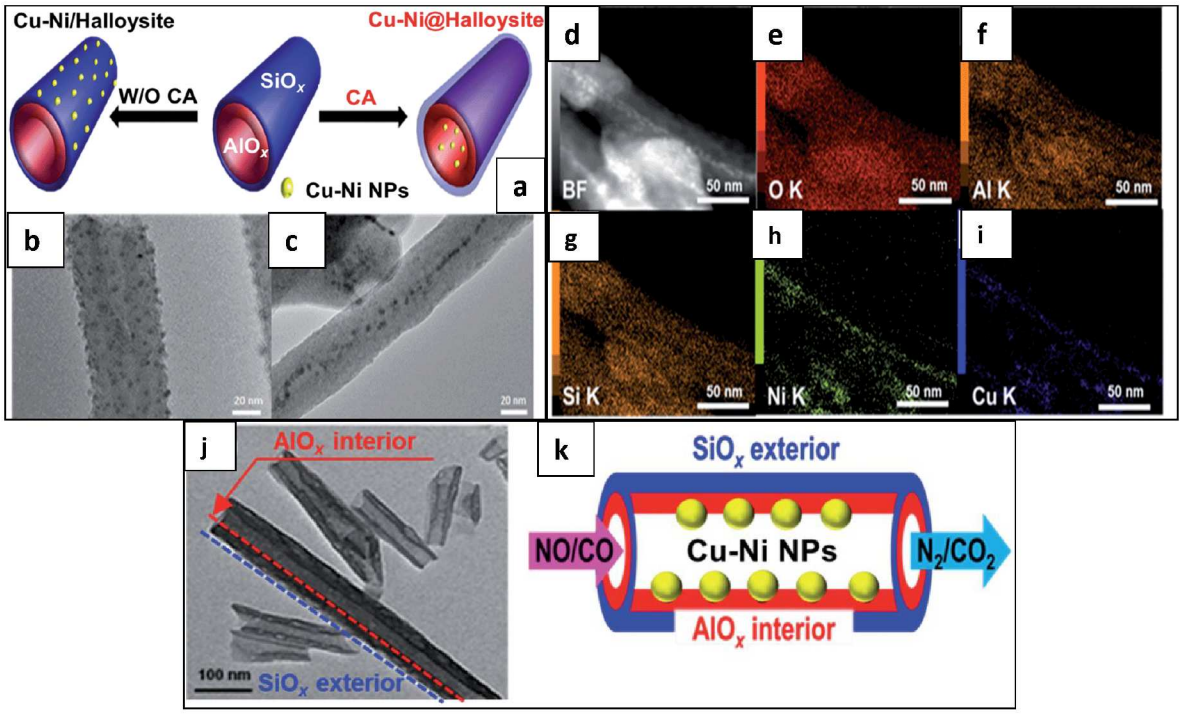

Fig. 33. (a) Schematic illustration of the selective dispersion of Cu-Ni nanoparticles over halloysite in the absence or presence of citrate (CA); TEM images of (b) Cu-Ni/halloysite and (c) Cu-Ni@halloysite; (d) Annular-dark field image of Cu-Ni@halloysite; (e-i) Corresponding elemental-mapping images; (j) TEM image of halloysite and (k) motor vehicle exhaust purification by Cu-Ni@halloysite. Reproduced from [32] with permission from the Royal Society of Chemistry.

Cu–Ni@halloysite with interior metal encapsulation efficiently catalyzes purification of simulated motor vehicle exhaust comprising nitrogen monoxide (NO) and carbon monoxide (CO) near the activation temperature of Pt-based exhaust catalysts, <400°C, showing its potential as an alternative catalyst.

We assume gas-phase catalysis could be developed for pollutants removal using core-shell nanoclay reactors containing two-type metal particles selectively located on the different surfaces of halloysite tubes.

4.3.Hydrogen production and storage

To decrease the CO_2 emission and protect the atmosphere, the research focus is sifting towards environmentally sustainable resources like hydrogen[178]. However, hydrogen usage requires its effective storage and safe transportation[179, 180] and nanoporous hydrogen storage materials are the most attractive for this[181, 182]. Despite many hydrogen storages by sorbents or coordination with hydrides were developed, the search for effective and safe media for hydrogen accumulation and controlled release is importaint[183, 184]. Borohydrides and aminoborane are regarded as promising hydrogen storage options[185, 186]. However, the alkaline byproducts lead to reaction yield decrease and catalyst deactivation. The methanolysis of hydrides in alcohols like methanol, ethanol, or ethylene glycol instead of water is more attractive. This reaction is characterized by low activation energy and occurred at much lower temperatures as compared to decomposition in aqueous media. Much attention is attracted to the development of effective catalysts for decomposition or methanolysis of borohydrides or aminoboranes. These materials should provide high hydrogen capacity and readily accelerate the hydrogen release[187]. Halloysite

clay nanotubes may be a compromise storage material with nanoporosity reaching 500 m^2/g after acid etching, also combined with the catalytic ability for hydrogen production.

Since halloysite nanotubes are bio-compatible and inexpensive clays, it may be an environmentally benign catalytic system with a good storage capacity. Various amine-functionalized halloysite nanotubes were applied as metal-free catalysts for hydrogen production via methanolysis of sodium borohydride [188].

Typically, halloysite-based catalysts for hydrogen generation are modified with (3-aminopropyl)triethoxysilane (APTES) [189], ethylenediamine (EDA), diethylenetriamine (DETA), triethylenetetramine (TETA), and tris(2-aminoethyl)amine (TAEA), and polyethyleneimine (PEI) (Fig. 34) [188]. Catalytic activity increased proportionally to the number of amine groups and the PEI modified catalyst has demonstrated the best performances.

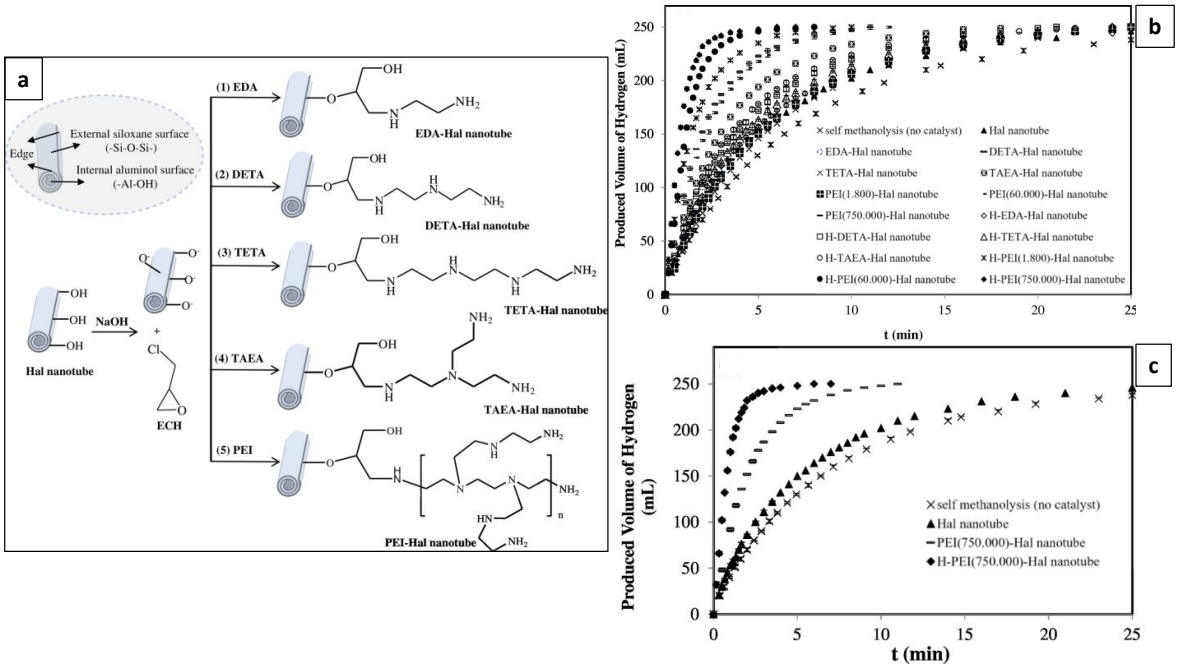

Fig. 34. (a) Scheme of halloysite modified with amine-based agents and (b, c) performance of resulted catalysts in the methanolysis of $NaBH_4$ for hydrogen production vs time (catalyst: 50 mg, 20 mL, 125 mM $NaBH_4$ at 298 K). Reprinted from [188], copyright (2017) with permission from Elsevier.

Halloysite nanotubes (HNTs) were modified with (3-aminopropyl)triethoxysilane (APTES) followed by treatment with HCl to obtain mod-HNT (HNTs-NH_2·HCl) support [189]. It was used as a metal-free catalyst for H_2 production through the methanolysis of sodium borohydride. This study was not focused on selective modification of the inner surface of halloysite; however, it was assumed that the Si-OR group of APTES mostly reacts with outer surface and edge of the nanotubes. These mod-HNT catalysts showed greater reusability with high catalytic activity after 10th usage, providing 100% conversion at each time.

Halloysite-based cobalt mesocatalysts were also used for hydrogen production by decomposition of sodium borohydride [23, 83]. The azines, as well as silanes, were used for ligand-assisted metal impregnation on the outer surface and intercalation into the nanotubes (Fig. 35). The chelating agent strongly affected hydrogen evolution. Over the best such mesocatalyst, produced using ketazine as the complexation agent, and containing 16 wt% of cobalt, a maximum hydrogen evolution rate of 3 L/min×g(cat) was achieved. These catalysts lose 30-60%

of activity after the first reaction cycle. This azine linkage enhances cobalt ions' adsorption into halloysite nanotubes twice higher.

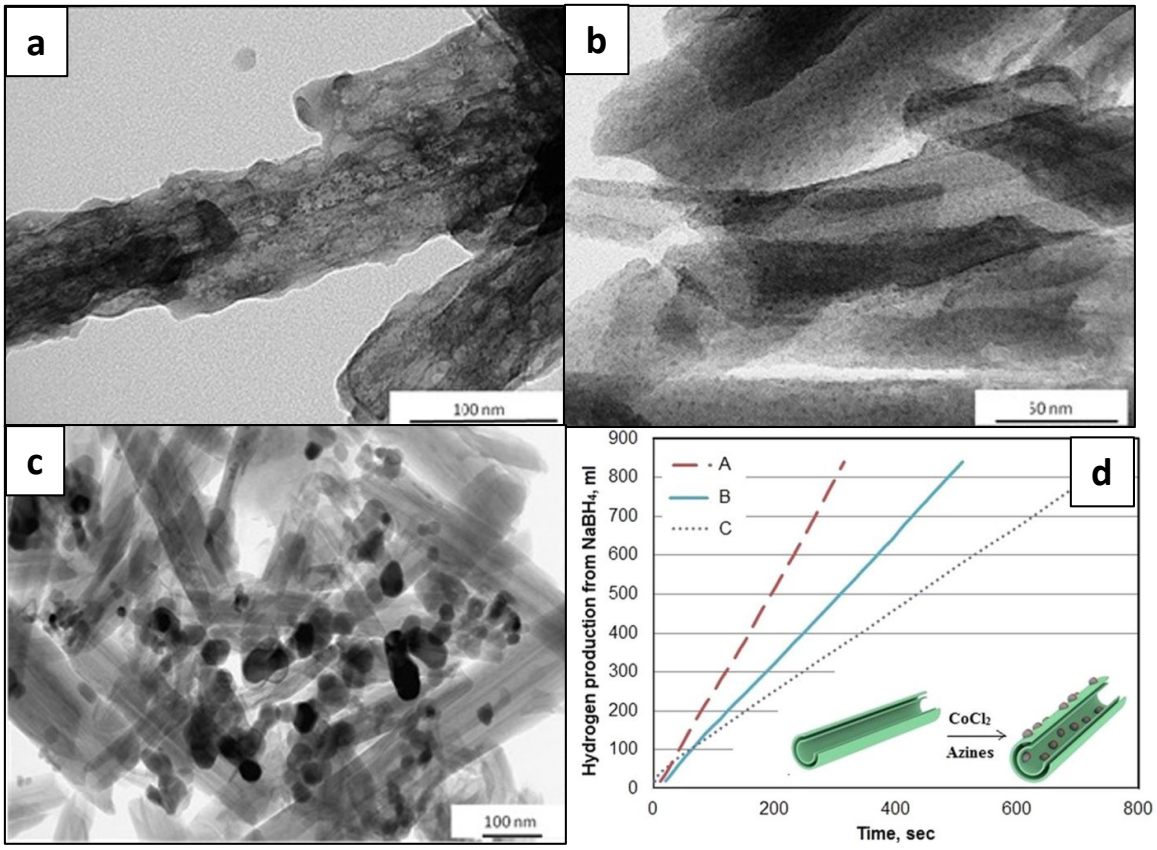

Fig. 35. (a-c) TEM images for halloysite-based mesocatalyst, obtained using ketazine as the complexation agent; (d) its hydrogen production from sodium borohydride decomposition. Reprinted from [83], copyright (2018) with permission from Elsevier.

Another promising application of halloysite nanotubes is as a support for Ru particles for the catalytic decomposition of ammonia to produce CO_x-free hydrogen as the feed gas for a proton exchange membrane fuel cell [190]. These nanotubes also have been used as a support for FeNi and BFeNi alloys, where metal nanoparticles were dispersed with the co-impregnation method. The resulting catalysts were highly active in decomposition of PH_3 into yellow phosphorus and hydrogen at a low temperature [191]. Si–O and OH groups on halloysite surface, strongly interact with metal ions, providing good metal dispersion and enhancing catalytic activity.

Halloysite nanotubes were applied as catalytic support for hydrogen storage methods based on ammonia borane decomposition [192]. It had enhanced stability, mechanical property and prevented metal leaching. Thus, the bimetallic Cu-Co catalyst supported on poly (diallyldimethylammonium (PDDA) chloride) functionalized halloysite nanotubes demonstrated high activity in hydrolytic dehydrogenation of ammonia borane. The coating of halloysite nanotubes with PDDA is beneficial for deposition of Cu and Co nanoparticles with high dispersion. It gave high total turnover frequency of 30.8 molH_2/(mol of metal per min), low activation energy of 35.15 kJ $mol^{-1,}$ and high recycling stability (>90% conversion at 10th reuse) (Fig. 36).

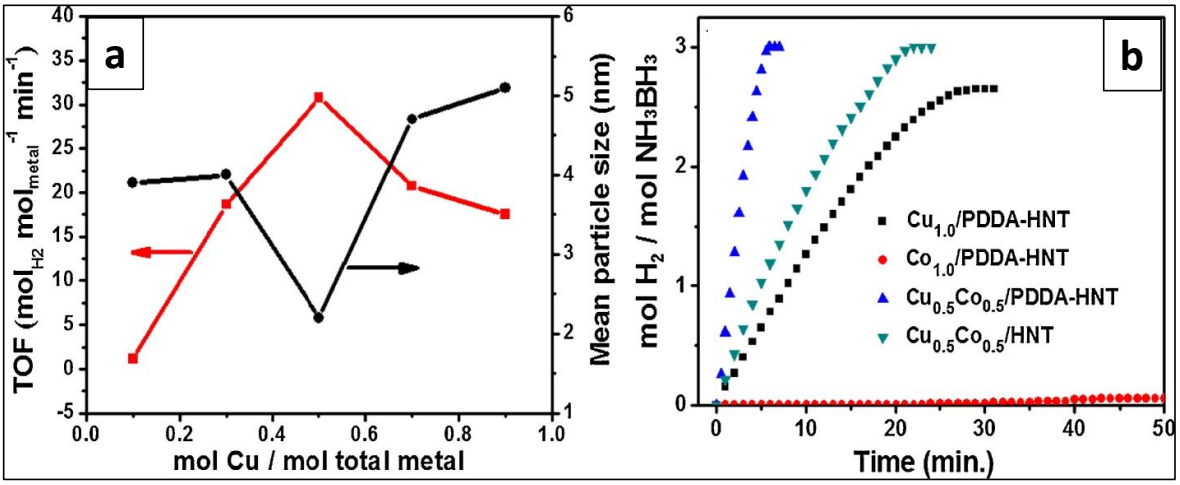

Fig. 36. Hydrogen generation with hydrolysis of aqueous amino borane (0.2 M, 5 mL) at 25°C (a) and the corresponding TOF value and mean particle size versus Cu molar content (Cu/(Cu + Co)) in Cu_XCo_{1-X}/PDDA-HNT (x = 0.1, 0.3, 0.5, 0.7, 0.9) as well as time-dependent hydrogen generation (b) for halloysite supported catalysts. Reprinted from [192], copyright (2018) with permission from Elsevier.

The decoration of nanotubes' surface by PDDA leads to dispersed ultrafine metal nanoparticles located predominantly on the outer surface. Co may cause the excess coverage of Cu active sites (higher Co loading gives lower catalytic activity).

An efficient thermal dehydrogenation was carried out by encapsulation of ammonia borane into halloysite supported Pd catalyst [193]. Halloysite adjusted the amino borane particle size due to their incorporation into the internal lumen. The functional groups also decorated the external surface of nanotubes with a uniform nanolayer. Pd nanoparticles improved catalytic activity, reducing the decomposition temperature, improving purity of hydrogen release, and suppressing emission of volatile by-products. Nanoconfinement of amino borane in halloysite enhances kinetics of H_2 release at 60 °C (for comparison, when neat amino borane was used, no H_2 is evolved at 80 °C).

Bimetallic AgPd nanoalloy supported on polydopamine-coated halloysite nanotubes (PDA-HNT) was applied for hydrogen generation [194]. The modification of nanotubes by polydopamine enhances the dispersion of AgPd (Fig. 37, a-f). By varying the Ag/Pd molar ratio, activity of the AgPd/PDA-HNT catalysts was controlled. Ag_3Pd_2/PDA-HNT system exhibited the highest TOF value of 90 mol(H_2) per mol catalyst (Fig. 37, g-h).

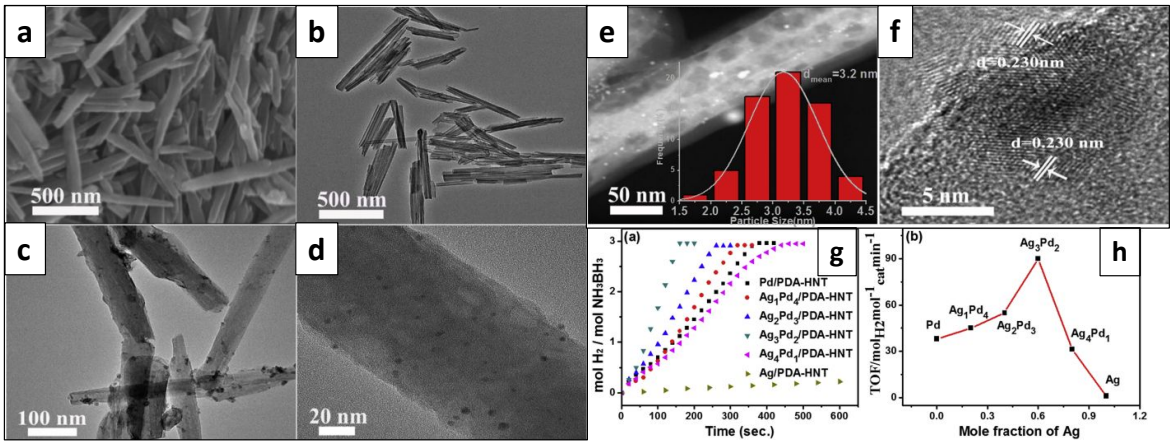

Fig. 37. (a) SEM and (b) TEM images of halloysite nanotubes; (c, d) TEM images of Ag_3Pd_2/PDA-HNTs catalyst; (e) HAADF-image of Ag_3Pd_2/PDA-HNTs nanocatalysts, AgPd alloy nanoparticles corresponding size histogram (inset), (f) HRTEM image of Ag_3Pd_2/PDA-HNTs catalyst; (g) Plots of reaction time versus volume of hydrogen released from the hydrolysis of amino borane (0.2 M, 5 mL) catalyzed by AgPd/PDA-HNT nanocatalysts with different compositions (including Ag/PDA-HNT, Ag_1Pd_4/PDA-HNT, Ag_2Pd_3/PDA-HNT, Ag_3Pd_2/PDA-HNT, Ag_4Pd_1/PDA-HNT, Pd/PDA-HNT), $n_{catalyst}/n_{amino\ borane}$ = 0.0125, T=25 °C; (h) Plot of TOF over nanocatalysts at different Ag:Pd mole ratios. Reprinted from [194], copyright (2018) with permission from Elsevier.

The acid-treated nanotubes and halloysite decorated with hexagonal boron nitride nanoparticles were used as a hydrogen storage medium [195]. These nanoclay-based composites exhibited superior storage capacity at 138 - 175 °C, which makes them promising materials for solid-state hydrogen storage.

Similar research was reported in [196], where boron nitride modified acid-treated halloysite was used. Halloysite support provided uniform dispersion of nitride nanoparticles in lumens and wall interlayer spacing leading to higher hydrogen adsorption.

Halloysite hybridized with a metal-organic framework (MOFs) was tested for hydrogen adsorption ability [197]. The MOFs were carbonized by calcination followed by Pd impregnation to produce a composite with a high specific surface area, uniform pore size, and large pore volume. These textural properties benefit the hydrogen adsorption. The Al-containing MOFs demonstrated higher hydrogen capacity compared to Zn-based samples, which proved the predominant influence of metal selectivity (Fig. 38).

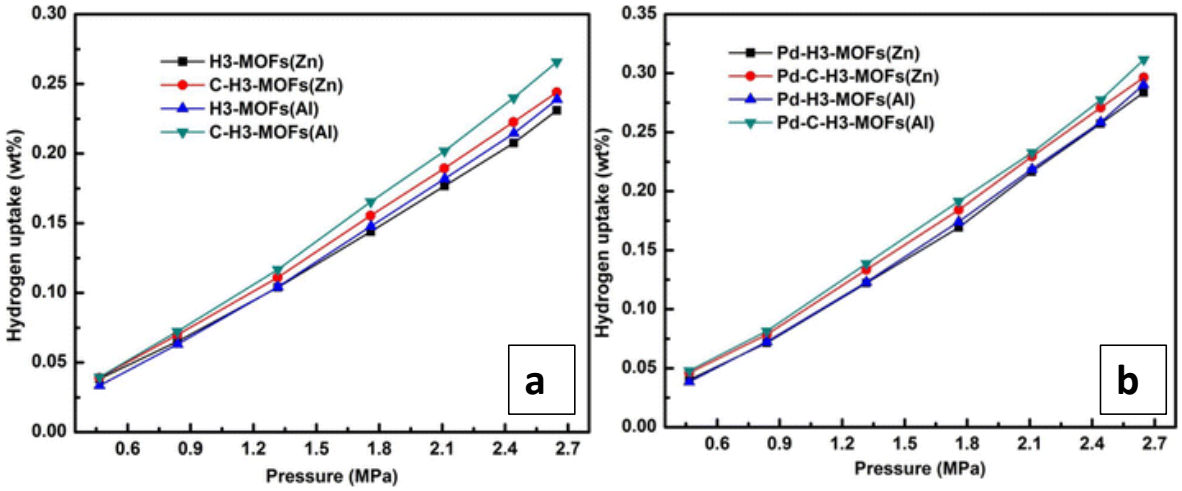

Fig. 38. Hydrogen adsorption isotherms of (a) H3-MOFs(Zn), H3-MOFs(Al), C-H3-MOFs(Zn), C-H3-MOFs(Al) samples, and (b) Pd-containing counterparts (where 3 is the concentration of mixed acid solution). CC BY license, 2017, Springer Nature, Nanoscale research letters[197]

Halloysite-supported polyaniline was reported as potential room-temperature hydrogen storage materials [198]. High hydrogen capacity of 0.78wt.% was due to controlled lumen size. The chemisorption sites are formed through the solid-state milling of polyaniline with the halloysite. Covering of the outer aluminosilicate surface by polyaniline or its penetration into the lumen led to narrowed inner cavity, thus regulating the ability for hydrogen uptake.

High specific surface area and porosity, good cation-exchange capacity, and strong adsorbability of halloysite nanotubes are perfect for hydrogen storage. Contrary to zeolites, carbon nanotubes, and metal-organic frameworks, halloysite is low-cost, biocompatible, and abundantly available natural clay. It may be selectively modified enabling release of gas adsorbed. Development of green technologies for halloysite-based hybrid materials for hydrogen operations is quite promising.

5. Conclusions and prospective

Halloysite is a cheap and abundant aluminosilicate with opportunities for tuning structural and chemical properties, and it is safe and environment-friendly. This tubular nanoclay has SiO_2 outer and Al_2O_3 inner surfaces. Halloysite enables nanoarchitectural core-shell catalytic systems serving as a support for the immobilization of the metal phase. Loading these clay nanotubes with 2-5 nm diameter Au, Pt, Pd, Ru, Rh, Au, Ag, Co, CoMo, Fe_2O_3, Cu-Ni, ZrO_2, and CdS particles or placing these metals outside the tubes demonstrated stable and efficient catalysis. The halloysite nanotubes have to be exploited as a template for design of advanced inorganic-organic hybrid materials used as catalytic support both for homogeneous and heterogeneous catalysis. Due to the unique chemistry, it's external and internal surfaces are differently charged, enabling selective immobilization of functional groups onto inner or outer halloysite surfaces. The functional group may be positioned on the proper surface allowing for controlled catalyst selectivity. This allows for designing the catalysts with tuned wettability for processes in aqueous media or under two-phase conditions (oil-water). The modification of the halloysite tubes' surface with hydrophobic shell protects active components from water leaching. The functionalization with ligands allows for complexation of metal particles, facilitates their immobilization, and controls localization. This is a facile *in situ* procedure to fabricate mesocatalysts with well-dispersed non-agglomerated nanoparticles for enhanced catalytic performance. Such design allows loading one metal selectively inside the nanotubes and a second metal bonding onto the outer tube's surface, producing a dual-metal catalytic system. Nanoclay encapsulation of metal nanoparticles in core-shell structures prevents their aggregation at high temperatures of 400-500 ºC.

Future trends for advances with these materials as a component of hydrogenation catalysts allow for reactants and molecules diffusion control by the modification of nanotubes with ionic liquids and suspended nanoparticles. An attractive approach for the design of selective catalysts is a modification of the halloysite surface by dendrimers or amines. The selective amine functionalities allow for strong anchoring of metal nanoparticles with their selective inner/outer localization. The amino-modified halloysite opens the opportunity for fabrication of hydroformylation catalysts, especially for two-phase condition catalysis. It provides the basis for the effective heterogeneous transformation of syn-gas to value-added chemicals over stable heterogeneous catalysts. Catalytic performance of halloysite-based systems both in dry reforming of methane and Fisher-Tropsch synthesis allows for the tandem process over a one-type catalyst to produce the value-added chemicals or hydrocarbon fuels from methane and carbon dioxide. Therefore, it is an available natural resource to produce clean synthetic fuels as an alternative to those from petroleum feedstocks and CO_2 utilization to reduce the toxic wastes emission through green chemical production.

The application of halloysite as an agent for templating of different organic molecules opens opportunities to fabricate the hybrid organic-inorganic composites with enhanced properties for catalytic transformations. The advances of halloysite-based hybrid functional materials will impact the design of core-shell catalysts for a wide range of applications.

The halloysite-based composites are promising materials for high-temperature mesocatalysts with enhanced properties. Their high thermal and mechanical strength allow usage of halloysite nanotubes as "skeleton" for reinforcement of mesoporous silicates or aluminosilicates (e.g. MCM-41), to develop stronger thermostable materials for oil refining catalysts. Halloysite may be used as a template for well-ordered silica or aluminosilicate (including zeolites) growth

inside/outside of the nanotubes to introduce the higher porosity and surface area in the catalytic support. Its specific surface area can be increased to 400-800 m^2/g by synthesis of halloysite-silica mesoscale composite thus achieving higher dispersion of active phase particles. This development may be extended with tuning acidity of halloysite by acid etching. The adjustment of acid properties helps to improve the activity in acid-catalyzed C-S bond scission and C-C bond isomerization. Halloysite is a pure aluminosilicate clay, and it may be used as a silica and alumina source for the crystallization of zeolites with a desirable porous arrangement, textural properties, and acidity making the synthesis cheaper.

Halloysite nanotubes may act as an arming component for enhancing the thermal and mechanical stability of their catalysts. The 10-15 nm inner lumen of the halloysite provides a transport channel for diffusing reactants and reinforcing hybrid materials allowing to enhance catalysts' lifetime. Therefore, halloysite has a great potential for the supported mesocatalysts for hydrotreating, isomerization, and hydrocracking processes.

Halloysite nanotubes are prospective for hydrogen storage: they have a specific surface area up to 400 m^2/g, high porosity and cation-exchange capacity, and strong absorbability. Different from zeolites, carbon nanotubes, and metal-organic frameworks, halloysite is a low-cost, bio-safe, and abundantly available natural material. Due to the wide opportunities for its modifications, halloysite-based materials may enhance green technologies for hydrogen usage as an energy source replacing fossil fuels.

Another direction is introducing the clay tubes as nano-confined reactors. The outer tube’s surface could be hydrophobized with organosilanes while the lumen is loaded with metal nanoparticles. This architectural strategy allows for using these systems for biphasic catalysis and is interesting for bio-oil hydrofining without the stage of water removal. As for transition metal sulfide-based catalysts, this conception of loading the internal cavity allows for protection of active species from coking and leaching. This approach also may be applicable for the layered materials design because the assembly of multilayered sulfides is limited by the inner diameter of halloysite nanotubes. The intercalation of metal nanoparticles into the more acidic tubular lumen provides stronger bonding of active species, enhancing the dispersion.

The future trends in the clay nanotube-based metal-core catalysts for hydroprocessing are as follows:

(1) Outer tubes’ surface functionalization with zeolites and structured mesoporous silica to increase textural properties of composites with bimodal pore size distribution and catalysts for heavy oil and residue upgrading (hydrotreating and hydrocracking).
(2) Tuning acidity of halloysite by acid etching and/or zeolites formation inside/outside the surface of the nanotubes for acid-catalyzed reactions (alkanes and xylenes isomerization, hydrocracking).
(3) Multi-shell structure formation with nanoparticles and ionic liquids for biphase catalysis and diffusion control of reactants and products (selective hydrogenation, hydroformylation).
(4) Halloysite-based catalysts with active phase protection (noble metals promoted or transition metals sulfides and phosphides core-shell nanosystems) for hydrotreating and S, N, O species removal.
(5) New zeolites or structured mesoporous materials synthesis from halloysite (both as a Si/Al precursor and template of low cost).
(6) The nanotubes surface modification and passivators loading for protective layers and fluid catalytic cracking additives.

Halloysite nanoclay is a cheap and environment-friendly material, available at thousand tons, which promises an industrial scale-up of the proposed catalytic processes with enhanced efficiency.

Acknowledgments

This work was supported by the Russian Science Foundation (RSF project № 19-79-10016 in parts of petrochemical and oil refining hydroprocesses). YL thanks for a partial support Louisiana Board of Regents LEQSF(2021)- RDD-03 grant. The authors thank Maria Rubtsova from Gubkin University for technical help, and Faith Scott from Louisiana Technical University for English editing.

References

1. Y. Lvov, W. Wang, L. Zhang and R. Fakhrullin, *Advanced Materials*, 2016, **28**, 1227-1250.
2. G. Lazzara, G. Cavallaro, A. Panchal, R. Fakhrullin, A. Stavitskaya, V. Vinokurov and Y. Lvov, *Current Opinion in Colloid & Interface Science*, 2018, **35**, 42-50.
3. D. Papoulis, *Applied Clay Science*, 2019, **168**, 164-174.
4. P. Yuan, D. Tan and F. Annabi-Bergaya, *Applied Clay Science*, 2015, **112-113**, 75-93.
5. M. Massaro, C. G. Colletti, G. Lazzara, S. Milioto, R. Noto and S. Riela, *Journal of Materials Chemistry A*, 2017, **5**, 13276-13293.
6. Y. Lvov, A. Panchal, Y. Fu, R. Fakhrullin, M. Kryuchkova, S. Batasheva, A. Stavitskaya, A. Glotov and V. Vinokurov, *Langmuir*, 2019, **35**, 8646-8657.
7. A. Glotov, A. Stavitskaya, A. Novikov, A. Semenov, E. Ivanov, P. Gushchin, Y. Darrat, V. Vinokurov and Y. Lvov, in *Nanomaterials from Clay Minerals*, eds. A. Wang and W. Wang, Elsevier, 2019, pp. 203-256.
8. S. Sadjadi, *Applied Clay Science*, 2020, **189**, 31.
9. S. Sadjadi, M. Malmir, N. Pourmohammad, S. Ahmadi and M. M. Heravi, *Res. Chem. Intermed.*, 2019, **45**, 4349-4366.
10. A. Glotov, N. Levshakov, A. Stavitskaya, M. Artemova, P. Gushchin, E. Ivanov, V. Vinokurov and Y. Lvov, *Chem. Commun.*, 2019, **55**, 5507-5510.
11. J. Keeling, 2015, pp. 96-115.
12. W. O. Yah, H. Xu, H. Soejima, W. Ma, Y. Lvov and A. Takahara, *Journal of the American Chemical Society*, 2012, **134**, 12134-12137.
13. A. Glotov, A. Novikov, A. Stavitskaya, V. Nedolivko, D. Kopitsyn, A. Kuchierskaya, E. Ivanov, V. Stytsenko, V. Vinokurov and Y. Lvov, *Catalysis Today*, 2020.
14. T. Rostamzadeh, M. S. Islam Khan, K. Riche', Y. M. Lvov, A. V. Stavitskaya and J. B. Wiley, *Langmuir*, 2017, **33**, 13051-13059.
15. E. Abdullayev, A. Joshi, W. Wei, Y. Zhao and Y. Lvov, *ACS Nano*, 2012, **6**, 7216-7226.
16. M. Massaro, G. Lazzara, R. Noto and S. Riela, *Rend. Lincei.-Sci. Fis. Nat.*, 9.
17. Y. M. Lvov, M. M. DeVilliers and R. F. Fakhrullin, *Expert Opinion on Drug Delivery*, 2016, **13**, 977-986.
18. R. R. Price, B. P. Gaber and Y. Lvov, *Journal of microencapsulation*, 2001, **18**, 713-722.
19. M. Saif and H. Asif, *Journal of the Chilean Chemical Society*, 2015, **60**, 2949-2953.
20. D. M.E Phd and Y. Agrawal, *Reviews on Advanced Materials Science*, 2012, **30**, 282-295.
21. M. Liu, Z. Jia, D. Jia and C. Zhou, *Progress in Polymer Science*, 2014, **39**, 1498-1525.
22. A. Panchal, G. Fakhrullina, R. Fakhrullin and Y. Lvov, *Nanoscale*, 2018, **10**, 18205-18216.

23. A. Glotov, A. Stavitskaya, Y. Chudakov, E. Ivanov, W. Huang, V. Vinokurov, A. Zolotukhina, A. Maximov, E. Karakhanov and Y. Lvov, *Bull. Chem. Soc. Jpn.*, 2019, **92**, 61-69.
24. O. S. Patrusheva, K. P. Volcho and N. F. Salakhutdinov, *Russ. Chem. Rev.*, 2018, **87**, 771-796.
25. E. Nazimova, A. Pavlova, O. Mikhalchenko, I. Il'ina, D. Korchagina, T. y. Tolstikova, K. Volcho and N. Salakhutdinov, *Medicinal Chemistry Research*, 2016, **25**, 1369-1383.
26. M. N. Timofeeva, K. P. Volcho, O. S. Mikhalchenko, V. N. Panchenko, V. V. Krupskaya, S. V. Tsybulya, A. Gil, M. A. Vicente and N. F. Salakhutdinov, *Journal of Molecular Catalysis A: Chemical*, 2015, **398**, 26-34.
27. M. N. Timofeeva, V. N. Panchenko, A. Gil, S. V. Zakusin, V. V. Krupskaya, K. P. Volcho and M. A. Vicente, *Catalysis Communications*, 2015, **69**, 234-238.
28. A. Y. Sidorenko, A. V. Kravtsova, A. Aho, I. Heinmaa, J. Warna, H. Pazniak, K. P. Volcho, N. F. Salakhutdinov, D. Y. Murzin and V. E. Agabekov, *J. Catal.*, 2019, **374**, 360-377.
29. V. A. Vinokurov, A. V. Stavitskaya, A. P. Glotov, A. A. Novikov, A. V. Zolotukhina, M. S. Kotelev, P. A. Gushchin, E. V. Ivanov, Y. Darrat and Y. M. Lvov, *Chem. Rec.*, 2018, **18**, 858-867.
30. V. A. Vinokurov, A. V. Stavitskaya, Y. A. Chudakov, E. V. Ivanov, L. K. Shrestha, K. Ariga, Y. A. Darrat and Y. M. Lvov, *Science and Technology of Advanced Materials*, 2017, **18**, 147-151.
31. B. Micó-Vicent, F. M. Martínez-Verdú, A. Novikov, A. Stavitskaya, V. Vinokurov, E. Rozhina, R. Fakhrullin, R. Yendluri and Y. Lvov, *Advanced Functional Materials*, 2018, **28**, 1703553.
32. N. M. Sanchez-Ballester, G. V. Ramesh, T. Tanabe, E. Koudelkova, J. Liu, L. K. Shrestha, Y. Lvov, J. P. Hill, K. Ariga and H. Abe, *Journal of Materials Chemistry A*, 2015, **3**, 6614-6619.
33. V. Vinokurov, A. Glotov, Y. Chudakov, A. Stavitskaya, E. Ivanov, P. Gushchin, A. Zolotukhina, A. Maximov, E. Karakhanov and Y. Lvov, *Ind. Eng. Chem. Res.*, 2017, **56**, 14043-14052.
34. M. Karaismailoglu, H. E. Figen and S. Z. Baykara, *Acta Phys. Pol. A*, 2018, **134**, 57-60.
35. K. Ariga, H. Abe, Q. Ji and Y. M. Lvov, in *Functional Polymer Composites with Nanoclays*, The Royal Society of Chemistry, 2017, pp. 207-222.
36. A. V. Stavitskaya, E. A. Kozlova, A. Y. Kurenkova, A. P. Glotov, D. S. Selischev, E. V. Ivanov, D. V. Kozlov, V. A. Vinokurov, R. F. Fakhrullin and Y. M. Lvov, *Chemistry – A European Journal*, 2020, **26**, 13085-13092.
37. V. A. Vinokurov, A. V. Stavitskaya, E. V. Ivanov, P. A. Gushchin, D. V. Kozlov, A. Y. Kurenkova, P. A. Kolinko, E. A. Kozlova and Y. M. Lvov, *ACS Sustainable Chemistry & Engineering*, 2017, **5**, 11316-11323.
38. N. Bahri-Laleh, S. Sadjadi and A. Poater, *Journal of Colloid and Interface Science*, 2018, **531**, 421-432.
39. J. Hamdi, A. A. Blanco, B. Diehl, J. B. Wiley and M. L. Trudell, *Org. Lett.*, 2019, **21**, 3471-3475.
40. P. Krishnaiah, C. T. Ratnam and S. Manickam, *Applied Clay Science*, 2017, **135**, 583-595.
41. M. Massaro, C. G. Colletti, G. Buscemi, S. Cataldo, S. Guernelli, G. Lazzara, L. F. Liotta, F. Parisi, A. Pettignano and S. Riela, *New J. Chem.*, 2018, **42**, 13938-13947.
42. M. Massaro, S. Riela, G. Cavallaro, C. G. Colletti, S. Milioto, R. Noto, F. Parisi and G. Lazzara, *Journal of Molecular Catalysis A: Chemical*, 2015, **408**, 12-19.
43. M. Massaro, S. Riela, G. Cavallaro, M. Gruttadauria, S. Milioto, R. Noto and G. Lazzara, *Journal of Organometallic Chemistry*, 2014, **749**, 410-415.

44. S. Sadjadi, M. Akbari, E. Monflier, M. M. Heravi and B. Leger, *New J. Chem.*, 2018, **42**, 15733-15742.
45. S. Sadjadi and M. Atai, *Applied Clay Science*, 2018, **153**, 78-89.
46. S. Sadjadi, M. M. Heravi and S. S. Kazemi, *Carbohydrate Polymers*, 2018, **200**, 183-190.
47. S. Sadjadi, M. M. Heravi and M. Malmir, *Carbohydrate Polymers*, 2018, **186**, 25-34.
48. S. Sadjadi, M. M. Heravi, M. Malmir and F. Noritajer, *Materials Chemistry and Physics*, 2019, **223**, 380-390.
49. S. Sadjadi, F. Koohestani, N. Bahri-Laleh and K. Didehban, *J. Solid State Chem.*, 2019, **271**, 59-66.
50. S. Sadjadi, M. Malmir, M. M. Heravi and F. G. Kahangi, *International Journal of Biological Macromolecules*, 2018, **118**, 1903-1911.
51. A. P. Glotov, A. V. Stavitskaya, Y. A. Chudakov, M. I. Artemova, E. M. Smirnova, N. R. Demikhova, T. N. Shabalina, A. A. Gureev and V. A. Vinokurov, *Pet. Chem.*, 2018, **58**, 1221-1226.
52. V. V. Nedolivko, G. O. Zasypalov, Y. A. Chudakov, A. V. Vutolkina, A. Pimerzin and A. P. Glotov, *Russ. Chem. Bull.*, 2020, **69**, 260-264.
53. S. Sadjadi, F. Ghoreyshi Kahangi and M. M. Heravi, *Polyhedron*, 2020, **175**, 114210.
54. S. Dehghani, S. Sadjadi, N. Bahri-Laleh, M. Nekoomanesh-Haghighi and A. Poater, *Appl. Organomet. Chem.*, 2019, **33**, 10.
55. S. Sadjadi, M. Akbari and M. M. Heravi, *ACS Omega*, 2019, **4**, 19442-19451.
56. S. Sadjadi, M. Akbari, B. Leger, E. Monflier and M. M. Heravi, *Acs Sustainable Chemistry & Engineering*, 2019, **7**, 6720-6731.
57. S. Sadjadi and F. Koohestani, *J. Mol. Liq.*, 2020, **301**, 9.
58. S. Sadjadi, G. Lazzara, M. M. Heravi and G. Cavallaro, *Applied Clay Science*, 2019, **182**, 14.
59. S. Sadjadi and M. Tavakolian, *ChemistrySelect*, 2019, **4**, 3369-3375.
60. M. Z. Z. Cai, H. Dai, Y. Liu, J. Mao, X. Chen, C. He *Advances in Chemical Engineering and Science*, 2011, **1**, 15-19.
61. Z.-L. Cheng and W. Sun, *Chinese Chemical Letters*, 2016, **27**, 81-84.
62. A. Philip, J. Lihavainen, M. Keinänen and T. T. Pakkanen, *Applied Clay Science*, 2017, **143**, 80-88.
63. Y. H. Ahmad, A. T. Mohamed, K. A. Mahmoud, A. S. Aljaber and S. Y. Al-Qaradawi, *RSC Adv.*, 2019, **9**, 32928-32935.
64. P. Liu and M. Zhao, *Applied Surface Science*, 2009, **255**, 3989-3993.
65. M. Zou, M. Du, M. Zhang, T. Yang, H. Zhu, P. Wang and S. Bao, *Materials Research Bulletin*, 2015, **61**, 375-382.
66. M. Massaro, C. G. Colletti, B. Fiore, V. La Parola, G. Lazzara, S. Guernelli, N. Zaccheroni and S. Riela, *Appl. Organomet. Chem.*, 2019, **33**, 11.
67. A. P. Glotov, M. I. Artemova, N. R. Demikhova, E. M. Smirnova, E. V. Ivanov, P. A. Gushchin, S. V. Egazar'yants and V. A. Vinokurov, *Pet. Chem.*, 2019, **59**, 1226-1234.
68. J. A. Torres-Luna, S. Moreno, R. Molina and J. G. Carriazo, *Energy & Fuels*, 2019, **33**, 12647-12655.
69. J. A. Torres-Luna, S. Moreno, R. Molina and J. G. Carriazo, *Energy & Fuels*, 2018, **32**, 9782-9792.
70. V. M. Abbasov, H. C. Ibrahimov, G. S. Mukhtarova and E. Abdullayev, *Fuel*, 2016, **184**, 555-558.
71. A. Hasanova, A. Alizade, R. Ahmadova, G. Mukhtarova and V. Abbasov, *Appl. Petrochem. Res.*, 2019, **9**, 199-209.
72. G. S. Mukhtarova, *Process. Petrochem. Oil Refin.*, 2015, **16**, 120-130.
73. G. S. Mukhtarova, A. B. Hasanova, A. D. Guliyev, M. E. Huseynova, L. A. Mahmudova, A. E. Alizada, H. J. Ibrahimov and V. M. Abbasov, *Process. Petrochem. Oil Refin.*, 2018, **19**, 206-210.

74. A. B. Hasanova, *Process. Petrochem. Oil Refin.*, 2019, **20**, 449-457.
75. G. S. Muktarova, A. B. Hasanova, S. F. Ahmedbeyova, A. D. Guliyev, H. C. Ibrahimov and V. M. Abbasov, *Chem. Probl.*, 2018, 537-543.
76. G. S. Muhtarova, Z. M. Ibrahimova, A. B. Hasanova, H. C. Ibrahimov and V. M. Abbasov, *Tekhnologii nefti i gaza*, 2018, 9-14.
77. V. Abbasov, T. Mammadova, N. Aliyeva, M. Abbasov, N. Movsumov, A. Joshi, Y. Lvov and E. Abdullayev, *Fuel*, 2016, **181**, 55-63.
78. V. Abbasov, T. Mammadova, N. Andrushenko, N. Hasankhanova, Y. Lvov and E. Abdullayev, *Fuel*, 2014, **117**, 552-555.
79. S. Chen, J. Li, Y. Zhang, D. Zhang and J. Zhu, *Journal of Natural Gas Chemistry*, 2012, **21**, 426-430.
80. V. P. Ananikov, *Nanomaterials*, 2019, **9**, 1197.
81. C. Sanchez, B. Julián, P. Belleville and M. Popall, *Journal of Materials Chemistry*, 2005, **15**, 3559-3592.
82. C. Laberty-Robert, K. Vallé, F. Pereira and C. Sanchez, *Chemical Society Reviews*, 2011, **40**, 961-1005.
83. V. Vinokurov, A. Stavitskaya, A. Glotov, A. Ostudin, M. Sosna, P. Gushchin, Y. Darrat and Y. Lvov, *J. Solid State Chem.*, 2018, **268**, 182-189.
84. S. Battistoni, A. Dimonte, E. Ubaldi, Y. Lvov and V. Erokhin, *Journal of Nanoscience and Nanotechnology*, 2017, **17**, 5310-5317.
85. S. Sadjadi, F. Koohestani, B. Leger and E. Monflier, *Appl. Organomet. Chem.*, 13.
86. S. Sadjadi, M. Malmir, G. Lazzara, G. Cavallaro and M. M. Heravi, *Scientific reports*, 2020, **10**, 2039.
87. E. Karakhanov, A. Maximov, M. Terenina, V. Vinokurov, L. Kulikov, D. Makeeva and A. Glotov, *Catalysis Today*, 2020, **357**, 176-184.
88. A. Glotov, A. Vutolkina, A. Pimerzin, V. Nedolivko, G. Zasypalov, V. Stytsenko, E. Karakhanov and V. Vinokurov, *Catalysts*, 2020, **10**, 537.
89. R. D. Neal, Y. Inoue, R. A. Hughes and S. Neretina, *The Journal of Physical Chemistry C*, 2019, **123**, 12894-12901.
90. J. Strachan, C. Barnett, A. F. Masters and T. Maschmeyer, *ACS Catalysis*, 2020, **10**, 5516-5521.
91. T. Aditya, A. Pal and T. Pal, *Chem. Commun.*, 2015, **51**, 9410-9431.
92. P. Zhao, X. Feng, D. Huang, G. Yang and D. Astruc, *Coordination Chemistry Reviews*, 2015, **287**, 114-136.
93. Z. D. Pozun, S. E. Rodenbusch, E. Keller, K. Tran, W. Tang, K. J. Stevenson and G. Henkelman, *The Journal of Physical Chemistry C*, 2013, **117**, 7598-7604.
94. S. Das and S. Jana, *Dalton Trans.*, 2015, **44**, 8906-8916.
95. G. K. Dedzo and C. Detellier, *Advanced Functional Materials*, 2018, **28**, 12.
96. G. K. Dedzo, G. Ngnie and C. Detellier, *ACS Applied Materials & Interfaces*, 2016, **8**, 4862-4869.
97. X. B. Gao, F. Tang and Z. X. Jin, *Langmuir*, 2019, **35**, 14651-14658.
98. D. Gorbunov, M. Nenasheva, M. Terenina, Y. Kardasheva, A. Maksimov and E. Karakhanov, *ChemistrySelect*, 2020, **5**, 6407-6414.
99. D. N. Gorbunov, M. V. Nenasheva, R. P. Matsukevich, M. V. Terenina, F. N. Putilin, Y. S. Kardasheva, A. L. Maksimov and E. A. Karakhanov, *Pet. Chem.*, 2019, **59**, 1009-1016.
100. R. Franke, D. Selent and A. Börner, *Chemical Reviews*, 2012, **112**, 5675-5732.
101. M. L. Clarke, *Angewandte Chemie International Edition*, 2016, **55**, 13377-13377.
102. G. M. Torres, R. Frauenlob, R. Franke and A. Börner, *Catalysis Science & Technology*, 2015, **5**, 34-54.
103. D. Gorbunov, D. Safronova, Y. Kardasheva, A. Maximov, E. Rosenberg and E. Karakhanov, *ACS Applied Materials & Interfaces*, 2018, **10**, 26566-26575.

104. J. Tang, P. J. Quinlan and K. C. Tam, *Soft Matter*, 2015, **11**, 3512-3529.
105. D. Gonzalez Ortiz, C. Pochat-Bohatier, J. Cambedouzou, M. Bechelany and P. Miele, *Engineering*, 2020, **6**, 468-482.
106. O. L. Armstrong, S. N. Baxter, F. L. Deepak and P. J. Thomas, *Chem. Commun.*, 2020, **56**, 4801-4803.
107. F. Chang, C. M. Vis, W. Ciptonugroho and P. C. A. Bruijnincx, *Green Chemistry*, 2021, **23**, 2575-2594.
108. A. L. Sadgar, T. S. Deore and R. V. Jayaram, *ACS Omega*, 2020, **5**, 12224-12235.
109. D. Stehl, N. Milojevic, S. Stock, R. Schomacker and R. von Klitzing, *Ind. Eng. Chem. Res.*, 2019, **58**, 2524-2536.
110. D. Stehl, T. Skale, L. Hohl, Y. Lvov, J. Koetz, M. Kraume, A. Drews and R. von Klitzing, *ACS Applied Nano Materials*, 2020, **3**, 11743-11751.
111. M. V. Kulikova, *Catalysis Today*, 2020, **348**, 89-94.
112. H. Jahangiri, J. Bennett, P. Mahjoubi, K. Wilson and S. Gu, *Catalysis Science & Technology*, 2014, **4**, 2210-2229.
113. A. Y. Krylova, *Solid Fuel Chemistry*, 2014, **48**, 22-35.
114. Z. Gholami, Z. Tišler and V. Rubáš, *Catalysis Reviews*, 2020, 1-84.
115. E. Peluso, C. Galarraga and H. de Lasa, *Chemical Engineering Science*, 2001, **56**, 1239-1245.
116. E. Iglesia, S. L. Soled, J. E. Baumgartner and S. C. Reyes, *J. Catal.*, 1995, **153**, 108-122.
117. W. D. Shafer, M. K. Gnanamani, U. M. Graham, J. Yang, C. M. Masuku, G. Jacobs and B. H. Davis, *Catalysts*, 2019, **9**, 259.
118. R.-J. Liu, Y. Xu, Y. Qiao, Z.-H. Li and X.-B. Ma, *Fuel Processing Technology*, 2015, **139**, 25-32.
119. A. Stavitskaya, K. Mazurova, M. Kotelev, O. Eliseev, P. Gushchin, A. Glotov, R. Kazantsev, V. Vinokurov and Y. Lvov, *Molecules (Basel, Switzerland)*, 2020, **25**.
120. E. Karakhanov, A. Maximov, A. Zolotukhina, V. Vinokurov, E. Ivanov and A. Glotov, *Catalysts*, 2020, **10**, 15.
121. A. Glotov, A. Vutolkina, M. Artemova, N. Demikhova, E. Smirnova, E. Roldugina, A. Stavitskaya, E. Ivanov, S. Egazar'yants and V. Vinokurov, *Applied Catalysis A: General*, 2020, **603**, 117764.
122. M. Guisnet, N. S. Gnep and S. Morin, *Microporous and Mesoporous Materials*, 2000, **35-36**, 47-59.
123. A. Glotov, N. Demikhova, M. Rubtsova, D. Melnikov, D. Tsaplin, P. Gushchin, S. Egazar'yants, A. Maximov, E. Karakhanov and V. Vinokurov, *Catalysis Today*, 2021.
124. M. Guisnet, *Catalysis Today*, 2013, **218-219**, 123-134.
125. A. P. Glotov, E. A. Roldugina, M. I. Artemova, E. M. Smirnova, N. R. Demikhova, V. D. Stytsenko, S. V. Egazar'yants, A. L. Maksimov and V. A. Vinokurov, *Russ. J. Appl. Chem.*, 2018, **91**, 1353-1362.
126. A. Corma and E. Sastre, *J. Catal.*, 1991, **129**, 177-185.
127. L. Fu, H. Yang, A. Tang and Y. Hu, *Nano Research*, 2017, **10**, 2782-2799.
128. Z. Shu, Y. Chen, J. Zhou, T. Li, Z. Sheng, C. Tao and Y. Wang, *Applied Clay Science*, 2016, **132-133**, 114-121.
129. R. Bingre, B. Louis and P. Nguyen, *Catalysts*, 2018, **8**, 163.
130. A. P. Glotov, A. V. Vutolkina, N. A. Vinogradov, A. A. Pimerzin, V. A. Vinokurov and A. A. Pimerzin, *Catalysis Today*, 2020.
131. E. Naranov, O. Golubev, K. Zanaveskin, A. Guseva, P. Nikulshin, Y. Kolyagin, A. Maximov and E. Karakhanov, *ACS Omega*, 2020, **5**, 6611-6618.
132. E. R. Naranov, O. V. Golubev, A. I. Guseva, P. A. Nikulshin, A. L. Maksimov and E. A. Karakhanov, *Pet. Chem.*, 2017, **57**, 1151-1155.
133. A. V. Vutolkina, A. P. Glotov, A. V. Zanina, D. F. Makhmutov, A. L. Maximov, S. V. Egazar'yants and E. A. Karakhanov, *Catalysis Today*, 2019, **329**, 156-166.

134. R. Sahu, B. J. Song, J. S. Im, Y.-P. Jeon and C. W. Lee, *Journal of Industrial and Engineering Chemistry*, 2015, **27**, 12-24.
135. P. Dugkhuntod and C. Wattanakit, *Catalysts*, 2020, **10**, 245.
136. A. Galadima and O. Muraza, *Journal of Industrial and Engineering Chemistry*, 2018, **61**, 265-280.
137. D. Verboekend, N. Nuttens, R. Locus, J. Van Aelst, P. Verolme, J. C. Groen, J. Pérez-Ramírez and B. F. Sels, *Chemical Society Reviews*, 2016, **45**, 3331-3352.
138. A. Corma, A. Martinez, V. Martinezsoria and J. B. Monton, *J. Catal.*, 1995, **153**, 25-31.
139. A. R. Hasanova, *Process. Petrochem. Oil Refin.*, 2019, **20**, 314-320.
140. T. A. Mammadova, A. R. Hasanova, M. M. Abbasov, E. S. Abdullayev, V. M. Abbasov and S. A. Mammadkhanova, *Process. Petrochem. Oil Refin.*, 2017, **18**, 381-389.
141. A. Pimerzin, A. Mozhaev, A. Varakin, K. Maslakov and P. Nikulshin, *Applied Catalysis B: Environmental*, 2017, **205**, 93-103.
142. D. Ishutenko, P. Nikulshin and A. Pimerzin, *Catalysis Today*, 2016, **271**, 16-27.
143. P. A. Nikulshin, D. I. Ishutenko, A. A. Mozhaev, K. I. Maslakov and A. A. Pimerzin, *J. Catal.*, 2014, **312**, 152-169.
144. P. A. Nikulshin, V. A. Salnikov, A. V. Mozhaev, P. P. Minaev, V. M. Kogan and A. A. Pimerzin, *J. Catal.*, 2014, **309**, 386-396.
145. A. Pimerzin, A. Roganov, A. Mozhaev, K. Maslakov, P. Nikulshin and A. Pimerzin, *Fuel Processing Technology*, 2018, **173**, 56-65.
146. A. Kokliukhin, M. Nikulshina, A. Sheldaisov-Meshcheryakov, A. Mozhaev and P. Nikulshin, *Catalysis Letters*, 2018, **148**, 2869-2879.
147. A. N. Varakin, V. A. Salnikov, M. S. Nikulshina, K. I. Maslakov, A. V. Mozhaev and P. A. Nikulshin, *Catalysis Today*, 2017, **292**, 110-120.
148. A. A. Pimerzin, D. I. Ishutenko, A. V. Mozhaev, V. M. Kapustin, E. A. Chernysheva, A. V. Maximova, A. A. Pimerzin and P. A. Nikulshin, *Fuel Processing Technology*, 2017, **156**, 98-106.
149. A. A. Pimerzin, P. A. Nikul'shin, A. V. Mozhaev and A. A. Pimerzin, *Pet. Chem.*, 2013, **53**, 245-254.
150. A. V. Vutolkina, I. G. Baygildin, A. P. Glotov, K. A. Cherednichenko, A. L. Maksimov and E. A. Karakhanov, *Applied Catalysis B: Environmental*, 2021, **282**, 119616.
151. A. Glotov, N. Levshakov, A. Vutolkina, S. Lysenko, E. Karakhanov and V. Vinokurov, *Catalysis Today*, 2019, **329**, 135-141.
152. E. A. Karakhanov, A. P. Glotov, A. G. Nikiforova, A. V. Vutolkina, A. O. Ivanov, S. V. Kardashev, A. L. Maksimov and S. V. Lysenko, *Fuel Processing Technology*, 2016, **153**, 50-57.
153. S. Nair, A. H. M. Shahadat Hussain and B. J. Tatarchuk, *Fuel*, 2013, **105**, 695-704.
154. O. V. Potapenko, V. P. Doronin and T. P. Sorokina, *Pet. Chem.*, 2012, **52**, 55-59.
155. T. Henmi and K. Wada, *Clay Minerals*, 2018, **10**, 231-245.
156. Y. Em, A. Stoporev, A. Semenov, A. Glotov, E. Smirnova, G. Villevald, V. Vinokurov, A. Manakov and Y. Lvov, *ACS Sustainable Chemistry & Engineering*, 2020, **8**, 7860-7868.
157. R. K. Parsapur, S. Chatterjee and K.-W. Huang, *ACS Energy Letters*, 2020, **5**, 2881-2885.
158. V. V. Nedolivko, G. O. Zasypalov, A. V. Vutolkina, P. A. Gushchin, V. A. Vinokurov, L. A. Kulikov, S. V. Egazar'yants, E. A. Karakhanov, A. L. Maksimov and A. P. Glotov, *Russ. J. Appl. Chem.*, 2020, **93**, 765-787.
159. D. Pakhare and J. Spivey, *Chemical Society Reviews*, 2014, **43**, 7813-7837.
160. N. A. K. Aramouni, J. G. Touma, B. A. Tarboush, J. Zeaiter and M. N. Ahmad, *Renewable and Sustainable Energy Reviews*, 2018, **82**, 2570-2585.
161. W.-J. Jang, J.-O. Shim, H.-M. Kim, S.-Y. Yoo and H.-S. Roh, *Catalysis Today*, 2019, **324**, 15-26.

162. M. Akri, S. Zhao, X. Li, K. Zang, A. F. Lee, M. A. Isaacs, W. Xi, Y. Gangarajula, J. Luo, Y. Ren, Y.-T. Cui, L. Li, Y. Su, X. Pan, W. Wen, Y. Pan, K. Wilson, L. Li, B. Qiao, H. Ishii, Y.-F. Liao, A. Wang, X. Wang and T. Zhang, *Nature Communications*, 2019, **10**, 5181.
163. S. Arora and R. Prasad, *RSC Adv.*, 2016, **6**, 108668-108688.
164. M. Lu, J. Fang, L. Han, K. Faungnawakij, H. Li, S. Cai, L. Shi, H. Jiang and D. Zhang, *Nanoscale*, 2018, **10**.
165. Z. Zhao, P. Ren and W. Li, *RSC Adv.*, 2016, **6**, 49487-49496.
166. C. Peng, D. Yu, L. Wang, X. Yu and Z. Zhao, *Journal of Materials Chemistry A*, 2021.
167. H. Dai, *Science Bulletin*, 2015, **60**, 1708-1710.
168. V. N. Rogozhnikov, A. V. Kulikov, D. I. Potemkin, A. P. Glotov, G. O. Zasypalov and P. V. Snytnikov, *Catalysis Communications*, 2021, **149**, 106198.
169. V. N. Rogozhnikov, D. I. Potemkin, V. P. Pakharukova, V. D. Belyaev, V. V. Nedolivko, A. P. Glotov, V. A. Sobyanin and P. V. Snytnikov, *Int. J. Hydrog. Energy*, 2021.
170. K. Fujiwara, K. Okuyama and S. E. Pratsinis, *Environmental Science: Nano*, 2017, **4**, 2076-2092.
171. V. N. Rogozhnikov, A. N. Salanov, D. I. Potemkin, A. P. Glotov, S. V. Boev and P. V. Snytnikov, *Materials Letters*, 2021, **283**, 128855.
172. W. J. Li and M. Y. Wey, *Sci. Total Environ.*, 2019, **675**, 397-407.
173. L. Kang, L. P. Han, J. B. He, H. R. Li, T. T. Yan, G. R. Chen, J. P. Zhang, L. Y. Shi and D. S. Zhang, *Environ. Sci. Technol.*, 2019, **53**, 938-945.
174. J. Ouyang, Z. Zhao, H. Yang, Y. Zhang and A. Tang, *Applied Clay Science*, 2018, **152**, 221-229.
175. J. Ouyang, Z. Zhao, Y. Zhang and H. Yang, *Journal of Colloid and Interface Science*, 2017, **505**, 430-436.
176. Z. Zhou, J. Ouyang, H. Yang and A. Tang, *Applied Clay Science*, 2016, **121-122**, 63-70.
177. X. Zhang, P. Wang, X. Wu, S. Lv and J. Dai, *Catalysis Communications*, 2016, **83**, 18-21.
178. A. Schneemann, J. L. White, S. Kang, S. Jeong, L. F. Wan, E. S. Cho, T. W. Heo, D. Prendergast, J. J. Urban, B. C. Wood, M. D. Allendorf and V. Stavila, *Chemical Reviews*, 2018, **118**, 10775-10839.
179. M. E. Konnova, S. V. Vostrikov, A. A. Pimerzin and S. P. Verevkin, *The Journal of Chemical Thermodynamics*, 2021, **159**, 106455.
180. R. Moradi and K. M. Groth, *Int. J. Hydrog. Energy*, 2019, **44**, 12254-12269.
181. V. N. Emel'yanenko, M. A. Varfolomeev, S. P. Verevkin, K. Stark, K. Müller, M. Müller, A. Bösmann, P. Wasserscheid and W. Arlt, *The Journal of Physical Chemistry C*, 2015, **119**, 26381-26389.
182. S. P. Verevkin, A. A. Pimerzin and L.-X. Sun, *The Journal of Chemical Thermodynamics*, 2020, **144**, 106057.
183. M. Mohan, V. K. Sharma, E. A. Kumar and V. Gayathri, *Energy Storage*, 2019, **1**, e35.
184. Y. Zhao, W. Kong, Z. Jin, Y. Fu, W. Wang, Y. Zhang, J. Liu and B. Zhang, *Applied Energy*, 2018, **222**, 180-188.
185. C. W. Hamilton, R. T. Baker, A. Staubitz and I. Manners, *Chemical Society Reviews*, 2009, **38**, 279-293.
186. G. Chen, L. N. Zakharov, M. E. Bowden, A. J. Karkamkar, S. M. Whittemore, E. B. Garner, T. C. Mikulas, D. A. Dixon, T. Autrey and S.-Y. Liu, *Journal of the American Chemical Society*, 2015, **137**, 134-137.
187. L. Yin, Y. Feng, X. Zhou, K. Dai, X. Gao, Y. Zhao and B. Zhang, *Chemistry Letters*, 2019, **48**, 1084-1087.
188. N. Sahiner and S. B. Sengel, *Applied Clay Science*, 2017, **146**, 517-525.
189. N. Sahiner and S. B. Sengel, *Fuel Processing Technology*, 2017, **158**, 1-8.
190. L. Wang, J. Chen, L. Ge, Z. Zhu and V. Rudolph, *Energy & Fuels*, 2011, **25**, 3408-3416.

191. X. Tang, L. Li, B. Shen and C. Wang, *Chemosphere*, 2013, **91**, 1368-1373.
192. Y. Liu, J. Zhang, H. J. Guan, Y. F. Zhao, J. H. Yang and B. Zhang, *Applied Surface Science*, 2018, **427**, 106-113.
193. Y. N. Feng, X. P. Zhou, J. H. Yang, X. Y. Gao, L. X. Yin, Y. F. Zhao and B. Zhang, *Acs Sustainable Chemistry & Engineering*, 2020, **8**, 2122-2129.
194. Y. Liu, H. J. Guan, J. Zhang, Y. F. Zhao, J. H. Yang and B. Zhang, *Int. J. Hydrog. Energy*, 2018, **43**, 2754-2762.
195. R. N. Muthu, S. Rajashabala and R. Kannan, in *Dae Solid State Physics Symposium 2015*, eds. R. Chitra, S. Bhattacharya and N. K. Sahoo, Amer Inst Physics, Melville, 2016, vol. 1731.
196. R. N. Muthu, S. Rajashabala and R. Kannan, *Renew. Energy*, 2016, **90**, 554-564.
197. J. Jin, J. Ouyang and H. M. Yang, *Nanoscale Res. Lett.*, 2017, **12**, 9.
198. N. F. Attia, M. M. Menemparabath, S. Arepalli and K. E. Geckeler, *Int. J. Hydrog. Energy*, 2013, **38**, 9251-9262.